Bifurcation Analysis and Control of a Fighter Aircraft

by

Pierre-Etienne AUBIN

Ancien élève de l'Ecole polytechnique, Palaiseau, France (1987-1990)
Ingénieur de l'armement

Submitted to the Department of Aeronautics and Astronautics
in partial fulfillment of the requirements for the degree of

Master of Science in Aeronautics and Astronautics

at the

MASSACHUSETTS INSTITUTE OF TECHNOLOGY.

February 1993

Author .....
Department of Aeronautics and Astronautics
December 8, 1992

Certified by .....
Rudrapatna V. Ramnath
Adjunct Professor of Aeronautics and Astronautics
Thesis Supervisor

Accepted by .....
Professor Harold Y. Wachman
Chairman, Departement Graduate Committee

Bifurcation Analysis and Control of a Fighter Aircraft

by

Pierre-Etienne AUBIN

Submitted to the Department of Aeronautics and Astronautics
on December 8, 1992, in partial fulfillment of the
requirements for the degree of
Master of Science in Aeronautics and Astronautics

Abstract

The equations of flight dynamics can be written in the form of a first order system of nonlinear differential equations. Linear approximations of this system are usually accurate enough to deal with low amplitude maneuvers involving only small angles of attack and sideslip. However, to predict the behavior of a plane at high angle of attack, one has to cope with many nonlinearities, both in the aerodynamic coefficients and in the mathematical model itself.

In this thesis, a system including nonlinear aerodynamic coefficients have been studied from the standpoint of the bifurcation theory. The bifurcation theory basically allows us to analyze how the equilibrium states of a differential system vary when parameters (typically, deflections of the rudder, the elevator or the ailerons) are varied.

This bifurcation analysis was successfully employed to predict such nonlinear phenomena as sudden jumps or departures into limit cycles. The occurrence of these phenomena have been confirmed by numerical simulations and time histories. Some applications of the bifurcation theory to control problems were investigated. Specifically, a control system aimed at avoiding jumps during lateral maneuvers was designed and the bifurcation surface concept was applied to the design of a classical control system, namely a yaw damper.

Thesis Supervisor: Rudrapatna V. Ramnath
Title: Professor of Aeronautics and Astronautics

Acknowledgements

I want to thank the Délégation Générale pour l'Armement of the French Ministry of Defense for supporting my studies at MIT.

I want to express my gratitude to Professor Rudrapatna V. Ramnath for giving me the opportunity to work on these original mathematical approaches to flight dynamics, for his guidance and friendliness and for his patient correction of this thesis.

I would like to thank all the people who have helped me and made my life easier, especially Mrs. Edith Roques at Sup'Aéro, who helped so much in preparing my application to MIT, Mrs. Valentine Girard at the French Embassy, Mrs. Elizabeth Zotos in the Aero/Astro Department at MIT, Pierre-Henri at the French Consulate, the Medical Department, the libraries and the Athena network staff.

Among all the friends we met this year, I am especially grateful to the Mahoney family. More than friends, you are now our American family.

Thank you also to Art and Margaret Kalb, Nancy Daly, Lynn Page, Karina and Eng-Soon Chan, Yuko and Takashi Maekawa, Christian Malis and Loïc Batel. You all deserve a gold medal in baby-sitting.

A very special thanks also to Etienne and Gwenaëlle Balmès. Your support and friendship helped us a lot. We hope you will come and join us in Paris next year.

To all our relatives who have crossed the Atlantic to help and visit us, *merci*!

Laure, Priscille, Lætitia and Henri, our American boy, this work is certainly not a masterpiece but it is for you, with all my love as a husband and a dad.

Contents

List of Figures

List of Tables

Chapter 1

Introduction

1.1 Linear and nonlinear models in flight dynamics

1.1.1 Linear models

In first approximation, aircraft dynamics are ruled by the equations of motion of a rigid body in which forces and moments due to weight, aerodynamic forces and thrust are inserted. In these equations, nonlinearities are many since both the mathematical model itself (presence of coupling terms such as pv, qr or nonlinear terms such as $\sin\alpha$, $\sin\phi\ldots$) and the aerodynamic model are nonlinear.

However, valid linearizations of the mathematical and aerodynamic models can be achieved in the limit of small angles of attack and sideslip. Thus far, the set of linearized equations of motion has been accurate enough for most of the applications. These applications include classical descriptions of lateral and longitudinal dynamics and control systems design [1, 2]. Thus, most of the civilian and military airplanes have been built based on these linear equations.

Nevertheless, as early as in the fifties, it appeared that coupling terms, usually neglected, were responsible for nonnegligible effects in high performance fighter aircraft: in 1948, the so-called *roll-coupling* phenomenon was predicted by Phillips [3] and was unfortunately experienced later by F-100 Super-Sabre fighters [4]. The cross-

coupling problem, which is also referred to as the roll-coupling or inertia-coupling problem, basically arises when an airplane performs high roll-rate maneuvers. Two dangerous phenomena can then be encountered. The first one is an instability of the short-period longitudinal and directional oscillations. The second one is known as auto-rotational rolling, in which the fighter can suddenly jump to a higher roll-rate, where, additionally, controls can become inefficient. All these phenomena can lead to high angle of attack or sideslip, causing unusual loading on the structure leading to accidents. Some studies [5, 6, 7, 4, 8] were devoted to this phenomenon in the late fifties but these studies were still based on linearized systems of equations.

But nowadays, the requirement for increased maneuverability has fostered the use of fully nonlinear models.

1.1.2 "Maneuverability [...], the difference between life and death"

These words from an army official [9] demonstrate the concern for increased maneuverability in the next generation of combat aircraft. One of the basic requirements for enhanced maneuverability is the ability to fly at angles of attack of at least 50 degrees. No less than three experimental programs are currently underway in the US in order to investigate flight at high angles of attack, namely the Grumman X-29 forward swept wing fighter, the Rockwell-MBB X-31 Enhanced Fighter Maneuverability (EFM) project, incorporating thrust vectoring, and the NASA F/A-18 High Angle of Attack Research Vehicle (HARV). The X-29 and the HARV programs have already reached angles of attack up to fifty five or sixty degrees. And one can remember the Soviet Su-27 "cobra maneuver" featuring flight at more than 90 degrees of angle of attack, though only in a transient manner.

According to a German expert [10], so-called *supermaneuverability* shall include both post-stall (PST) and direct force (DFM) capabilities. PST is the ability to maneuver beyond stall angle and DFM is the ability to follow a flight path independently of the fuselage attitude, allowing the supermaneuverable fighter to point and shoot

first. Thus, flight dynamicists have much to do and one of their major concerns is to develop adequate models. The first prerequisite for an accurate dynamic model is a complete aerodynamic model. But aerodynamics at high alpha are especially difficult ...

1.1.3 Aerodynamic peculiarities of flight at high angle of attack

Flight at high angle-of-attack features many complex phenomena, which have been described to some extent in [11, 12] and, more recently and extensively, in [13]. First of all, stability derivatives happen to have nonlinear variations with angles of attack and sideslip and to depend heavily and nonlinearly on roll or pitch rates for instance. Some of these nonlinearities have been tentatively included in the model studied in this thesis in the form of second order polynomials.

One of the most surprising nonlinear effects is that side forces and moments can develop at zero angle of sideslip, for sufficiently high angle of attack. Thus lateral and longitudinal motions are definitely coupled. Another typical nonlinear phenomenon is the well-known *wing-rock*, which is a high amplitude rigid body oscillation. Wing-rock can be mathematically interpreted as a limit cycle and is due to asymmetric and successive leading edge vortex bursts.

In the bizarre nonlinear phenomenology, one can also come across aerodynamic hysteresis, such as that which affect the rolling moment coefficient versus the angle of sideslip on Figure 1-1. This demonstrates that aerodynamic coefficients also depend on the past history of the flow.

These are some of the difficulties and delights of flight dynamics at high angles of attack. They are just intended to give an idea of the complexity and variety of the phenomena to be included in models. As a matter of fact, in recent computationnal surveys, aerodynamic models were taken into account in the form of tabular data. Once a proper aerodynamic model has been included in the equations of motion, specific methods have to be applied in order to analyze the fully nonlinear system.

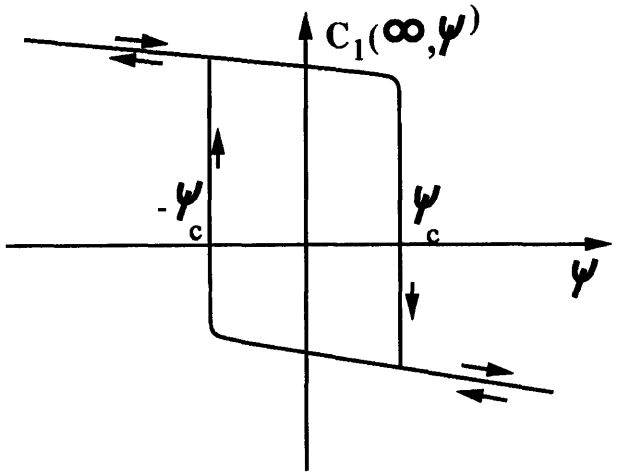

Figure 1-1: Aerodynamic hysteresis on the rolling moment coefficient

The key method is the bifurcation theory.

1.1.4 The bifurcation theory, a new powerful tool in nonlinear flight dynamics

Bifurcation theory itself is far from being new since it was invented first by Poincaré at the late nineteenth century. Hopf, in the forties, and Thom [14] have also been great contributors, among others. However, the application of bifurcation theory to issues in flight dynamics is fairly recent and has been pioneered in the early eighties by Guicheteau [15], Mehra [16, 17] and Schy [18, 19, 20].

The first success of bifurcation theory was to give an account for the aforementioned old cross-coupling problem [15, 18]. This approach mainly consists in computing the value of the equilibrium states[1] of the system constituted by the equations of motion when one or more parameter (typically, the ailerons, the rudder or the elevator deflection) is varied. Thus, for example, one can easily obtain the equilibrium roll-rate for any combination of the control surfaces deflections. These equilibrium surfaces allow a great deal of prediction since they tell which equilibrium state the dynamic system is to be attracted to. Based on this kind of analysis, cross-coupling phenomena

[1] An equlibrium state of a differential system $\dot{x} = f(x)$ is a state where $\dot{x} = 0$. A linear system has only one equilibrium state, which is zero, but a nonlinear system may have many nontrivial equilibrium states.

such as auto-rotationnal rolling were interpreted as "jumps" or "catastrophes".

The same type of approach has been applied to the more complex problem of high angle of attack dynamics [15, 17, 16, 20, 21, 22, 23] and noticeable results such as spin departure prediction have been obtained.

1.2 Statement of purpose

Nevertheless, in all these articles, fully nonlinear equations and aerodynamic datas from wind tunnel are used. Thus, sophisticated mathematical methods, so-called *continuation methods*, are needed, in addition to the bifurcation theory itself, to compute the various equilibrium states and their stability. This is beyond the scope of this thesis, and, consequently, a simpler model has been used in this study, one in which aerodynamic nonlinearities are included in the form of polynomials with constant coefficients. This simplification allows straightforward computations with a software specialized in polynomial processing such as *Matlab* but preserves the variety of all the nonlinear phenomena. Another advantage of this simpler aerodynamic model is that it allows parametric studies along with a more thorough understanding of the phenomena.

Thus, based on this nonlinear but simple model, this thesis presents a bifurcation analysis of the longitudinal and lateral dynamics of a fighter aircraft. Some strategies to control nonlinear phenomena in the largest possible range of the control deflections are investigated.

1.3 Organization of the report

This thesis is divided into four chapters, including this introduction aimed at providing a historical background for bifurcation analysis applied to flight dynamics. Chapter 2 is dedicated to an introduction to the bifurcation theory itself and provides the necessary tools to analyze linear and nonlinear systems. The first purpose of Chapter 2 is to make clear when a nonlinear system can be validly approximated by

its linearized system. The answer is: always, for small perturbations about an equilibrium point, except when the jacobian matrix of the nonlinear system has eigenvalues with zero real parts. Then, Chapter 2 answers the question: "what happen when there is a zero eigenvalue?" through the center manifold theorem and the bifurcation theory, which specifically deals with system dependence on one (or more) parameter.

Chapter 3 is the application of these tools to the study of the longitudinal and lateral dynamics of a fighter airplane. Nonlinear phenomena such as jumps and limit cycles are identified and analyzed through the bifurcation theory and confirmed by numerical simulations on complete differential systems.

Chapter 4 investigates some hints given in the aforementioned articles in order to provide efficient control of nonlinear phenomena. The bifurcation theory is applied to design original control laws coupling the rudder and the ailerons to avoid jumps.

Chapter 2

Introduction to the Bifurcation Theory

2.1 Introduction

In many physical situations, a model including a system of coupled ordinary nonlinear equations arises naturally.

This is the case in flight dynamics, where the equations of motion of a rigid airplane can be symbolically written as

$$\dot{x} = f(x), \tag{2.1}$$

where $f : R^n \longrightarrow R^n$ is a smooth function of the state vector x.

The stability[1] of such a dynamical system is obviously a crucial issue. This problem was originally discussed by Henri Poincaré and by Liapunov. They related the stability of system 2.1 about the equilibrium point x_0 to that of the linearized system 2.2

$$\dot{\zeta} = Df(x_0)\zeta, \tag{2.2}$$

[1]By stability, it is meant here local stability. Given an equilibrium point $x = x_0, \dot{x}(x_0) = 0$, this point is said to be locally stable if any trajectory in a neighborhood of x_0 at $t = t_1$ remains in this neighborhood at $t > t_1$. The equilibrium point x_0 is asynptotically stable if, furthermore, $x(t)$ goes to x_0 when t goes to infinity.

where $Df(x_0)$ is the Jacobian matrix of f, computed in x_0. Thus, to begin with, it seems important to review some features about linear systems. Then, a modern version of Poincaré-Liapunov's theory is explained. It appears that phenomena specific to nonlinear equations arise only when a real eigenvalue of the Jacobian matrix is zero or when the real part of a pair of complex conjugate eigenvalues is zero. A new theory is thus needed to adress this case, whose basis is the so-called *Center Manifold Theorem.* Eventually, after these necessary preliminaries, the bifurcation theory itself is exposed.

There are many textbooks dealing with the basics of linear systems, such as [24]. The theory of nonlinear systems is still under the scope of current research. A comprehensive introduction, written to the intention of engineers and including a very large bibliography is that by Holmes and Guckenheimer [25].

2.2 The linear system $\dot{x} = Ax$

2.2.1 General theory

A linear system is defined by

$$\dot{x} = Ax, x(0) = x_0 \tag{2.3}$$

where A is $n \times n$ matrix with constant real coefficients and $x \in R^n$. For this system, the only equilibrium point is $x = 0$. Since the solution of this system can be written as

$$x(t) = x_0 e^{At}, \tag{2.4}$$

the stability of this equilibrium depends on the sign of the eigenvalues of the matrix A in the following way:

Theorem 1 *The equilibrium point 0 of system 2.3 is unique and is stable if and only if the real part of the eigenvalues of the matrix A are non positive.*

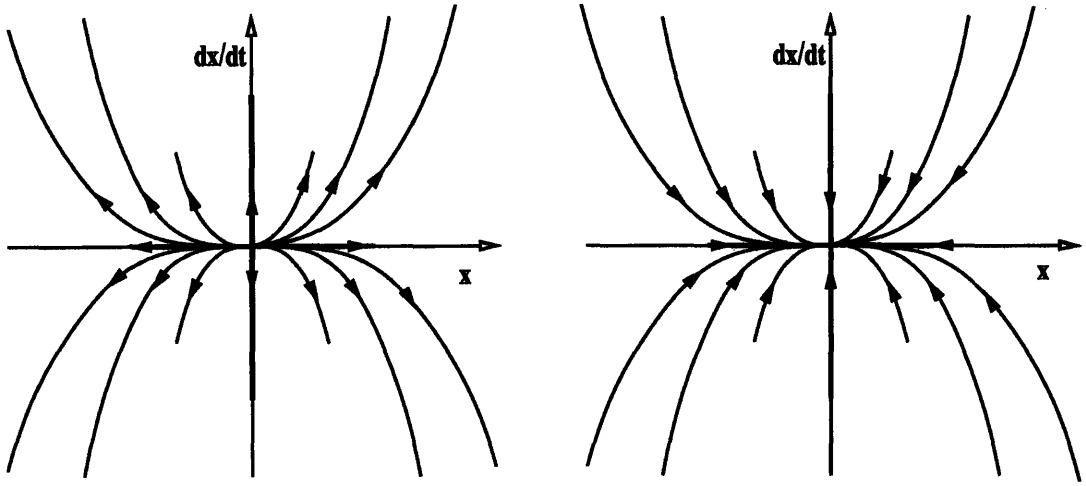

Figure 2-1: Stable node (left) and unstable node

2.2.2 The two dimensional case

The two dimensional case is of some importance because it allows to represents either a first order system with two variables such as

$$\begin{aligned} \dot{x_1} &= a_{11}x_1 + a_{12}x_2 \\ \dot{x_2} &= a_{21}x_1 + a_{22}x_2, \end{aligned} \tag{2.5}$$

either a second order phenomenon with one variable such as

$$\ddot{x} = a\dot{x} + bx + c, \tag{2.6}$$

which can be put in the form of system 2.5 by letting $x = x_1$ and $\dot{x} = x_2$.

If A is a 2×2 real valued matrix, the different types of equilibria can be classified in terms of the sign of the two eigenvalues λ_1 and λ_2 of the matrix A.

λ_1 and λ_2 are non zero, real, distinct and of same sign

The equilibrium point is called a *node*, stable if λ_1 and λ_2 are negative and unstable if λ_1 and λ_2 are positive. The aspect of the trajectories near the equilibrium point can be represented in the *phase plane*, which is the plane $(x, \dot{x})$. In this case the so-called *phase portrait* looks like that represented on Figure 2-1. On this figure, the arrows denote the direction of increasing time. It can be also noticed that the trajectories

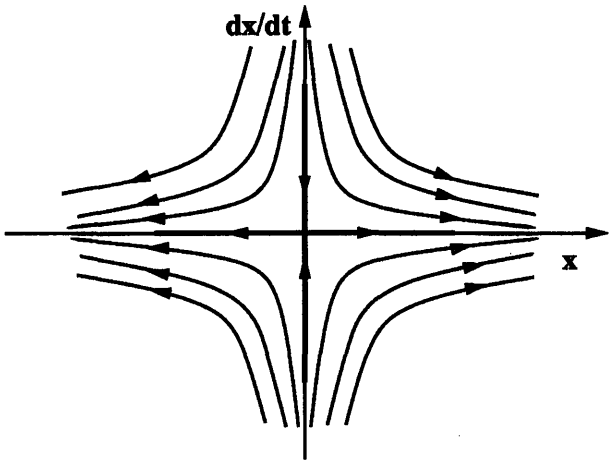

Figure 2-2: Saddle

approach the equilibrium point along two specific directions, which are nothing but the eigenvectors of the matrix A. This fact is of great importance and is discussed later under the notion of *invariant subspaces.*

λ_1 and λ_2 are non zero, real, distinct and of opposite sign

The equilibrium point is now called a *saddle* and is unstable. The phase portrait near the equilibrium point looks like that represented on Figure 2-2.

λ_1 and λ_2 are non zero, real and equal

Two subcases arise in this case. If the matrix A can be put in a diagonal form then the origin can be approached or left in all directions. This is due to the fact that such a matrix is equivalent to identity matrix, implying that every non zero vector is an eigenvector. In this case, the equilibrium point is called a *proper node.*

If the matrix A can not be put in a diagonal form then the origin can be approached in only one direction, due to the fact that, in this case, there is only one eigenvector. The equilibrium point is called an *improper node.* The phase portrait in these two cases is sketched on Figure 2-3.

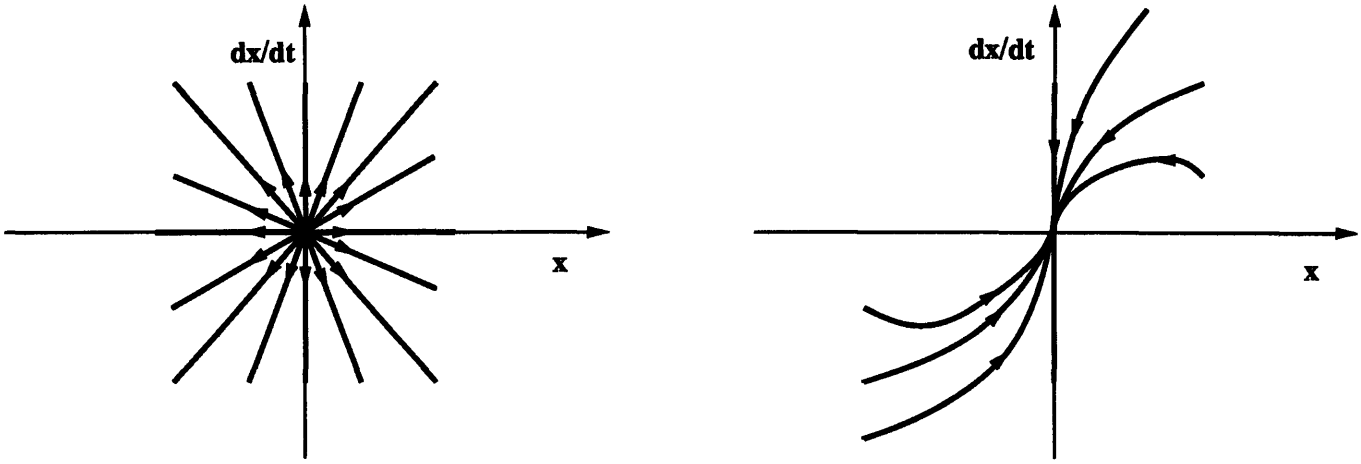

Figure 2-3: Proper node (left) and improper node

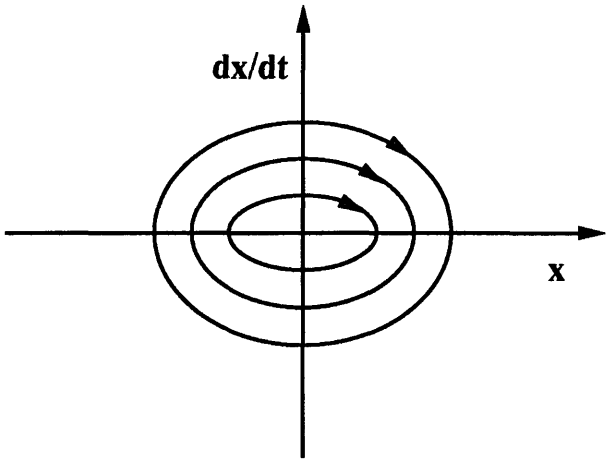

Figure 2-4: Vortex

λ_1 and λ_2 are complex conjugate and have zero real part

The equilibrium point is called a *center* or *vortex.* In this case, the equilibrium is stable but not asynptotically stable. The phase portrait is sketched on Figure 2-4.

λ_1 and λ_2 are complex conjugate and have non zero real part

The equilibrium point is a *focus* or a *spiral point.* It is stable if the real part of λ_1 and λ_2 is negative and unstable if the real part is positive. These two cases are sketched on Figure 2-5. This ends the zoology of all the possible types of equlibrium in the two dimensional case. Before dealing with the nonlinear case, some definitions are needed and a section is to be devoted to the study of the notion of *invariant spaces.*

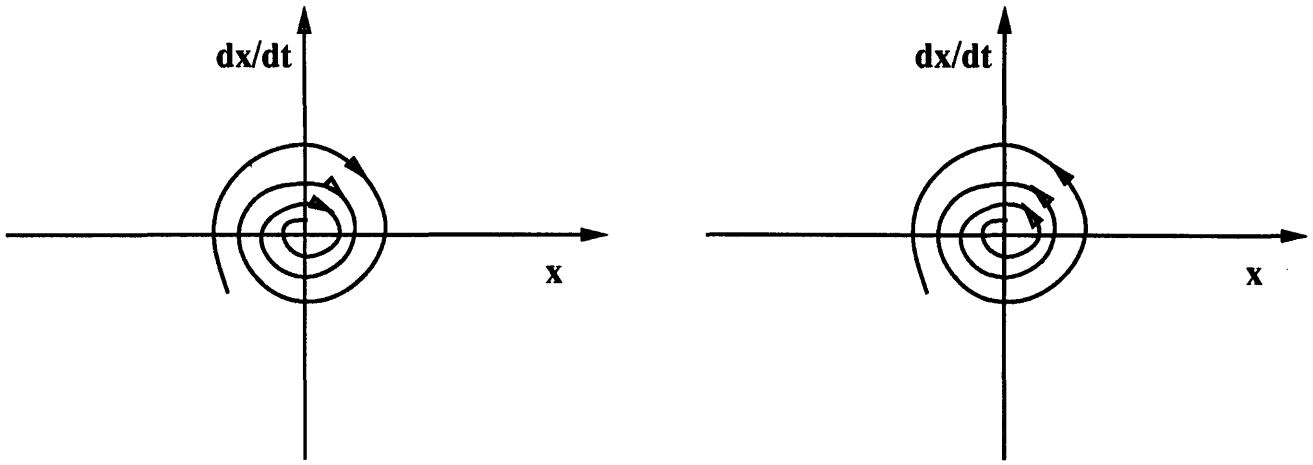

Figure 2-5: Stable focus (left) and unstable focus

2.3 Invariant spaces

In the previous schemes of two dimensional flows near their equilibrium point, it has been noted that the trajectories approached the equilibrium point along special directions, at least in the case of real eigenvalues. These directions are the eigenvectors of the matrix A. These eigenvectors are said to be invariant under the flow of A. This means that a solution of system 2.3 with an eigenvector as an initial condition remains on this eigenvector. The proof of this fact can be stated as follows:

If v_i is an eigenvector of A with a real eigenvalue λ_i, then $Av_i = \lambda_i v_i$. If v_i is the initial condition, then the solution of system 2.3 writes $x(t) = e^{tA}v_i$. But

$$e^{tA}v_i = [1 + tA + \frac{t^2A^2}{2} + \ldots]v_i = v_i + t\lambda_i v_i + \ldots = e^{t\lambda_i}v_i. \tag{2.7}$$

Thus, the solution does remain in the v_i direction.

If λ_i and $\bar{\lambda_i}$ are two complex conjugate eigenvalues with eigenvectors v_i^1 and v_i^2, then v_i^1 and v_i^2 are no more invariant separatly i.e. a trajectory whose initial condition is on v_i^1 or v_i^2 does not remain on v_i^1 or v_i^2. Nevertheless, what remains true is that a trajectory whose inital condition is in the plane spanned by v_i^1 and v_i^2 remains in this plane. So, the plane itself is invariant. Thus, one can define the more general concept of *invariant subspace.*

Definition 1 *The subspace spanned by the eigenvectors whose eigenvalues have a negative real part is called the* stable subspace *and is denoted E^s, the subspace spanned by the eigenvectors whose eigenvalues have a positive real part is called the* unstable subspace *and is denoted E^u, the subspace spanned by the eigenvectors whose eigenvalues have a zero real part is called the* center subspace *and is denoted E^c. On a stable subspace, the solutions decay, on an unstable subspace, the solutions increase, on a center subspace, the solutions either oscillate or remain constant.*

To finish with, the following example [25], which features a three dimensional flow, illustrates explicitly this concept of invariant subspaces. The matrix

$$A = \begin{bmatrix} -1 & -1 & 0 \\ 1 & -1 & 0 \\ 0 & 0 & 2 \end{bmatrix} \tag{2.8}$$

has the eigenvalues $\{2, \frac{-1+i}{2}, \frac{-1-i}{2}\}$ and the invariant subspaces $E^s = span\{(1,0,0),(1,1,0)\}$, $E^u = \{(0,0,1)\}$ and $E^c = \emptyset$ and the phase portrait near the origin can be represented as sketched on Figure 2-6. On this example, one can see that a solution beginning in the plane $E^s = span\{(1,0,0),(1,1,0)\}$ will remain in this plane although each of the eigenvectors (1,0,0) and (1,1,0) is not invariant separatly since the typical trajectory in E^s is a spiral.

This notion of invariant space is very efficient to analyze the flow in multiple dimension cases and is to be extended in the next section to the case of nonlinear systems under the notion of *stable*, *unstable* or *center manifolds*.

2.4 The nonlinear system $\dot{x} = f(x)$

It is now possible to come back to the nonlinear system

$$\dot{x} = f(x), \tag{2.9}$$

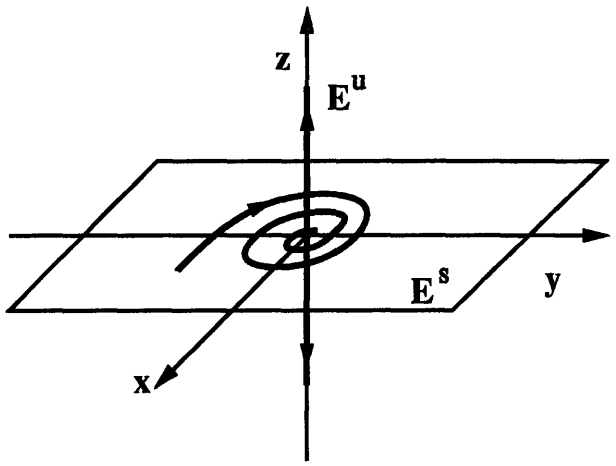

Figure 2-6: Invariant subspaces for matrix A

where $x \in R^n$ and f is a smooth function. Our purpose is still to inquire about the stability of the equilibria of this system. The first difference with linear systems is that nonlinear systems can exhibit multiple equilibrium points and a good start in studying system 2.9 is to find its zeros or equilibria or stationnary solutions. These equilbria are denoted $\bar{x}$. Then, one can linearize the system 2.9 in the following way:

$$\dot{\zeta} = Df(\bar{x})\zeta, \tag{2.10}$$

where $\zeta \in R^n$ and $Df(\bar{x})$ is the Jacobian matrix[2] of f computed in $\bar{x}$.

The question is then: how are the stability of the nonlinear system 2.9 and that of the linearized system 2.10 related?

The Poincaré-Liapunov's theory just gives the answer: the linearized system 2.10 describes properly the behavior of the nonlinear system 2.9 in the neighborhood of an equilibrium point $\bar{x}$ if the jacobian matrix $Df(\bar{x})$ has no zero eigenvalue or eigenvalue with zero real part.

2.4.1 The non degenerate equilibrium case

To state a modern version of this theorem, some more definitions are needed.

[2]The jacobian matrix is defined by $(Df(x))_{i,j} = \frac{\partial f_i}{\partial x_j} for 1 \leq i, j \leq n$.

Definition 2 *When the jacobian matrix $Df(\bar{x})$ has no zero eigenvalue or eigenvalue with zero real part, the equilibrium point $\bar{x}$ is said to be a* hyperbolic *or* non degenerate *equilibrium point.*

Furthermore, the locally stable and unstable manifolds of $\bar{x}$, $W^s_{loc} and W^u_{loc}$ are defined in the following way:

Definition 3 *If $U \subset R^n$ is a neighborhood of the fixed point $\bar{x}$ and $\phi_t(x_0)$ is a solution of system 2.9 equal to x_0 at $t = 0$, then*
$W^s_{loc} = \{x_0 \in U \mid \phi_t(x_0) \to \bar{x} \text{ as } t \to \infty \text{ and } \phi_t(x_0) \in U \text{ for all } t \geq 0\}$,
and
$W^u_{loc} = \{x_0 \in U \mid \phi_t(x_0) \to \bar{x} \text{ as } t \to -\infty \text{ and } \phi_t(x_0) \in U \text{ for all } t \leq 0\}$.

W^s_{loc} and W^u_{loc} are analog to E^s and E^u in the linear case. It is now possible to state a version of the Poincaré-Liapunov's theorem in term of these definitions. This one is due to Hartman and Grobman (1981) and is quoted in [25, p. 13-14].

Theorem 2 *If $Df(\bar{x})$ has no zero or purely imaginary eigenvalues, then*

a. there is a homeomorphism h defined on some neighborhood U of $\bar{x}$ in R^n locally taking solutions of the nonlinear system 2.9 to those of the linearized system 2.10. The homeomorphism preserves the sense of the solutions.

b. there exist local stable and unstable manifolds W^s_{loc} and W^u_{loc} of the same dimension n_s and n_u as those of the subspaces E^s and E^u of the linearized system 2.10 and tangent to E^s and E^u at $\bar{x}$. Further, W^s_{loc} and W^u_{loc} are as smooth as f.

In other words, in the neighborhood of an hyperbolic equilibrium point, the solutions and the stable and unstable manifolds are just distorted but the stability of the equilibrium point remains the same as in the linearized case. This concept is illustrated on Figure 2-7. Thus, in the case of an hyperbolic equilibrium point, the situation is simple. Nevertheless, a question has been left unanswered: what happen when a zero or purely imaginary eigenvalue occurs?

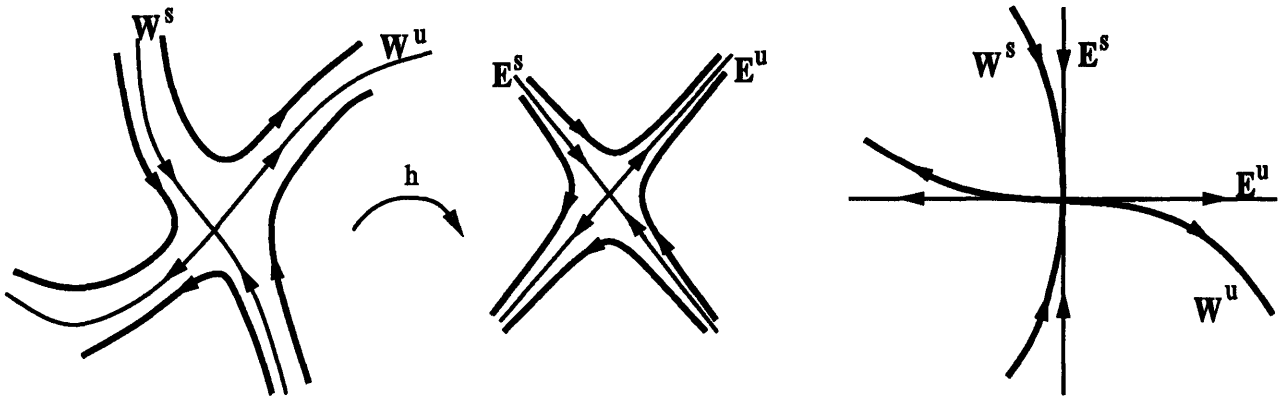

Figure 2-7: Nonlinear and linearized flow near an hyperbolic equilibrium point (left). Stable and unstable manifolds and subspaces

2.4.2 The degenerate equilibrium case

First of all, some other techniques can be used to inquire about the stability of any kind of fixed point. Thus, for example, if a continuous and positive function which decays along any trajectory in the neighborhood of the fixed point can be found, then this point is asynptotically stable. This function is called a Liapunov function. Typically, energy is a good candidate for a mechanical system.

Another interesting technique, which is going to be described in further details in the following section, is to find out what is the behaviour of the dynamical system in the so-called *center manifold.*

2.5 Center manifolds and the center manifold theorem

Definition 4 *A center manifold is defined as an invariant manifold tangent to the center subspace.*

The center manifold theorem states that such a center manifold exist but need not be unique [25, p. 127]

Theorem 3 *Center manifold theorem: let f be a C^r vector field on R^n vanishing at*

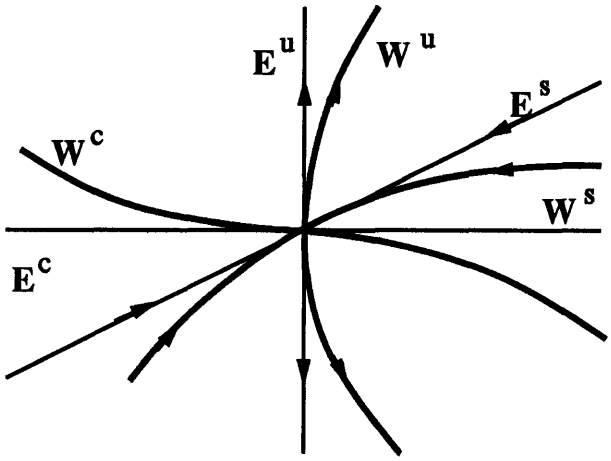

Figure 2-8: Stable, unstable and center manifolds and subspaces

the origin $(f(0) = 0)$ *and let* $A = Df(0)$. *Divide the spectrum of* A *into three parts,* σ_s, σ_u *and* σ_c *with*

$$\Re e\lambda \begin{cases} < 0 & if \quad \lambda \in \sigma_s, \\ > 0 & if \quad \lambda \in \sigma_u, \\ = 0 & if \quad \lambda \in \sigma_c. \end{cases}$$

Let the eigenspaces of σ_s, σ_u *and* σ_c *be* E^s, E^u *and* E^c. *Then, it exists* C^r *stable and unstable manifolds* W^s_{loc} *and* W^u_{loc} *tangent to* E^s *and* E^u *(this was already stated in the previous theorem) and a* C^{r-1} *center manifold* W^c *tangent to* E^c *at* 0. *The manifolds* W^s, W^u *and* W^c *are all invariant under the flow of* f. *The stable and unstable manifolds are unique but* W^c *need not be unique.*

The content of the center manifold theorem can be illustrated on Figure 2-8, where a center manifold tangent to the center eigenspace can be drawn but where no direction can be assigned to the flow. Thus, through the center manifold theorem, one can learn about the existence of the center manifolds but is still unable to say something about the stability of the flow in this manifold. This question is to be adressed in the next section.

2.6 Stability of center manifolds

The method proposed in [25, p. 130-138] consits in projecting the flow on the center manifold and in giving an approximate expression of this projected flow by a power series expansion.

Thus, the flow near an equilibrium point can be seen to be topologically equivalent to

$$\begin{aligned} \dot{\tilde{x}} &= \tilde{f}(\tilde{x}) \\ \dot{\tilde{y}} &= -\tilde{y} \\ \dot{\tilde{z}} &= \tilde{z}, \end{aligned}$$

where $(\tilde{x}, \tilde{y}, \tilde{z}) \in W^c \times W^s \times W^u$. If one can compute $\tilde{f}$, then one can determine the stability of the center manifold.

Assuming that the unstable manifold is empty, one can put the initial system 2.9 in the following form

$$\begin{aligned} \dot{x} &= Bx + f(x,y) \\ \dot{y} &= Cy + g(x,y), \end{aligned} \tag{2.11}$$

where B and C are $n \times n$ and $m \times m$ diagonal matrices with eigenvalues having respectively zero and negative real parts. If we assume also that the equilibrium point is O then f and g and their first partial derivatives vanish at the origin.

The crucial point of the method is that W^c can be represented as a graph near the origin, since it is tangent to the center subspace E^c. Thus,

$$W^c = \{(x,y) \mid y = h(x)\},$$

with

$$h(0) = Dh(0) = 0.$$

Thus,

$$\dot{y} = Dh(x)\dot{x} = Dh(x)[Bx + f(x,h(x))] = Ch(x) + g(x,h(x))$$

or

$$\mathcal{N}(h(x)) = Dh(x)[Bx + f(x,h(x))] - Ch(x) - g(x,h(x)) = 0$$

with the boundary conditions

$$h(0) = Dh(0) = 0.$$

If this partial differential equation for h cannot be solved exactly in the general case, a solution for h can be sought in the form of a series expansion. The following example illustrates this method. consider the system

$$\begin{aligned} \dot{u} &= v \\ \dot{v} &= -v + \alpha u^2 + \beta uv. \end{aligned} \tag{2.12}$$

This system has a single fixed point (0,0). The linear part of this system has 0 and - 1 eigenvalues. Putting it in diagonal form, one can come up with the following system, analog to 2.11,

$$\begin{aligned} \dot{x} &= \alpha(x+y)^2 - \beta(xy+y^2) \\ \dot{y} &= -y - \alpha(x+y)^2 + \beta(xy+y^2). \end{aligned}$$

Setting $h(x) = ax^2 + bx^3 + \ldots$ and computing $\mathcal{N}(h(x))$, one can determine that

$$h(x) = -\alpha x^2 + \alpha(4\alpha\beta)x^3 + O(x^4), \tag{2.13}$$

and so that

$$\dot{x} = \alpha(x+y)^2 - \beta(xy+y^2) = \alpha x^2 + \alpha(\beta - 2\alpha)x^3 + O(x^4). \tag{2.14}$$

Thus, when $\alpha > 0$, the center manifold is stable for $x < 0$ and unstable for $x > 0$, yielding the phase portrait on Figure 2-9.

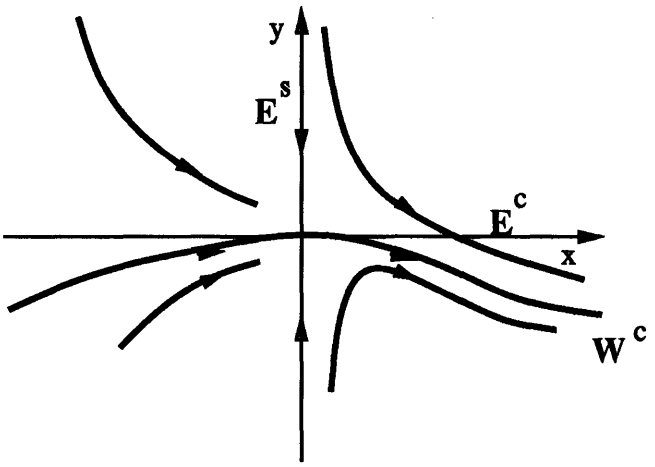

Figure 2-9: Local phase portrait and center manifold for system 2.12 and $\alpha > 0$

2.7 Bifurcation theory

2.7.1 Introduction

Another class of problems to which center manifold theorem is likely to be applied is the case of sytems depending on a parameter, such as

$$\dot{x} = f_\mu(x), \tag{2.15}$$

where $x \in R^n$, $\mu \in R$ and f_μ is smooth. The number of fixed points and their nature depends on the value of μ. The point (x_0, μ_0) at which these changes occur is called a *bifurcation point* and these changes occur through a real eigenvalue or the real part of a complex conjugate eigenvalue becoming zero.

2.7.2 Basic bifurcation models

There are four types of bifurcations for one dimensional parameters. They are described by the following equations:

$$\dot{x} = \mu - x^2 \text{ (Saddle-node)},$$
$$\dot{x} = \mu x - x^2 \text{ (Transcritical)},$$
$$\dot{x} = \mu x - x^3 \text{ (Pitchfork)},$$

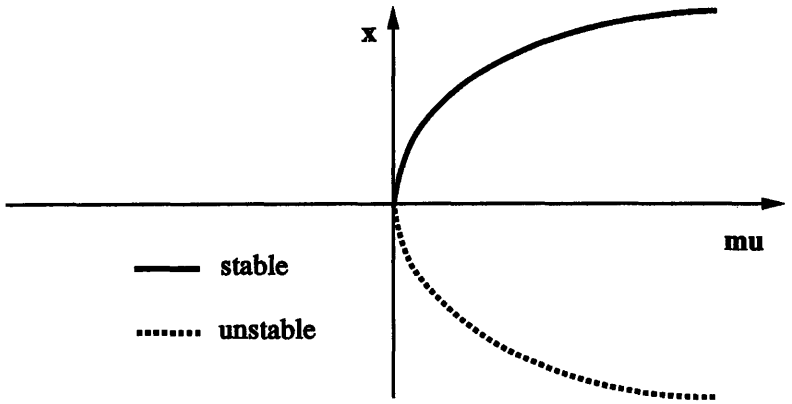

Figure 2-10: Bifurcation diagram for the saddle-node bifurcation

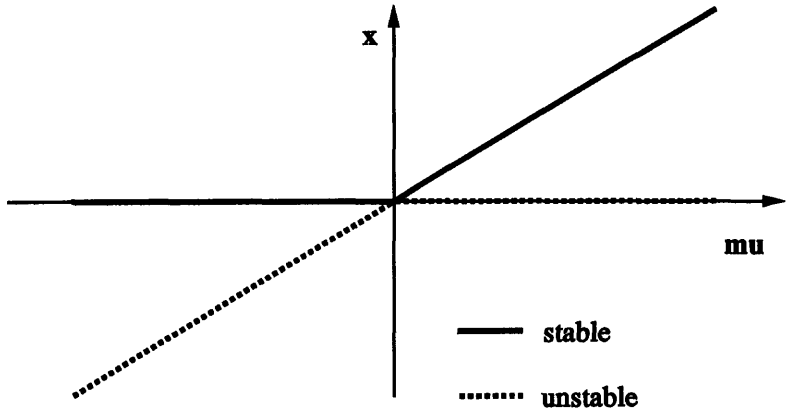

Figure 2-11: Bifurcation diagram for the transcritical bifurcation

and

$$\begin{cases} \dot{x} &= -y + x(\mu - (x^2 + y^2)) \quad (Hopf) \\ \dot{y} &= x + y(\mu - (x^2 + y^2)) \end{cases}$$

For each of these equations, one can draw a *bifurcation diagram*, which shows the number and the stability of the fixed points versus the value of the parameter μ. The four bifurcation diagrams are sketched on Figures 2-10 trough 2-13. These four systems are one or two dimensional but, through the center manifold theorem, one can reduce the study of a multi-dimensional system whose Jacobian matrix has a zero eigenvalue or a pair of purely imaginary eigenvalues at (x_0, μ_0) to that of its projection onto a center manifold. Thus bifurcations of multi-dimensional systems

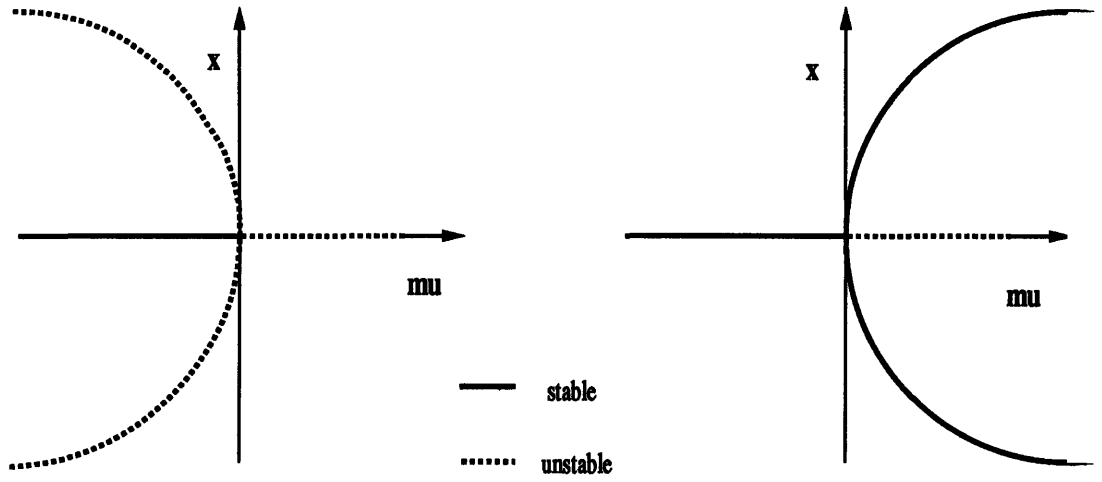

Figure 2-12: Bifurcation diagrams for the subcritical (left) and supercritical pitchfork bifurcation

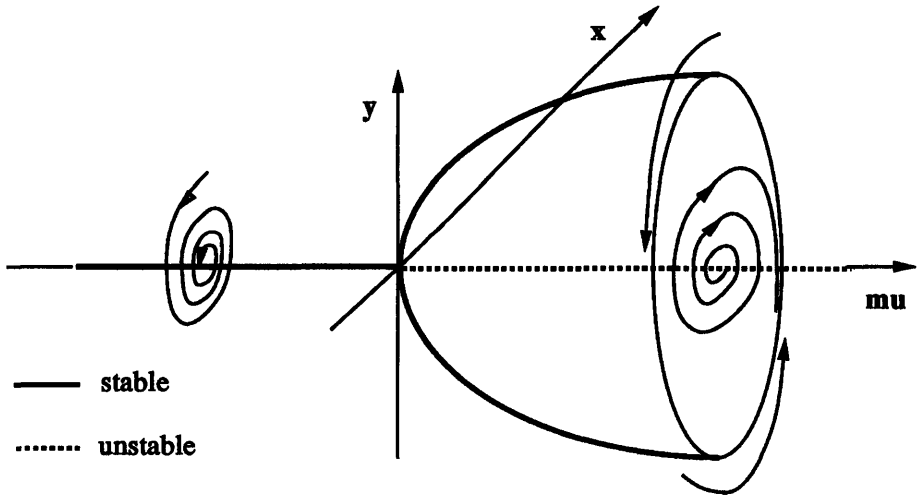

Figure 2-13: Bifurcation diagram for the Hopf bifurcation

can be compared with the previous four basic types. An example of this reduction for a parametrized system is helpful.

Consider the system

$$\begin{aligned} \dot{u} &= v \\ \dot{v} &= \beta u - u^2 - v, \end{aligned} \tag{2.16}$$

where β is a small variable parameter. At $\beta = 0$, the linearized system has 0 and -1 eigenvalues at $(u,v) = (0,0)$, with eigenvectors $(1,0)$ and $(1,-1)$. These two eigenvectors are a new frame in which the system 2.16 can be re-written as

$$\begin{aligned} \dot{x} &= \beta(x+y) - (x+y)^2 \\ \dot{y} &= -y - \beta(x+y) + (x+y)^2. \end{aligned} \tag{2.17}$$

A center manifold can now be sought in the form

$$y = h(x,\beta) = ax^2 + bx\beta + c\beta^2 + O(3), \tag{2.18}$$

where $O(3)$ means third order terms in x and β. After little algebra, whose details can be found in [25, p. 135], one can find that

$$y = (x^2 - \beta x) + O(3) \tag{2.19}$$

and that, in this two-dimensional center manifold,

$$\dot{x} = \beta(1-\beta)x - (1-\beta)x^2 + O(3). \tag{2.20}$$

This system can now be seen to be analog to the model of the transcritical bifurcation $\dot{x} = \mu x - x^2$, whose bifurcation diagram is sketched on Figure 2-11. The center manifold $y = h(x,\beta)$ itself is sketched on Figure 2-14.

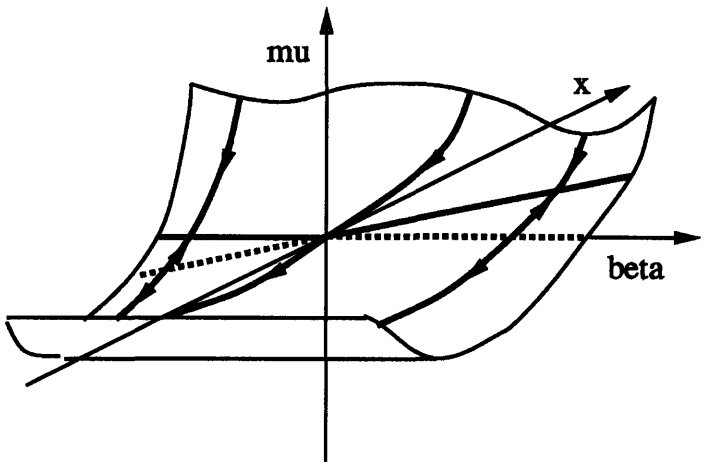

Figure 2-14: Two-dimensional center manifold for system 2.17

The conditions under which each of the four types of bifurcation occurs in multi-dimensional systems are now to be precised.

2.7.3 Saddle-node, transcritical and pitchfork bifurcations

Application of the center manifold reduction

It is now assumed that the system 2.15 has a zero real eigenvalue at (x_0, μ_0). This eigenvalue is also supposed to be simple: no other zero eigenvalue or pure imaginary eigenvalue occurs at (x_0, μ_0). Thus, one can figure out that, like in the previous example 2.16, it is possible to find a two-dimensional center manifold, in which the system 2.15 can be reduced to $\dot{\tilde{x}} = \tilde{f}_\mu(\tilde{x})$, where $(\tilde{x}, \mu) \in R \times R$. The assumption of a single zero eigenvalue is common to the first three types of bifurcation (saddle-node, transcritical and pitchfork) and one would now like to discriminate between these three possible cases. The answer is given in terms of the values of the coefficients of the series expansion of $\tilde{f}$ with respect to $\tilde{x}$ and μ.

For the saddle-node bifurcation as well as for the transcritical and pitchfork bifurcations, the zero real eigenvalue assumption implies that $(\partial \tilde{f}_{\mu_0}/\partial \tilde{x})(x_0) = 0$. But, specifically for the saddle-node case, one has $(\partial \tilde{f}_{\mu_0}/\partial \mu)(x_0) \neq 0$. It is thus implied by the implicit function theorem that the curve of equilibria is tangent to the line $\mu = \mu_0$. The additional condition $(\partial^2 \tilde{f}_{\mu_0}/\partial \tilde{x}^2)(x_0) \neq 0$ implies that this curve of

equilibria lies to one side of the line $\mu = \mu_0$. Eventually, there is a quadratic tangency with $\mu = \mu_0$ and, therefore, the local phase portrait of the original system 2.15 is topologically equivalent to that of a family $\dot{x} = \pm(\mu - \mu_0) \pm (x - x_0)$.

The transcritical bifurcation is likely to occur in families where 0 is constrained to be a fixed point for any μ: $\forall \mu \in R, \tilde{f}_\mu(x) = 0$. Thus, the hypothesis that $(\partial \tilde{f}_{\mu_0}/\partial \mu)(x_0) \neq 0$ is no more valid and has to be replaced by $(\partial^2 \tilde{f}_{\mu_0}/\partial \mu \partial \tilde{x})(x_0) \neq 0$.

For the pitchfork bifurcation, not only the constraint that 0 be a fixed point for any μ is required but also that there is a symmetry with respect to $\tilde{x}$: $\tilde{f}_\mu(-\tilde{x}) = -\tilde{f}_\mu(\tilde{x})$. Thus, the condition that $(\partial^2 \tilde{f}_{\mu_0}/\partial \tilde{x}^2)(x_0) \neq 0$ is not valid and has to be replaced by $(\partial^3 \tilde{f}_{\mu_0}/\partial \tilde{x}^3)(x_0) \neq 0$.

For a pitchfork bifurcation, one can see that the sign of $(\partial^3 \tilde{f}_{\mu_0}/\partial \tilde{x}^3)(x_0)$ determines the stability and the direction of the bifurcation branches. If $(\partial^3 \tilde{f}_{\mu_0}/\partial \tilde{x}^3)(x_0)$ is negative, then the bifurcation is said to be *supercritical*. The non-zero branches are stable and occur above the bifurcation value μ_0. If $(\partial^3 \tilde{f}_{\mu_0}/\partial \tilde{x}^3)(x_0)$ is positive, then the bifurcation is *subcritical*. These two kinds of pitchfork bifurcation are sketched on Figure 2-12.

Another theorem

This discrimination among the three kinds of bifurcation admitting a zero real eigenvalue was based on the process of reducing the problem to a family of one dimensional curves $\tilde{f}_\mu(\tilde{x})$ in the center manifold. Then, the hypothesis were made on $\tilde{f}_\mu$. Actually, a theorem can be stated which does not make use of this reduction process and whose hypothesis are done directly on the original system 2.15. Thus, for example, the following theorem can be stated for a saddle-node bifurcation:

Theorem 4 *-If the original multi-dimensional system 2.15 depends on a single parameter μ and has a fixed point (x_0, μ_0),*

-if, at (x_0, μ_0), the linearized system $D_x f_{\mu_0}$ has a simple zero real eigenvalue with right eigenvector v and left eigenvector w,

-if $w((\partial f_\mu/\partial \mu)(x_0, \mu_0) \neq 0$

-and if $w(D_x^2 f_{\mu_0}(x_0)(v, v)) \neq 0$

then (x_0, μ_0) *is a saddle-node bifurcation point and the phase portrait is equivalent to that of Figure 2-10.*

A more precise statement of this theorem appears in [25, p. 148]. Similar theorems can be formulated for pitchfork and transcritical bifurcations.

2.7.4 Hopf bifurcation

The last type of bifurcation is the Hopf bifurcation, which occurs when, at a fixed point (x_0, μ_0), the linearized system Df_{μ_0} has a simple pair of pure imaginary eigenvalues. A similar but a little more complicated reduction process (which makes use of the so-called *normal form theorem* [25, p. 138-145]) leads to a system which can be expressed in polar coordinates as

$$\begin{aligned} \dot{r} &= (a\mu + br^2)r \\ \dot{\theta} &= c + d\mu + er^2. \end{aligned} \tag{2.21}$$

If a and b are non zero, then $r_\mu = |a\mu/b|^{1/2}$ is the radius of a periodic orbit with $\theta = cste$. This family of periodic orbits is obviously invariant and is tangent to the center subspace in (x_0, μ_0), thus constituting a three-dimensional center manifold passing through (x_0, μ_0). The periodic orbits can be either stable or repelling, thus yielding subcritical or supercrtical bifurcations. The periodic orbits are also called *limit cycles*. The bifurcation diagram is sketched on Figure 2-13.

Chapter 3

Bifurcation Analysis of the Longitudinal and Lateral Dynamics of a fighter Aircraft

3.1 Introduction

The purpose of this chapter is to show how the bifurcation theory can be applied to dynamical systems in flight dynamics. An introductory example features an airplane model in a wind tunnel. It can be represented by a second order and one variable equation and has only one non-linearity. This non-linearity is due to the introduction of a nonlinear aerodynamic moment. This system exhibits a saddle node bifurcation. The main example features the equations of motion of an airplane in which an aerodynamic nonlinearity was also introduced. The system is of first order with five variables. Three control parameters, the aerodynamic controls provided by the ailerons, the rudder and the elevator are also present. Their combination is responsible for a wide variety of phenomena. On the various equilibrium diagrams presented below, saddle-nodes, pitchforks and Hopf bifurcations are present.

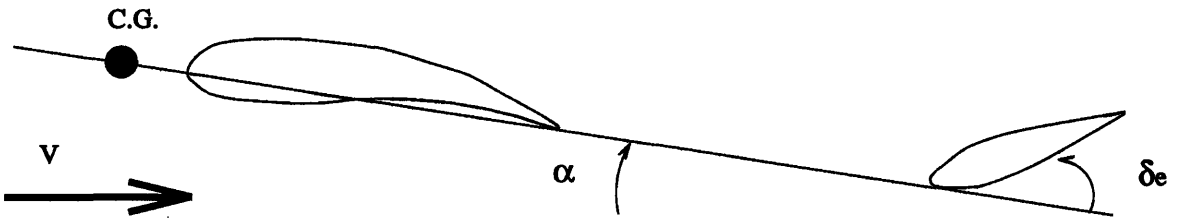

Figure 3-1: Geometry and notations for the airplane model

3.2 Introductory example: an airplane model in a wind tunnel

3.2.1 Description and equations of motion

In this example, an airplane model is placed in a wind tunnel. The model has only one degree of freedom, the angle of attack, since it can only rotate about a transversal axis passing through its center of gravity. On this model, the elevator is mobile and its deflection is measured by δe. This deflection is negative when the trailing edge of the elevator is up. The angle of attack is denoted α and is positive nose up. The geometry and the notations are represented on Figure 3-1. For a given elevator deflection δe, the equation of the motion about the transversal axis can be written as

$$I\ddot{\alpha} = \mathcal{M} + \mathcal{M}_{\delta e}\delta e, \tag{3.1}$$

where $\mathcal{M}$ is the aerodynamic moment due to the whole airplane except the elevator and $\mathcal{M}_{\delta e}\delta e$ is the aerodynamic moment due to the elevator. I is the moment of inertia about the transversal axis. Due to the fact that the transversal axis goes through the center of mass, there is no moment due to the weight of the aircraft.

Classically, $\mathcal{M}$ depends linearly on both α and $\dot{\alpha}$ and can be written as

$$\mathcal{M}_{linear} = \frac{1}{2}\rho S l V^2 (Cm_\alpha \alpha + Cm_{\dot{\alpha}}\dot{\alpha}), \tag{3.2}$$

where S and l are a reference surface and a reference length, ρ the air density, V the airspeed at infinity and where the coefficients Cm_α and $Cm_{\dot{\alpha}}$ are constant.

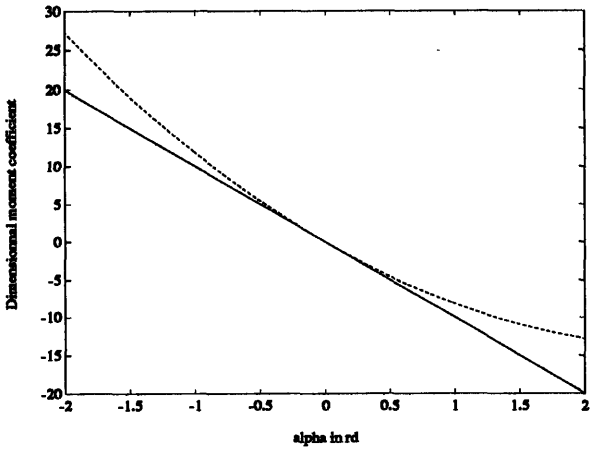

Figure 3-2: Linear and nonlinear aerodynamic moments

Nevertheless, at high angle of attack, this assumption that $\mathcal{M}$ is linear with α and $\dot{\alpha}$ does not remain true and one has to introduce some non-linearities in aerodynamics. In the real world, these aerodynamic nonlinearities are many, as it was stated in the Introduction. In this example, only the most simple non-linearity is introduced, a dependance of Cm in α^2. Thus, the nonlinear form of the aerodynamic moment is

$$\mathcal{M}_{nonlinear} = \frac{1}{2}\rho S l V^2 (Cm_\alpha \alpha + Cm_{\alpha\alpha}\alpha^2 + Cm_{\dot{\alpha}}\dot{\alpha}). \tag{3.3}$$

Upon substituting the expression of $\mathcal{M}_{nonlinear}$ into the equation of motion 3.1, one obtains

$$I\ddot{\alpha} = \frac{1}{2}\rho S l V^2 (Cm_\alpha \alpha + Cm_{\alpha\alpha}\alpha^2 + Cm_{\dot{\alpha}}\dot{\alpha} + Cm_{\delta e}\delta e), \tag{3.4}$$

which can be rewritten as

$$\ddot{\alpha} = m_\alpha \alpha + m_{\alpha\alpha}\alpha^2 + m_{\dot{\alpha}}\dot{\alpha} + m_{\delta e}\delta e, \tag{3.5}$$

where m_α, $m_{\alpha\alpha}$, $m_{\dot{\alpha}}$ and $m_{\delta e}$ are dimensional coefficients. The linear and non-linear "moments" $m_\alpha\alpha$ and $m_\alpha\alpha + m_{\alpha\alpha}\alpha^2$ are sketched on Figure 3-2, for $m_\alpha = -10$ and $m_{\alpha\alpha} = 1.8$. In this example $m_{\dot{\alpha}}$ and $m_{\delta e}$ are also taken respectively equal to -0.25 and -30. Since $m_{\alpha\alpha}$ is much smaller than m_α, the linear and non-linear moments remain close to each other, but this slight difference is going to induce radical changes in the equilibrium of the model. The new equation of motion 3.5 is a second order equation

which can be rewritten as a first order system with two variables by letting $x_1 = \alpha$ and $x_2 = \dot{\alpha}$. Then, equation 3.5 becomes

$$\begin{aligned} \dot{x_1} &= x_2 \\ \dot{x_2} &= m_\alpha x_1 + m_{\alpha\alpha} x_1^2 + m_{\dot{\alpha}} x_2 + m_{\delta e} \delta e. \end{aligned} \tag{3.6}$$

3.2.2 Equilibrium points

In the linear case ($m_{\alpha\alpha} = 0$), there is a unique equilibrium point, regardless of the value of the elevator deflection. This equilibrium point is characterized by

$$\bar{x_1^{lin}} = -\frac{m_{\delta e}}{m_\alpha} \delta e, \bar{x_2^{lin}} = 0. \tag{3.7}$$

The Jacobian matrix associated with this linear case is

$$Df^{lin} = \begin{bmatrix} 0 & 1 \\ m_\alpha & m_{\dot{\alpha}} \end{bmatrix} \tag{3.8}$$

The characteristic polynomial of this matrix is

$$\lambda^2 - m_{\dot{\alpha}} \lambda - m_\alpha = 0. \tag{3.9}$$

The sum of the two eigenvalues is $m_{\dot{\alpha}}$ and their product is $-m_\alpha$. As $m_{\dot{\alpha}}$ and m_α are both negative, the two eigenvalues are also both negative and the equilibrium point is a stable node.

In the nonlinear case, there are one, two or no equilibrium points, which is the first significant difference with the linear case: beyond a certain value of the elevator deflection, there are no more equilibrium points. This lower value of δe is given by the discriminant of

$$m_\alpha x_1 + m_{\alpha\alpha} x_1^2 + m_{\delta e} \delta e = 0 \tag{3.10}$$

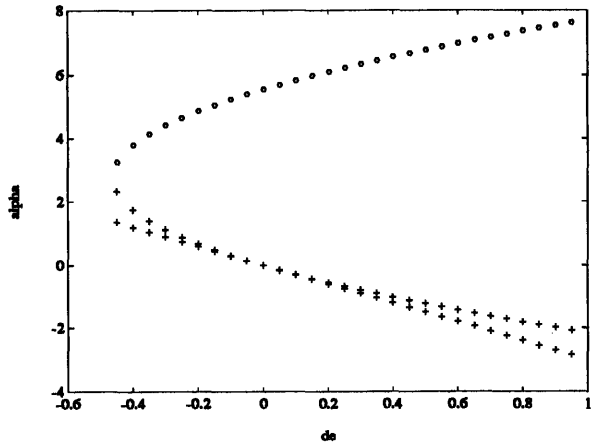

Figure 3-3: Bifurcation diagram for the airplane model. Equilibria marked with 'o' are unstable.

becoming zero i.e. for the value

$$\delta e = \delta e_{bif} = \frac{m_\alpha^2}{4 m_{\alpha\alpha} m_{\delta e}}. \tag{3.11}$$

At this point,

$$x_1 = x_{1bif} = -\frac{m_\alpha^2}{2 m_{\alpha\alpha}} \tag{3.12}$$

and the point $(x_{1bif}, x_2 = 0, \delta e_{bif})$ is a bifurcation point. The upper branch of equilibria is unstable, the lower branch is stable and tangent to the equilibrium curve of the linear case. The bifurcation diagram is sketched on Figure 3-3.

The main purpose of this example was to show how even a slight nonlinear perturbation of an aerodynamic moment can modify the nature of the behavior of an airplane. As a matter of fact, one can see on Figure 3-3 that the stable equilibrium points in the linear and nonlinear cases remain close from each other when they both exist and that the disappearance of the nonlinear equilibrium point is very sudden.

3.3 Longitudinal dynamics of a fighter

3.3.1 General equations

In this section, a system of five coupled ordinary differential equations is examined. These equations are representative of an airplane flying at a constant speed and where the gravity terms have been neglected. The original set of the equations of motion can be written, in the principal axis of the rigid airplane, as

$$\begin{aligned}
(W/g)(\dot{u} - rv + qw) &= X + T - W\sin\theta, \\
(W/g)(\dot{v} - pw + ru) &= Y + W\sin\phi\cos\theta, \\
(W/g)(\dot{w} + pv - qu) &= Z + W\cos\phi\cos\theta, \\
I_x\dot{p} + (I_z - I_y)qr &= \mathcal{L}, \\
I_y\dot{q} - (I_z - I_x)rp &= \mathcal{M}, \\
I_z\dot{r} + (I_y - I_x)pq &= \mathcal{N}, \\
\dot{\theta} &= q\cos\phi - r\sin\phi, \\
\dot{\phi} &= p + q\sin\phi\tan\theta + r\cos\phi\tan\theta, \\
\dot{\psi} &= q\sin\phi\sec\theta + r\cos\phi\sec\theta.
\end{aligned} \tag{3.13}$$

In this system, X, Y, Z, $\mathcal{L}$, $\mathcal{M}$ and $\mathcal{N}$ denote the aerodynamic forces and moments, T the thrust and W the weight of the airplane. Velocities and angular velocities are explicited on Figure 3-4. In the system 3.13, the first three equations are the force equations. Then come the three equations of angular momentum. The last three equations are geometric relationships between the various angles and angular velocities. From this complete set of equations (9 variables), a simplified set can be derived, where the following approximations are done: $u \simeq V$, $\beta \simeq v/V$, $\alpha \simeq w/V$ and V is a constant, an assumption whose effect is to remove the first force equation. The simplified set of equations is thus

$$\dot{\beta} = p\alpha - r + y + (g/V)\sin\phi\cos\theta,$$

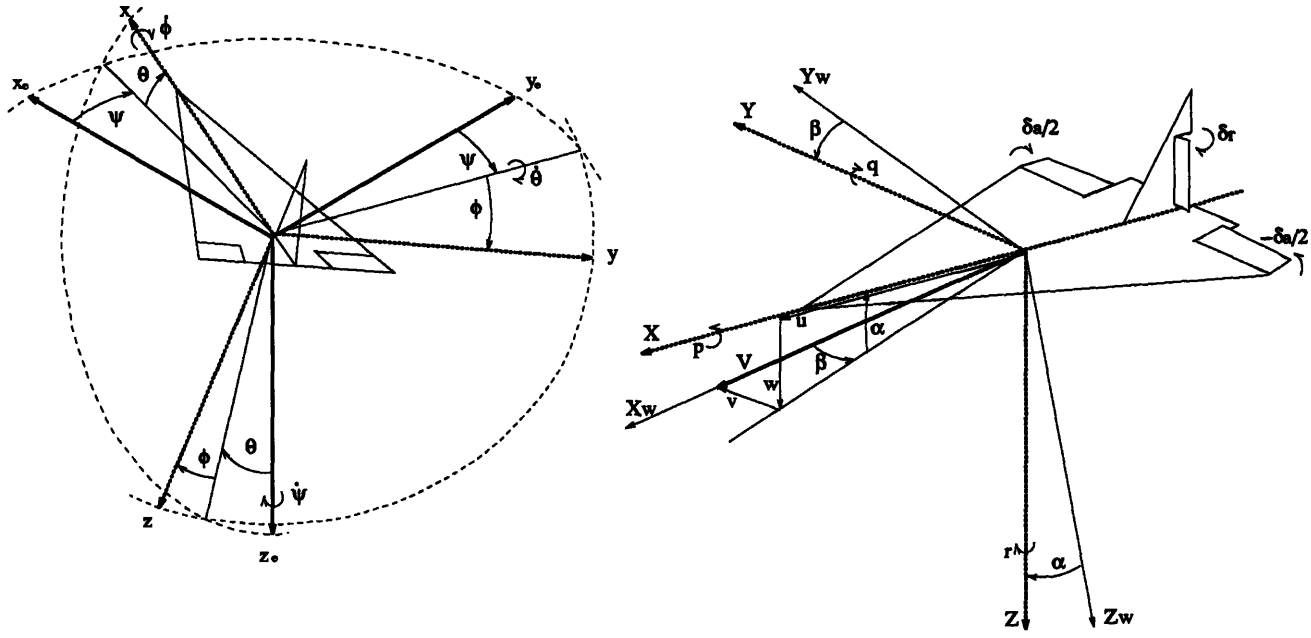

Figure 3-4: Orientations of earth (Xe, Ye, Ze), body (X, Y, Z) and wind (Xw, Yw, Zw) axes, linear and angular velocities and control deflections (the elevator deflection does not appear on this Figure: δe is positive when the trailing edge of the elevator is down)

$$
\begin{aligned}
\dot{\alpha} &= -p\beta + q + z + (g/V)\cos\phi\sin\theta, \\
\dot{q} &= i_2 rp + m, \\
\dot{r} &= -i_3 pq + n, \\
\dot{p} &= -i_1 qr + l, \\
\dot{\phi} &= p + q\sin\phi\tan\theta + r\cos\phi\tan\theta, \\
\dot{\theta} &= q\cos\phi - r\sin\phi,
\end{aligned}
\tag{3.14}
$$

where $i_1 = (I_z - I_y)/I_x$, $i_2 = (I_z - I_x)/I_y$, $i_3 = (I_y - I_x)/I_z$, $y = Y(g/WV)$, $z = Z(g/WV)$, $l = \mathcal{L}/I_x$, $m = \mathcal{M}/I_y$, $n = \mathcal{N}/I_z$. Substituting the values of the aerodynamic moments and forces yields

$$
\begin{aligned}
\dot{\beta} &= y_\beta\beta + p\alpha - r + (g/V)\sin\phi\cos\theta, \\
\dot{\alpha} &= z_\alpha\alpha - p\beta + q + (g/V)\cos\phi\sin\theta, \\
\dot{q} &= i_2 rp + \bar{m}_\alpha\alpha + \bar{m}_q q - m_{\dot{\alpha}} p\beta + (g/V)m_{\dot{\alpha}}\cos\phi\cos\theta + m_{\delta_e}\delta_e,
\end{aligned}
$$

$$
\begin{aligned}
\dot{r} &= -i_3 pq + n_\beta \beta + n_p p + n_r r + n_{\delta_a}\delta_a + n_{\delta_r}\delta_r, \\
\dot{p} &= -i_1 qr + l_\beta \beta + l_p p + l_r r + l_{r\alpha} r\alpha + l_q q + l_{\delta_a}\delta_a + l_{\delta_r}\delta_r, \\
\dot{\phi} &= p + q\sin\phi\tan\theta + r\cos\phi\tan\theta, \\
\dot{\theta} &= q\cos\phi - r\sin\phi,
\end{aligned}
\tag{3.15}
$$

where $\bar{m}_\alpha = m_\alpha + m_{\dot{\alpha}} z_\alpha$ and $\bar{m}_q = m_q + m_{\dot{\alpha}}$. The variables δ_a, δ_e and δ_r represent the ailerons, the elevator and the rudder deflections. Furthermore, in the expression of m, $\dot{\alpha}$ was replaced by the right-hand side of the second equation of system 3.14. Up to this stage, one can notice that a single aerodynamic non-linearity was introduced, namely the term $l_{r\alpha} r\alpha$ in the equation for $\dot{p}$, which represents a dependance of l_r with α. Nevertheless, the system 3.15 remains too complicated for an analysis based on simple computations and is used only for simulations. One can come up with a simpler set of equations by neglecting all the g/V terms, which is common practice because it decouples the first five equations from the last two, by neglecting a few aerodynamic forces and moments ($n_p p$ and $l_q q$), which are usually small, by neglecting the inertial term $i_1 qr$ and by setting δ_a and δ_r to be zero. These simplifications yield the following system:

$$
\begin{aligned}
\dot{\beta} &= y_\beta \beta + p\alpha - r, \\
\dot{\alpha} &= z_\alpha \alpha - p\beta + q, \\
\dot{q} &= i_2 rp + \bar{m}_\alpha \alpha + \bar{m}_q q - m_{\dot{\alpha}} p\beta + m_{\delta_e}\delta_e, \\
\dot{r} &= -i_3 pq + n_\beta \beta + n_r r, \\
\dot{p} &= l_\beta \beta + l_p p + l_r r + l_{r\alpha} r\alpha.
\end{aligned}
\tag{3.16}
$$

Before going to further computations, one must be aware of the validity domains and limitations of both systems 3.15 and 3.16. The system 3.15 is linearized with respect to α and β and, thus, cannot be expected to fully represent an airplane flying at high-angle of attack. Nevertheless, due to the introduction of nonlinear aerodynamics coefficients, this system has been seen to exhibit a great deal of phenomena

specific to nonlinear sytems. As noted before, the system 3.15 is still too complicated to be handled easily and the stability has sytematically been studied on the simplified system 3.16. Since all the nonlinearities of system 3.16 are in the form of polynomials, this system can be handled easily by a software package like *Matlab*, which specializes in polynomial processing. To be aware of the complexity of computations involving fully nonlinear equations with aerodynamic data coming from the wind tunnel, one is referred to the publications cited in the introduction of this thesis and especially to [17]. When done, simulations and time histories are made on both systems.

3.3.2 Equilibrium points

Although system 3.16 seems to be intricate, its equilibrium points can be found. From the first two equations, one can isolate q and r in terms of α and β. Substituting q and r in the following two equations yields a two equations system, linear in α and β and whose coefficients depends on the roll-rate p. Solving this system, one can come up with the expressions of α and β and, consequently, of q and r in term of p. Substituting these expressions in the last equation of system 3.16 yield a ninth order polynomial in p. Then *Matlab* is apt to solve for p, for different values of the parameter δe. For each real equilibrium roll-rate p_0, the whole equilibrium state vector $(\alpha_0, \beta_0, p_0, q_0, r_0)$ is computed. Then, the Jacobian matrix

$$Df = \begin{bmatrix} y_\beta & p & 0 & -1 & \alpha \\ -p & z_\alpha & 1 & 0 & -\beta \\ -m_{\dot{\alpha}}p & \bar{m}_\alpha & \bar{m}_q & i_2 p & i_2 r - m_{\dot{\alpha}}\beta \\ n_\beta & 0 & -i_3 p & n_r & -i_3 q \\ l_\beta & l_{r\alpha} r & 0 & l_r + l_{r\alpha}\alpha & l_p \end{bmatrix} \tag{3.17}$$

associated with the system 3.16 is evaluated, from which the stability of each equilibrium point can be determined. The *Matlab* routine associated with these computations is given in appendix A.

Two cases have be examined, which correspond to two different flight conditions,

namely for $M = 0.9, h = 20.000ft$ (Conditions I) and $M = 0.7, h = 0$ (Conditions II) for an hypothetical swept-wing fighter. The data used in this study are summarized in table 3.1 and are extracted from [26, p. 168].

Beside purely numerical investigations, some analytical computations can be done by hand in order to support numerical results. The stability of the basic solution $p = r = \beta = 0$, which always exists in the symetric case ($\delta a = \delta r = 0$) since the ninth order polynomial from which p is computed has no constant term, can be investigated this way.

It is recalled here that a bifurcation of equilibrium occur when the Jacobian matrix has one real eigenvalue going through zero or a pair of complex eigenvalues becoming purely imaginary. Since the determinant of a matrix is the product of its eigenvalues, another criterion to detect the occurence of a real eigenvalue becoming zero is that the determinant of the Jacobian matrix goes to zero itself. Thus, setting $p = r = \beta = 0$, one can write the determinant of the Jacobian matrix of the system 3.16 as

$$\det Df = \begin{vmatrix} y_\beta & 0 & 0 & -1 & \alpha \\ 0 & z_\alpha & 1 & 0 & 0 \\ 0 & \bar{m}_\alpha & \bar{m}_q & 0 & 0 \\ n_\beta & 0 & 0 & n_r & -i_3 q \\ l_\beta & 0 & 0 & l_r + l_{r\alpha}\alpha & l_p \end{vmatrix} \tag{3.18}$$

On the other hand, from the second and third equation of system 3.16, α and q can be written as

$$\alpha = -\frac{m_{\delta e}\delta e}{\bar{m}_\alpha - \bar{m}_q z_\alpha} = \alpha_{\delta e}\delta e \tag{3.19}$$

and

$$q = -\frac{m_{\delta e} z_\alpha \delta e}{\bar{m}_\alpha - \bar{m}_q z_\alpha} = q_{\delta e}\delta e. \tag{3.20}$$

Numerically, for flight conditions II, $\alpha_{\delta e} = -2.4836$ and $q_{\delta e} = -4.3364$. Using the usual rules for computing determinants, one can derive that the determinant of the Jacobian matrix is zero if and only if the following second order polynomial in δe is

	Condition I	Condition II		Condition I	Condition II
i_2	0.949	0.949	i_3	0.716	0.716
y_β	-0.196	-0.280	z_α	-1.329	-1.746
l_β	-9.990	-20.910	l_p	-3.933	-5.786
l_r	0.126	0.221	$l_{r\alpha}$	8.390	13.160
m_α	-23.18	-10.7	$m_{\dot{\alpha}}$	-0.173	-0.251
m_q	-0.814	-1.168	$m_{\delta e}$	-28.37	-31.64
n_β	5.67	8.88	n_r	-0.235	-0.377
$l_{\delta a}$	-45.83	-60.27	$l_{\delta r}$	7.64	10.05
$n_{\delta a}$	-0.921	-1.282	$n_{\delta r}$	-6.51	-8.30

Table 3.1: Aerodynamic coefficients

zero:

$$(y_\beta i_3 l_{r\alpha}\alpha_{\delta e}q_{\delta e} - n_\beta l_{r\alpha}\alpha_{\delta e}^2)\delta e^2 + (y_\beta l_r i_3 q_{\delta e} - i_3 l_\beta q_{\delta e} - n_\beta l_r \alpha_{\delta e} + n_r l_\beta \alpha_{\delta e})\delta e + (y_\beta n_r l_p - n_\beta l_p) = 0. \tag{3.21}$$

Numerically, still for flight conditions II, this polynomial becomes

$$-749.2432\delta e^2 - 79.4349\delta e + 50.7689 = 0, \tag{3.22}$$

whose roots are $\delta e = -0.3187$ rad and $\delta e = 0.2126$ rad. For these values of δe, bifurcations are expected. Since $p = 0$ remains an equilibrium point after the bifurcating point, the bifurcation is either a transcritical or a pitchfork. Since the airplane and the equations have a symmetry, a pitchfork bifurcation is expected. These facts are confirmed by the results of the *Matlab* routine associated with the stability computations, the results of which are now to be given.

3.3.3 Results and interpretation

The real equilibrium values of p are sketched versus the value of the control parameter δe. For each δe, there is a various number of equilibrium roll-rates in addition to the trivial solution $p = 0$. In the first case (flight conditions I), this equilibrium diagram is sketched on Figure 3-5, for values of δe between -0.5 rad and 0.3 rad. On this figure,

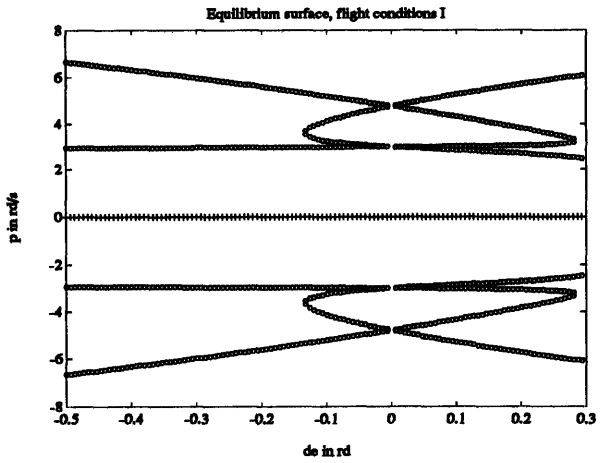

Figure 3-5: Equilibrium diagram for flight conditions I. Equilibria marked with 'o' are unstable.

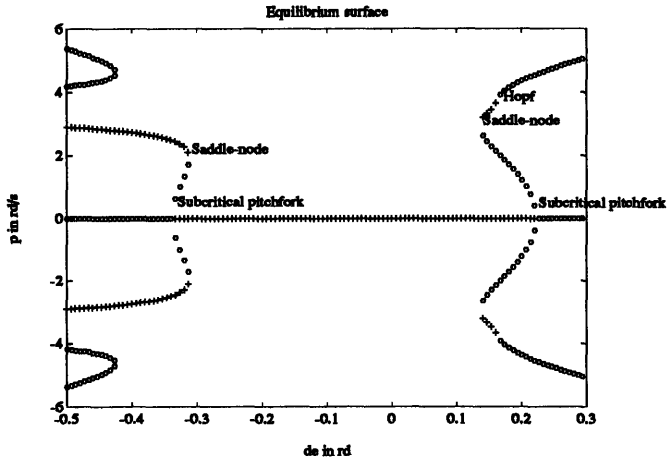

Figure 3-6: Equilibrium diagram for flight conditions II. Equilibria marked with 'o' are unstable.

one can see that the behavior of the aircraft is very sound: only the trivial solution is stable and the other branches are unstable. Thus, the airplane cannot jump from the trivial solution to an attractive solution characterized by high roll-rate, sideslip and angle of attack.

In the second case (flight conditions II), the equilibrium diagram, represented on Figure 3-6, is much more complicated and peculiar behavior of the airplane is expected when the elevator deflection varies from -0.5 rad (nose up) up to 0.3 rad (nose down).

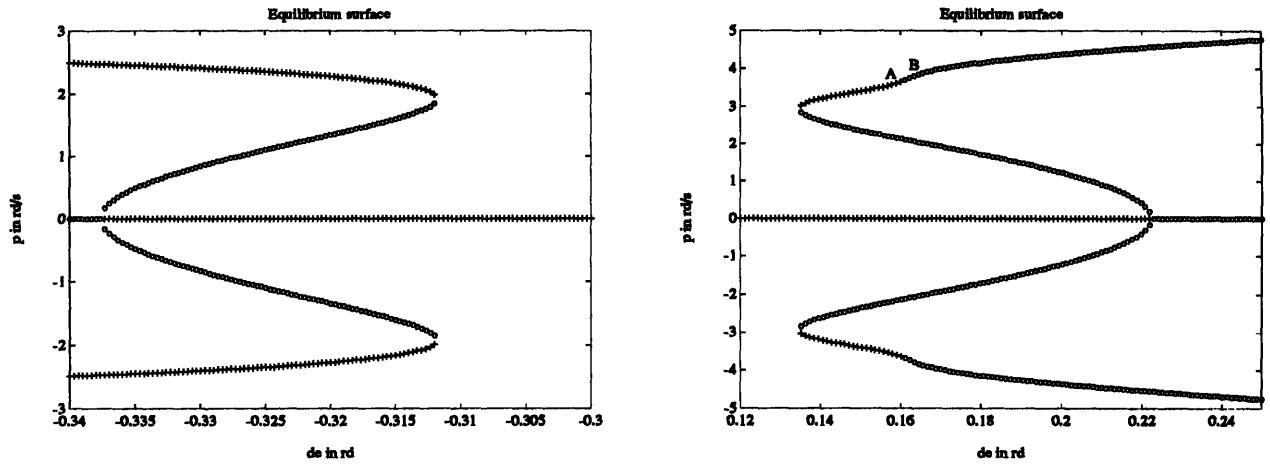

Figure 3-7: Enlargements of the equilibrium surface for negative δe (left) and positive δe

High positive values of the elevator deflection

At the right hand side of the equilibrium diagram, one can reckon three kinds of bifurcations. An enlargement of this area is given on the right hand side of Figure 3-7. First, one can see on this figure that the basic solution $p = 0$ becomes unstable for a value of δe of approximately 0.22 rad. This is the value predicted by the algebra done in the previous paragraph, which consisted in computing the value of δe at which the determinant of the stability matrix turned into zero. The shape of the equilibrium branches bifurcating from $(p = 0, \delta e \simeq 0.22)$ also confirms that the bifurcation is a subcritical pitchfork bifurcation.

The eigenvalues of the stability matrix corresponding to the trivial solution $p = 0$ are sketched on the left hand side of Figure 3-8. One can see that there is actually a real eigenvalue crossing the imaginary axis and becoming positive.

Coming back to Figure 3-7 (right), one can detect another type of bifurcation, namely a saddle-node bifurcation or rather two saddle-node bifurcations, since the equilibrium diagram is symmetrical with respect to $p = 0$. Each of these saddle-node bifurcations gives raise to two new branches of equilibria, a stable and an unstable one.

Then, each new stable branch turns itself into an unstable branch. The analysis of the eigenvalues of the stability matrix for these branches is provided on the right hand side of Figure 3-8 and shows that a pair of complex eigenvalues crosses the

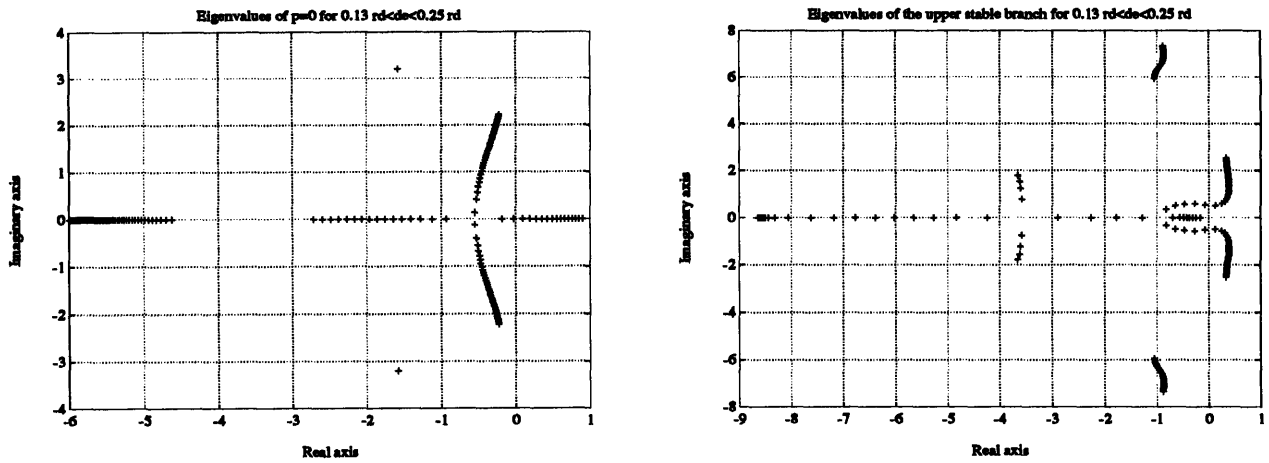

Figure 3-8: Eigenvalues of the stabilty matrix for 0.13 rad $< \delta e <$ 0.25 rad, corresponding to the trivial solution $p = 0$ (left) and to the stable branch of the saddle-node bifurcation (right)

imaginary axis. Thus a Hopf bifurcation occurs and limit cycles can be expected.

The power of these equilibrium diagrams lies in the fact that one can anticipate the behavior of the airplane merely on their basis. Thus, for values of δe less than 0.14 rad (occurrence of the saddle-node bifurcation), the trivial solution $p = 0$ can be predicted to be globally stable: regardless of the initial conditions, the airplane is attracted towards this trivial solution.

For values of δe between 0.14 rad and 0.16 rad (occurrence of the Hopf bifurcation), three different stable equilibria may occur: the trivial solution $p = 0$ and the highly hazardous solutions lying on the stable branches of the two saddle-node bifurcations. The unstable branches of the saddle-node bifurcations separates the attraction domains of the three stable equilibria.

For values of δe between 0.16 rad and 0.22 rad (occurrence of the pitchfork bifurcation), the airplane can now be attracted either towards the stable trivial solution either towards a stable limit cycle. The unstable branch of the saddle-node bifurcations still separates the respective domains of attraction.

Eventually, for values of δe greater than 0.22 rad, the basic solution is not stable and the airplane is now always attracted towards a limit cycle.

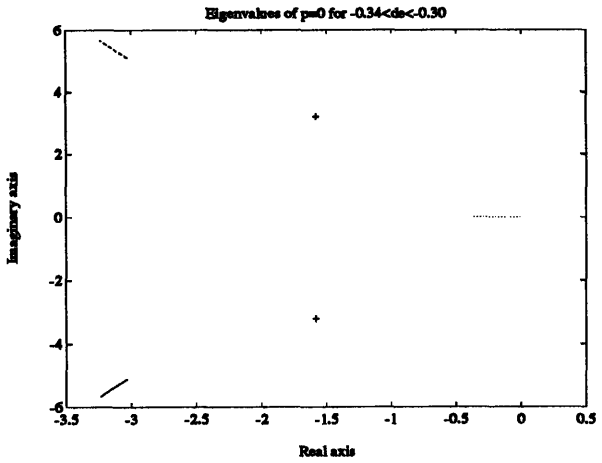

Figure 3-9: Eigenvalues of the stabilty matrix for -0.34 rad $< \delta e <$ -0.30 rad, corresponding to the trivial solution $p = 0$

High negative values of δe

The other side of the equilibrium diagram presented on Figure 3-6 has also been enlarged on the left hand side of Figure 3-7 and similarly shows bifurcation phenomena. First, another subcritical pitchfork bifurcation occurs for a value of δe of approximately -0.33 rad, as predicted by the previous computation of the zeros of the stability matrix determinant. On Figure 3-9, a diagram of the eigenvalues of the stability matrix for $p = 0$ in the neighborhood of $\delta e = -0.33$ rad reveals that a real eigenvalue crosses the imaginary axis. Thus the stability of the basic solution $p = 0$ is compromised at both ends of the possible range of the elevator deflection δe.

Furthermore, a pair of saddle-node bifurcations also occurs in this case, whose stable branches do not undergo Hopf bifurcation, unlike in the previous case. Thus, the airplane is likely to experience another class of phenomena, namely the autorotationnal rolling: for values of δe less than -0.33 rad, the airplane diverges from the basic solution $p = 0$ and jumps to a stable equilibrium characterised by high values of the angles of attack and sideslip. These high values of the state vector are responsible for excessive loads on the structure and can cause the loss of the airplane. This phenomenon is analog to the cross-coupling phenomenon, which was extensively studied in the fifties and sixties [3, 5, 4, 7, 6] and more recently in [18, 19, 20, 15].

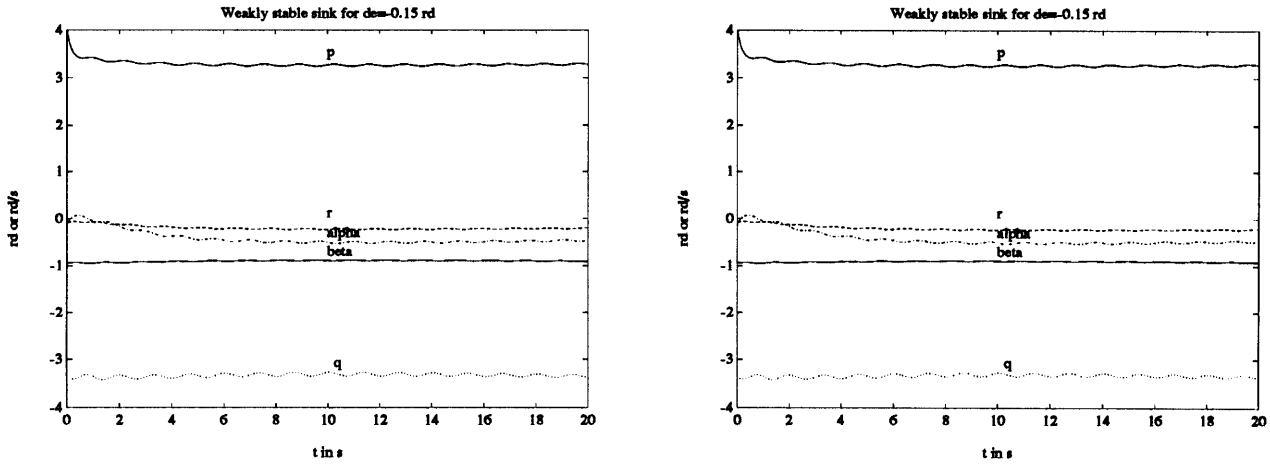

Figure 3-10: Simulation just before the Hopf bifurcation on simplified system 3.16 (left) and original system 3.15

Simulations

Some simulations have been done, which illustrate the behavior of the airplane for different values of δe. Each has been made both on the complete system 3.15 and on the simplified system 3.16. The purpose of this is to show that the bifurcation analysis made on the simplified system 3.16 remains qualitatively valid for the more realistic system 3.15. The main difference between the two systems is that the complete system 3.15 does not have real equilibrium states, such that all the time derivatives of the state vector are zero. This is due to the presence in the equations of gravity terms, which oscillate with θ. Thus, the equilibrium states of the system 3.16 are slightly perturbated in the case of the system 3.15.

First, the behavior of the airplane about the Hopf bifurcation has been simulated. From an equilibrium point corresponding to point A on Figure 3-7, which is located just before the Hopf bifurcation, the value of the roll-rate p has been perturbated. The value of δe corresponding to this simulation is 0.16 for system 3.16 and 0.15 for system 3.15. One can see on the simulations displayed on Figure 3-10 that the point A is actually stable and that the two sytems have qualitatively the same behavior. Then, another simulation was done at point B on Figure 3-7, which is located just after the Hopf bifurcation. It can now be seen on Figure 3-11 that the system undergoes a very sudden limit cycle, altough the elevator deflection has just gone from 0.16 rad up to 0.165 rad in the case of system 3.16 and from 0.15 rad up to 0.16 rad in the case of

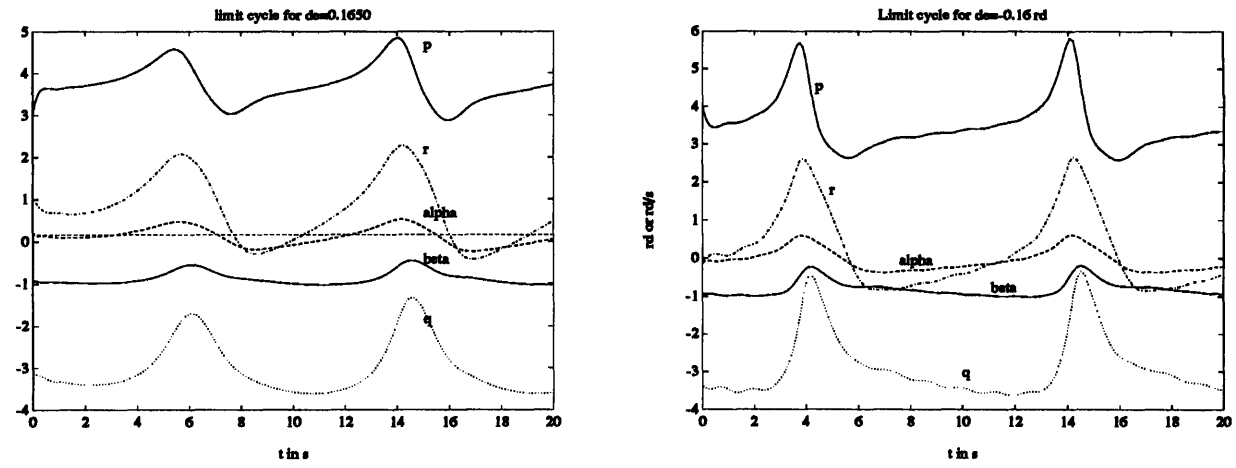

Figure 3-11: Simulation just beyond the Hopf bifurcation on simplified system 3.16 (left) and original system 3.15

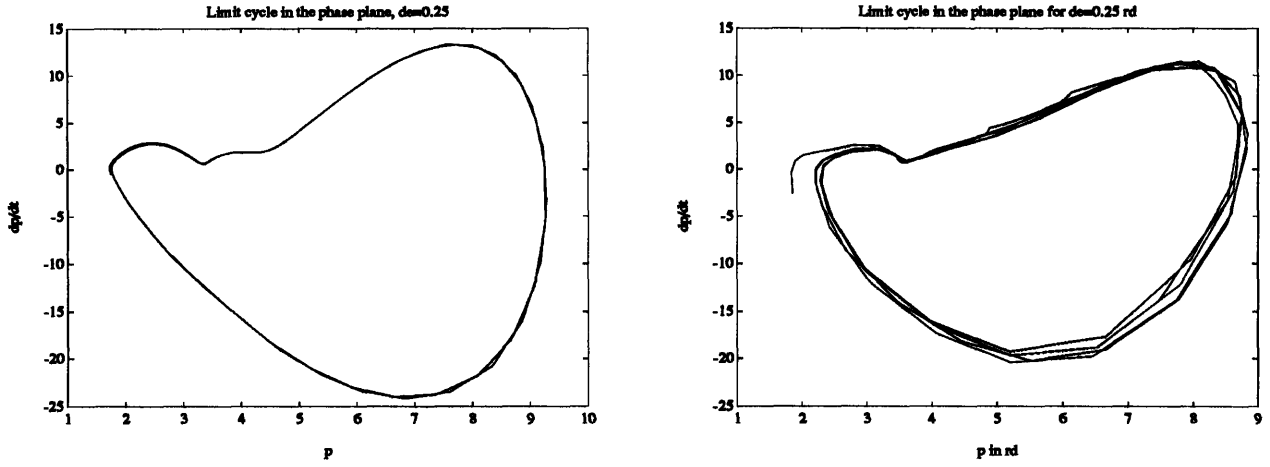

Figure 3-12: Shape of the limit cycle for $\delta e = 0.25$ for simplified system 3.16 (left) and original system 3.15

system 3.15.

The shape of the limit cycle in the phase plane $(p, \dot{p})$ is sketched on Figure 3-12. A clean closed curve appears in the case of the simplified system 3.16, and a more perturbed one appears in the case of system 3.15.

To conclude with simulations done at positive values of the elevator deflection, two more simulations have been done, showing the dependence of the behavior of the airplane on the initial conditions. For a same value of $\delta e = 0.20$ but for two different initial conditions on p, simulations show that the aircraft can be attracted either towards the stable trivial solution either towards the stable limit cycle. These two simulations are displayed on Figures 3-13 and 3-14. Once more, the qualitative

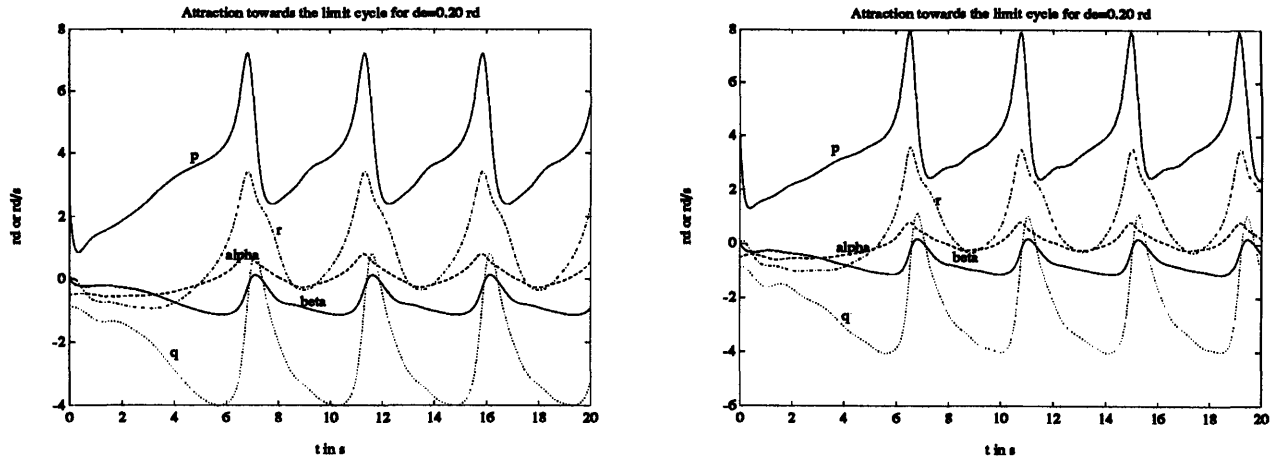

Figure 3-13: Attraction towards the limit cycle for $\delta e = 0.20$. $p_{ini} = 2.5$ rad/s in the case of system 3.16 and $p_{ini} = 4$ rad/s in the case of system 3.15

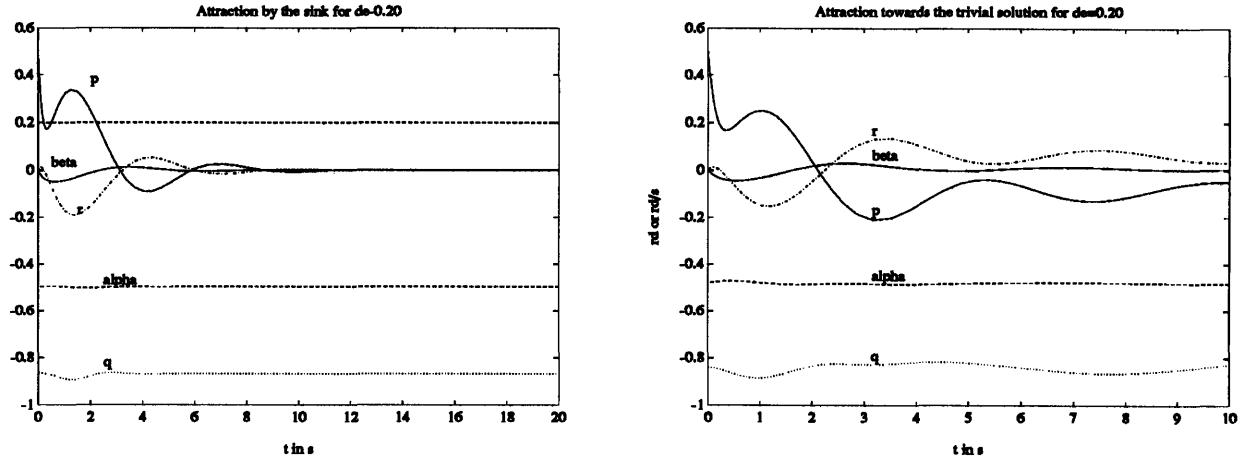

Figure 3-14: Attraction towards the trivial solution for $\delta e = 0.20$. $p_{ini} = 0.5$ rad/s in both cases

behavior of the two systems appears to be very similar.

Eventually, two simulations have been done in the case of negative values of the ailerons deflection, which show the phenomenon of auto-rotationnal rolling. The results appear on Figure 3-16 and have been obtained for a value of δe linearly varying from 0 to -0.4 rad. The principle of this simulation is to apply a small perturbation on the unstable equilibrium state ($p = 0$) that exists for δe = -0.40 rad. This perturbation is applied on the variable p ($p = 0.1$ rad at t = 5s) and causes the airplane to jump to high stable values of the state vector, as predicted by the equilibrium diagrams. The results are qualitatively similar in the two simulations, one being done with the simplified system 3.16 and the other with the more complex system 3.15.

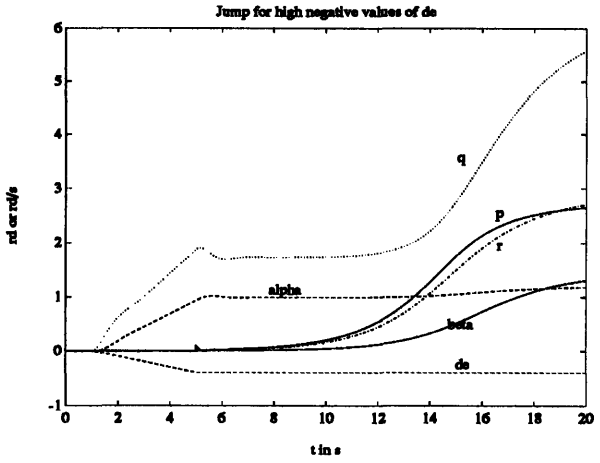

Figure 3-15: Left: jump to high values of the state vector. The simplified system 3.16 is used for the simulation

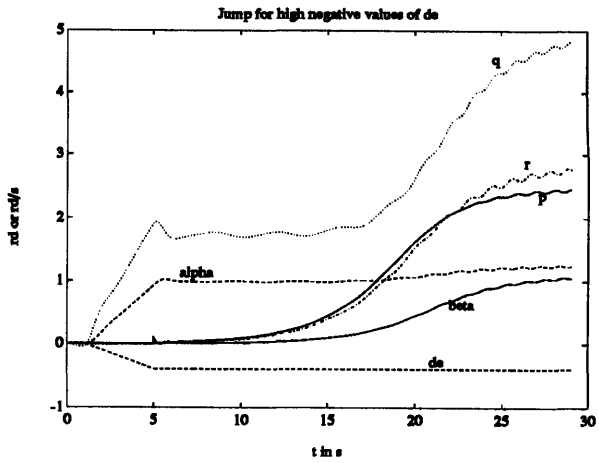

Figure 3-16: Right: jump to high values of the state vector. The complex system 3.15 is used for the simulation

3.4 Lateral dynamics of a fighter

The stability analysis developed in the previous section is now to be applied to the analysis of the equilibrium states obtained when the pilot moves the lateral control surfaces, namely the ailerons and the rudder. Because of the combination of the three control surfaces, a large variety of phenomena can be expected, including some interesting new combinations of bifurcations.

The sign of the control surfaces deflections is denoted on Figure 3-4. By convention, a positive ailerons deflection δa is caused by a stick going to the left and corresponds to a right aileron going down. A positive rudder deflection δr is caused by putting the foot to the left and corresponds to a rudder deflected to the left.

3.4.1 General equations

Both ailerons and rudder deflections have an impact on both yaw and roll rates, r and p. The major effect of an ailerons deflection is indeed on the roll-rate p but a secondary effect is also induced on the yaw-rate r. This is due to the fact that the aileron going down has a smaller drag than the aileron going up. Thus a positive ailerons deflection induces a negative roll-rate (major effect) and a negative yaw-

rate (secondary effect). These effects are expressed respectively by the mean of two coefficients $l_{\delta a}$ and $n_{\delta a}$, which are both negative. The values of these coefficients is given in table 3.1.

The major effect of a rudder deflection is to cause a yaw-rate through a moment with respect to the vertical axis. Neverthless, this moment has also a component with respect to the transversal axis and, thus, causes a roll-rate to appear. A positive rudder deflection (foot to the left) induces a negative yaw-rate and a positive roll-rate. The coefficients responsible for these effects are called $l_{\delta r}$ and $n_{\delta r}$ and are respectively positive and negative. Their values for flight conditions I and II is also given in table 3.1.

Therefore, the set of equations used for the stabilty analysis just results from the addition of the moments caused by the ailerons and rudder deflections to the simplified system 3.16. This new system writes

$$\begin{aligned}
\dot{\beta} &= y_\beta \beta + p\alpha - r, \\
\dot{\alpha} &= z_\alpha \alpha - p\beta + q, \\
\dot{q} &= i_2 rp + \bar{m}_\alpha \alpha + \bar{m}_q q - m_{\dot{\alpha}} p\beta + m_{\delta_e}\delta_e, \\
\dot{r} &= -i_3 pq + n_\beta \beta + n_r r + n_{\delta a}\delta a + n_{\delta r}\delta r, \\
\dot{p} &= l_\beta \beta + l_p p + l_r r + l_{r\alpha} r\alpha + l_{\delta a}\delta a + {}_{\delta r}\ \delta r.
\end{aligned} \tag{3.23}$$

The complete system 3.15, used for simulations, already includes the moments due to δa and δe and, thus, remains valid.

The ninth order polynomial used in the computation of the equilibrium states is different but the stability matrix remains the same since no derivative is taken with respect to the control deflections.

3.4.2 Equilibrium points

In the case of the lateral dynamics, any equilibrium state results from the combination of the three control deflections. Thus, not one but a large number of equilibrium

diagrams have to be plotted in order to account for the multiplicity of the possible situations. In each equilibrium diagram, two controls are set to be constant and the third one varies. In this study, the ailerons deflection is the parameter that varies.

The equilibrium diagrams have been plotted for flight conditions II and for six characteristic values of the elevator deflection, namely -0.35, -0.20, 0, 0.10, 0.15 and +0.30 rad. The values -0.35 rad and +0.30 rad are values of the elevator deflection at which the solution $p = 0$, when both δa and δe are zero, is unstable (cf Figure 3-7). For each of these values of the elevator deflection, the equilibrium diagram have been plotted for six values of the rudder delection, ranging from -0.5 rad up to 0 rad. Symmetrical diagrams could be obtained for positive values of the rudder deflection. This series of six sets of six diagrams is presented on Figures 3-17, 3-18, 3-19, 3-20, 3-21 and 3-22.

Examining these diagrams, one can come up with new classes of phenomena, which are now to be explained in the next subsection.

3.4.3 Interpretation

Equilibrium diagrams for $\delta e = 0$ rad

Figure 3-19 presents equilibrium diagrams for six different values of the rudder deflection. One can see on these various diagrams that the behavior of the airplane is very good for low values of the rudder deflection: the response to an ailerons deflection is quasi linear and there is a unique equilibrium state for a given value of the ailerons deflection.

Then, when the absolute value of the rudder deflection increases, saddle-node bifurcations appear, giving raise to jump phenomena. For example, for δr = -0.30 rad, there is a small jump when δa moves around 0.30 rad. A simulation illustrates this jump on Figure 3-23. The two parts of the Figure are representative of simulations done on the complete system 3.15 and on the simplified system 3.23. The results are totally similar in both cases. The simulations show the effect of slowly and linearly increasing the ailerons deflection from 0 up to 0.6 rad. The response of the airplane is

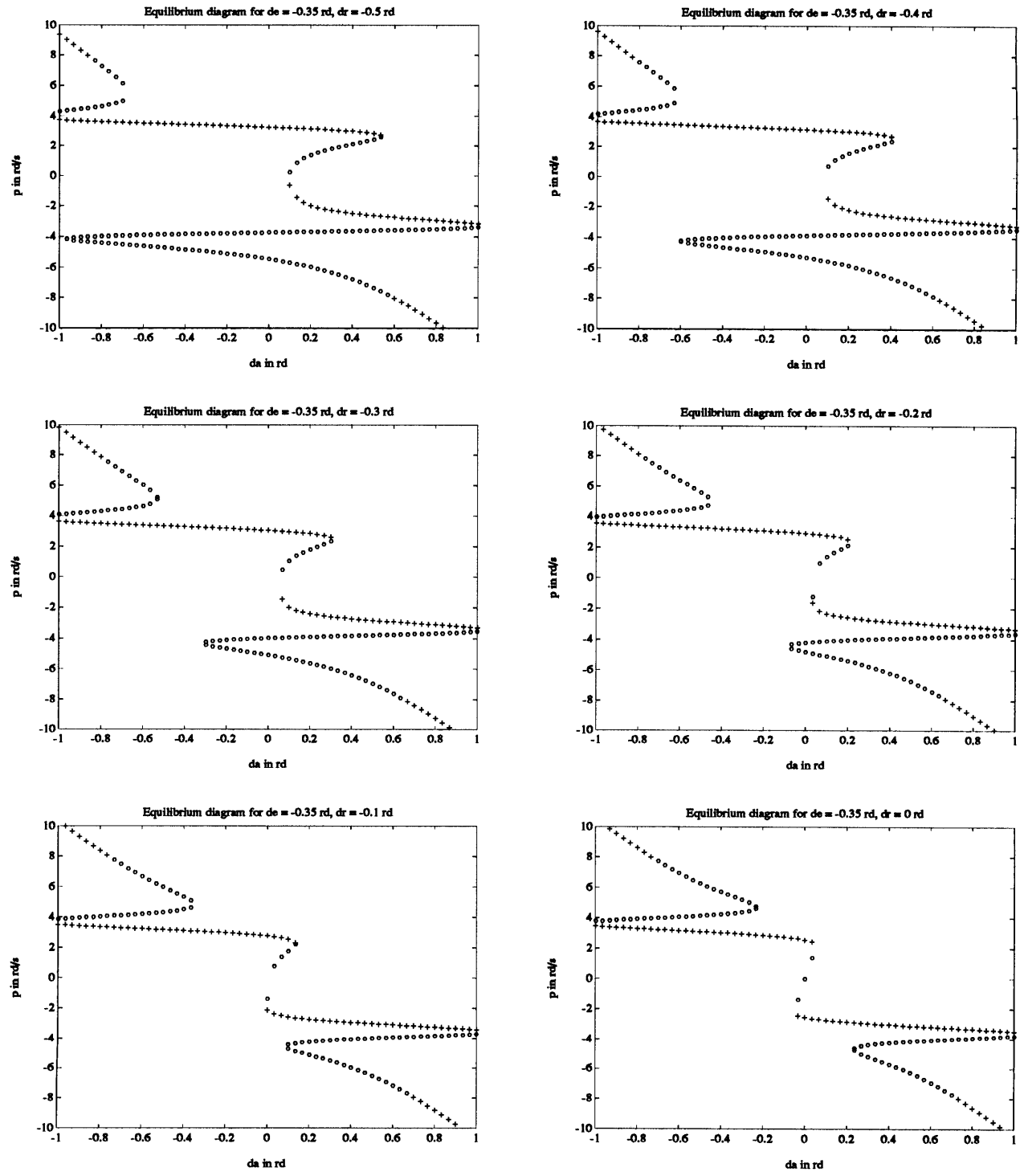

Figure 3-17: Equilibrium diagrams for δe = -0.35 rad. The 'o' points are unstable.

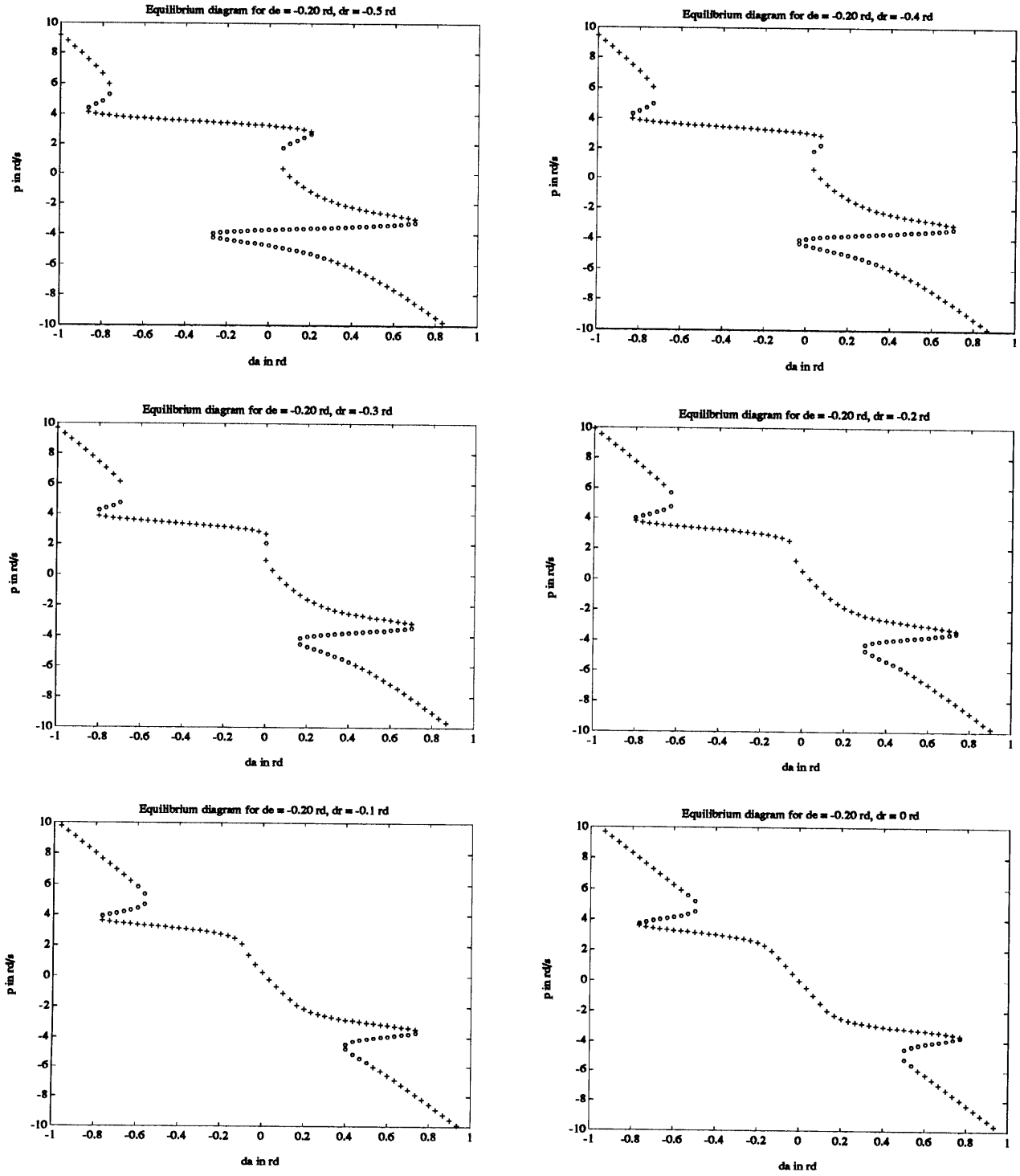

Figure 3-18: Equilibrium diagrams for δe = -0.2 rad. The 'o' points are unstable.

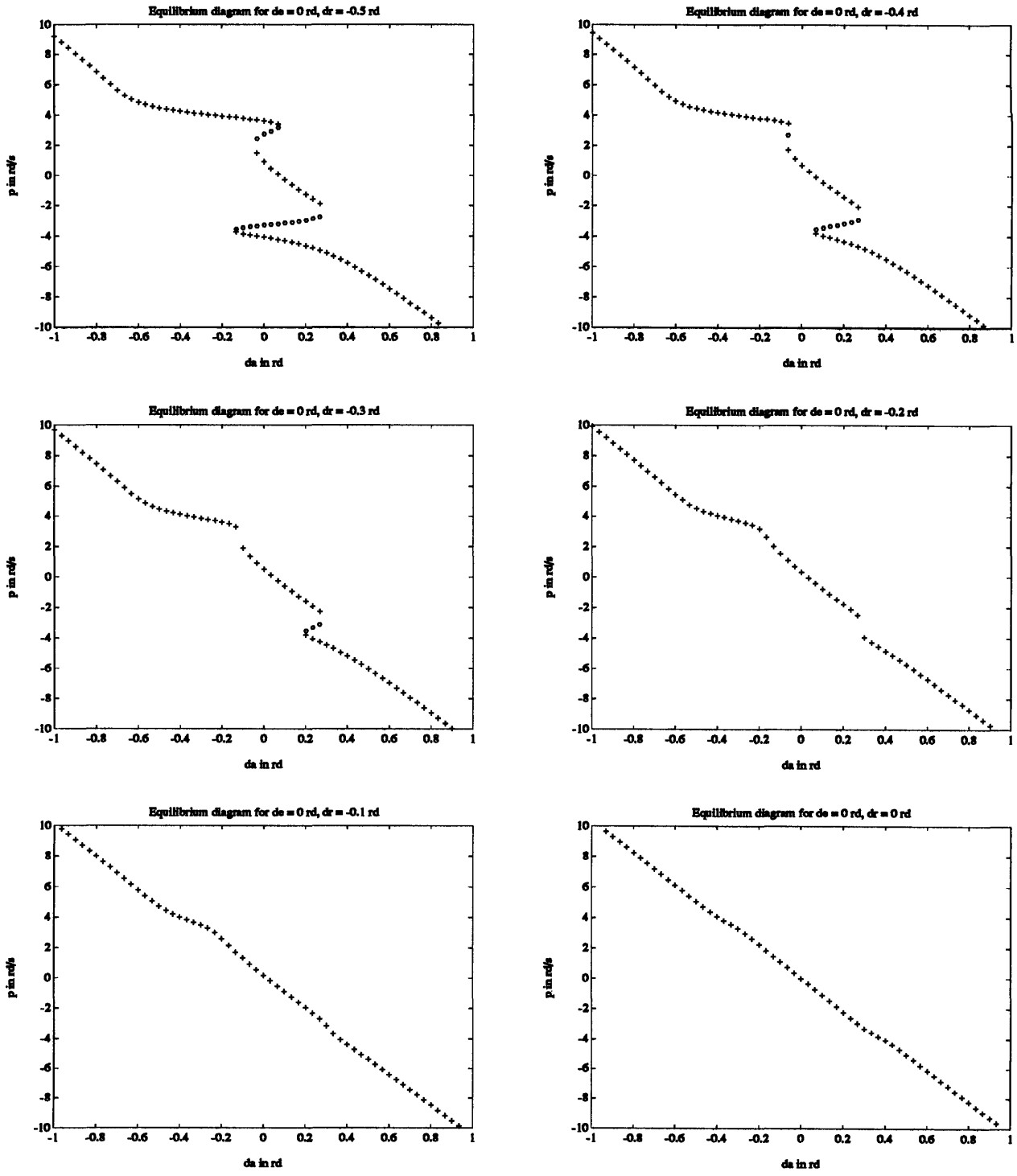

Figure 3-19: Equilibrium diagrams for $\delta e = 0$ rad. The 'o' points are unstable.

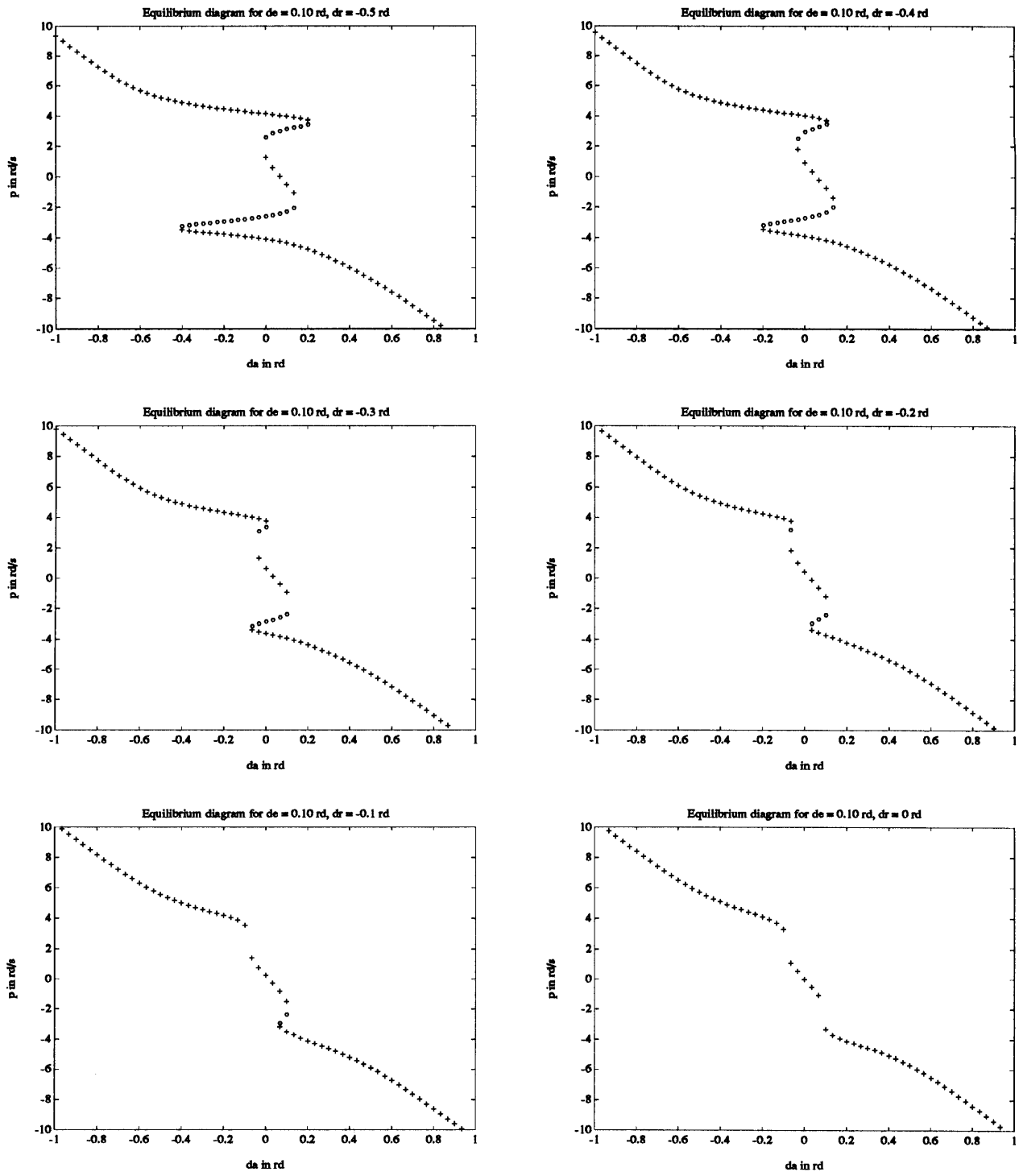

Figure 3-20: Equilibrium diagrams for $\delta e = 0.10$ rad. The 'o' points are unstable.

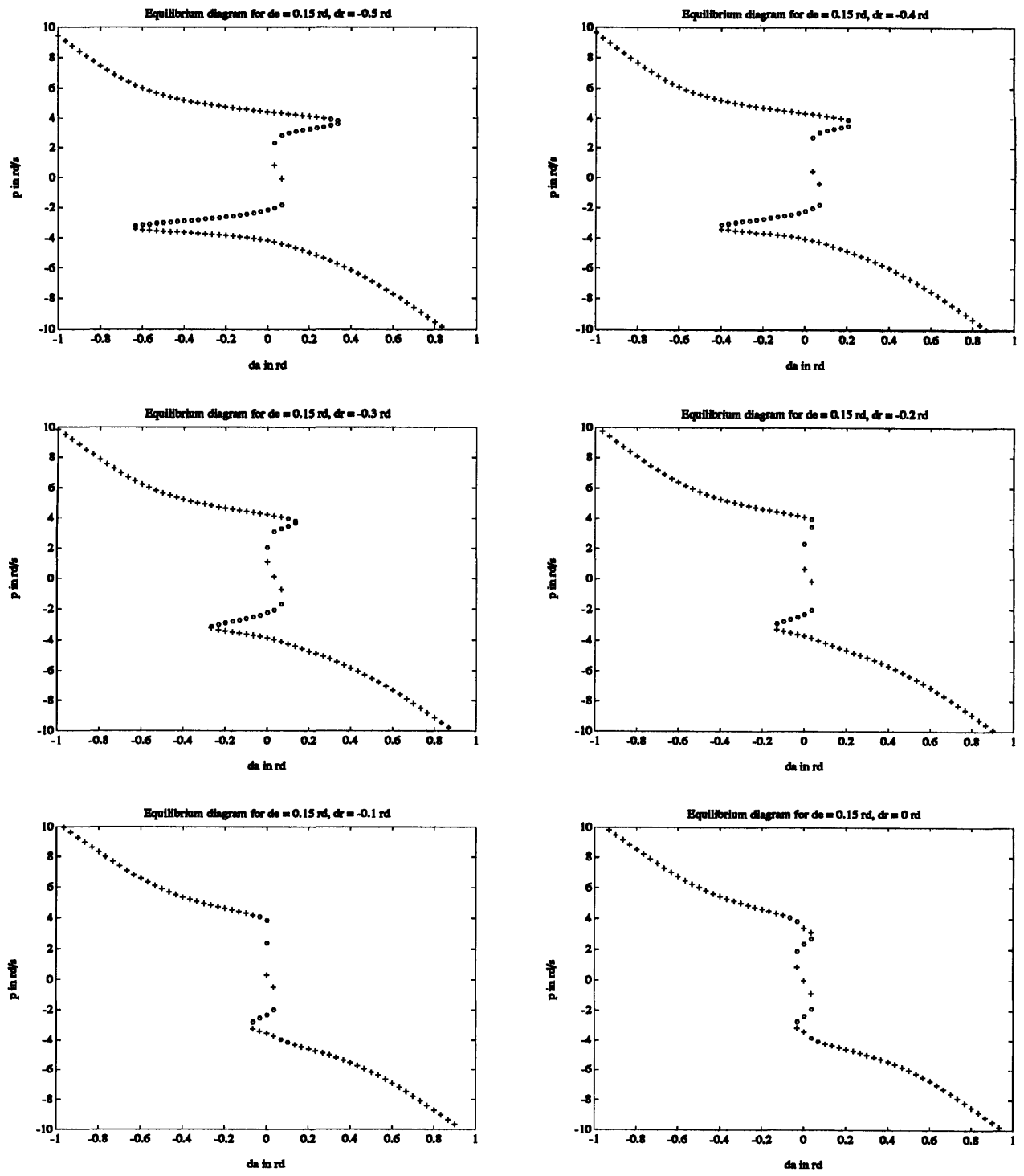

Figure 3-21: Equilibrium diagrams for $\delta e = 0.15$ rad. The 'o' points are unstable.

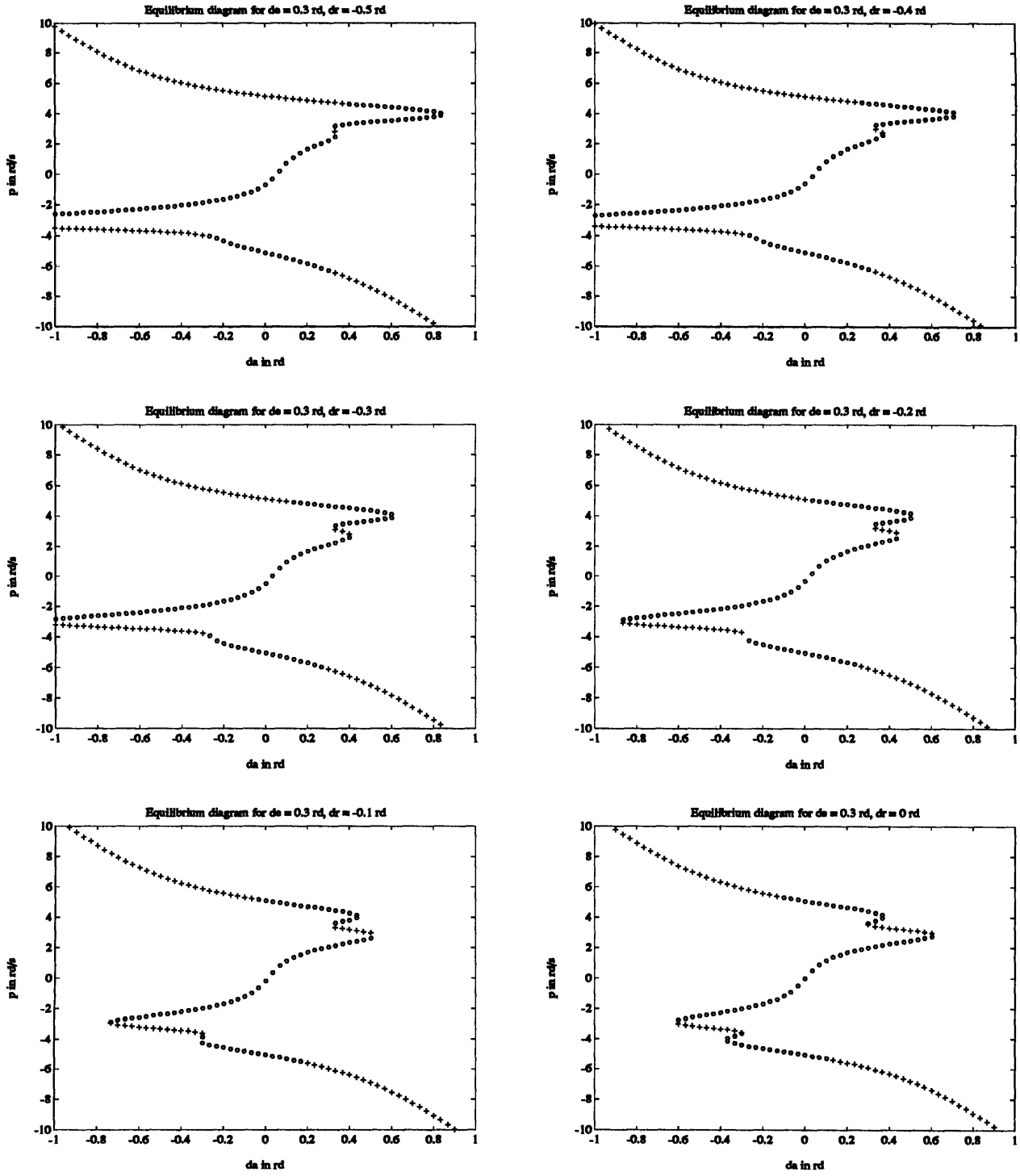

Figure 3-22: Equilibrium diagrams for $\delta e = 0.30$ rad. The 'o' points are unstable.

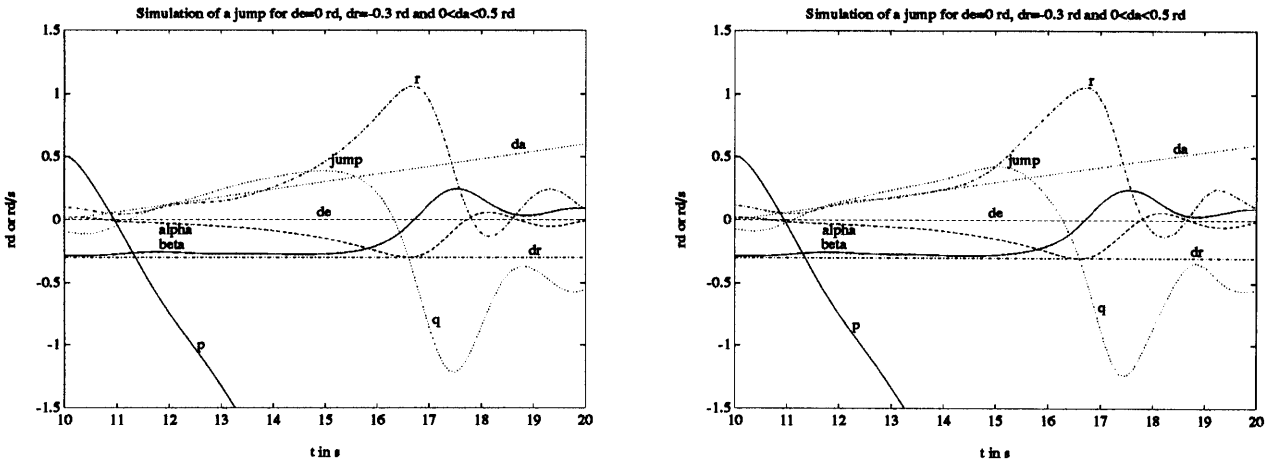

Figure 3-23: Simulation of a jump for $\delta e = 0$ rad and δr = -0.3 rad. Simulation on the simplified system is on the left.

quasi linear till the ailerons deflection exceeds a value of approximately 0.3 rad. There a jump can be observed in all the variables. For example, the pitch-rate q, which was growing positive, suddenly becomes negative. But other than these jump phenomena, there is no other weird phenomenon occuring for this value of the elevator deflection.

Equilibrium diagrams for δe = -0.2 rad

Life is not so simple in the case of a negative elevator deflection. There, one can see in Figure 3-18 that, along with jump phenomena and regular saddle-node bifurcations, a new type of bifurcation occurs, caused by the fusion of a saddle-node bifurcation and a subcritical Hopf bifurcation. On the equilibrium diagrams, this new type of bifurcation manifests itself as a saddle-node bifurcation whose both branches are unstable. This phenomenon appears even for $\delta r = 0$ rad. This phenomenon is to be analyzed more thoroughly on the equilibrium diagram presented on Figure 3-24, which corresponds to a rudder deflection of -0.20 rad. In this Figure, the two regular saddle-node bifurcations are denoted by A and A0, the two special bifurcations B and B0 and the two Hopf bifurcations H and H0.

First of all, it has been stated that the two points denoted H and H0 were subcritical Hopf bifurcations. The fact that they are actually Hopf bifurcations is proved by the eigenvalue diagram presented on Figure 3-25. On this diagram, the points

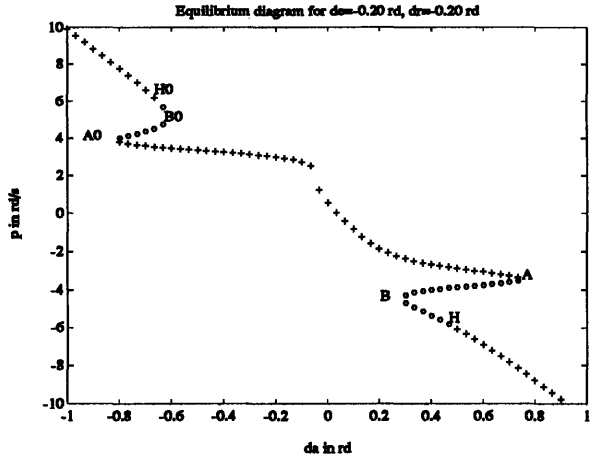

Figure 3-24: Equilibrium diagram for δe = -0.20 rad, δr = -0.20 rad

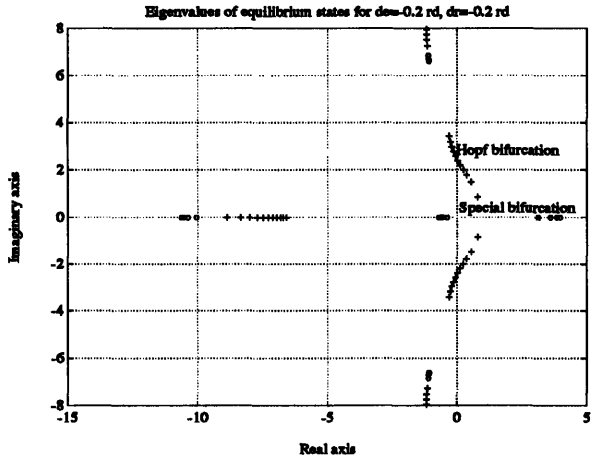

Figure 3-25: Eigenvalues diagram for δe = -0.20 rad and δr = -0.20 rad

marked with '+' symbols correspond to eigenvalues associated with the equilibrium points of the B-H branch of Figure 3-24. It can be seen that a complex pair of eigenvalues crosses the imaginary axis, thus causing a Hopf bifurcation to occur. Then, it can be seen that these Hopf bifurcations are subcritical because a simulation has shown that there are no stable limit cycles associated with the unstable equilibrium branches of the Hopf bifurcation, namely with the branches denoted B-H and B0-H0 on Figure 3-24. Thus, the limit cycles are associated with the stable branches of the Hopf bifurcations, namely the branches beginning at H and H0. A bifurcation diagram, similar to those presented in the previous chapter about bifurcation theory, is presented on Figure 3-26. These unstable limit cycles are believed to have no major effects on the dynamics of the airplane.

Coming back to Figure 3-24, one can now analyse the special bifurcations occuring

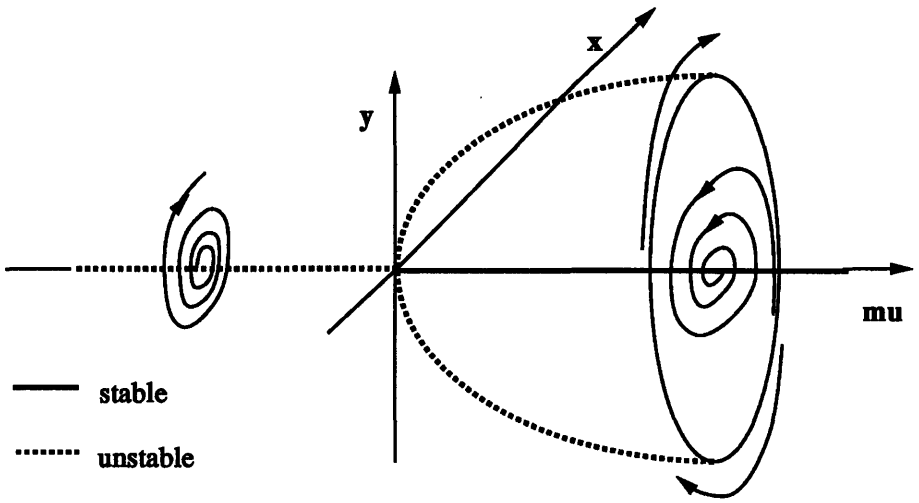

Figure 3-26: Subcritical Hopf bifurcation

	da (rd)	From A	0.2933	0.2900	0.2867	B
Eigenvalues			-9.9579	-9.8770	-9.7624	
			-1.1280 + 6.8726i	-1.1303 + 6.8997i	-1.1335 + 6.9381i	
			-1.1280 - 6.8726i	-1.1303 - 6.8997i	-1.1335 - 6.9381i	
			-0.3226	-0.2718	-0.1936	
			2.9285	2.8014	2.6149	
	da (rd)	B	0.2933	0.2900	0.2867	To H
Eigenvalues			-9.2816	-9.1467	-9.0457	
			-1.1465 + 7.1056i	-1.1501 + 7.1561i	-1.1527 + 7.1955i	
			-1.1465 - 7.1056i	-1.1501 - 7.1561i	-1.1527 - 7.1955i	
			0.3208	0.7377	0.8716 + 0.5151i	
			1.6458	1.1012	0.8716 - 0.5151i	

Table 3.2: Eigenvalues around the special saddle-node bifurcation, δe = -0.20 rad and δr = -0.20 rad

in B and B0. Interestingly enough, one can say that points B and B0 are bifurcation points because, there, a change in the number of equilibrium points does occur. Nevertheless, this change does not occur through a positive real eigenvalue crossing the imaginary as in a regular saddle-node bifurcation but rather through another real negative eigenvalue crossing the imaginary axis, becoming positive and then merging with the other positive real eigenvalue into a pair of complex eigenvalues with a positive real part. These fact are illustrated by the eigenvalues plot on Figure 3-25 and by the Table 3.2 presenting the eigenvalues around point B.

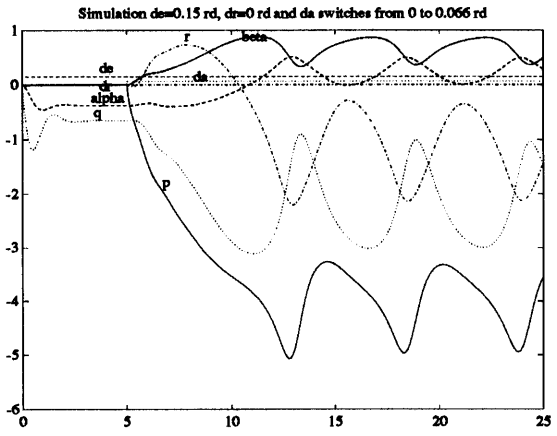

Figure 3-27: Simulation for $\delta e = 0.15$ rad and $\delta r = 0$ rad, when da goes from 0 to 0.066 rad

Equilibrium diagrams for $\delta e = 0.10$ and 0.15 rad

In these two cases, the solution $p = 0$ when $\delta a = \delta r = 0$ is stable. Nevertheless, one can see on Figures 3-20 and 3-21 that, in the case of positive elevator deflection, the relationship between the ailerons deflection δa and the equilibrium roll-rate p is very quickly distorted, even for small δa. Thus, for $\delta e = 0.10$ rad and $\delta r = 0$ (lower right corner of Figure 3-20), there are two jumps in the very neighborhood of $\delta a = 0$. For $\delta e = 0.15$ rad and $\delta r = 0$ (lower right corner of Figure 3-21), there are five equilibrium solutions near $\delta a = 0$, out of which three are stable: theoretically $\delta a = 0$ can yield a positive, a negative and a zero equilibrium roll-rate!

The case $\delta e = 0.15$ rad and $\delta r = 0$ also features an other interesting peculiarity: there are two successive Hopf bifurcations on the upper and lower branches. This phenomenon in itself is more extensively described in the following subsection dealing with the δe = -0.35 rad. The important thing to notice here is that stable limit cycles exist between the two Hopf bifurcations. Thus, in a certain range of ailerons deflection, very close from $\delta a = 0$, the airplane is going to be attracted towards dangerously high values of the equilibrium state vector, as shown in Figure 3-27. Such situations must be taken care of, either by limiting the range of possible elevator deflections (for example, no elevator deflection bigger than 0.1 rad) either by designing a stability augmentation system. Such issues are to be discussed in more details in the next chapter.

Equilibrium diagrams for δe = -0.35 rad

In this set of equilibrium diagrams, the solution $p = 0$ when both the ailerons deflection and the rudder deflection are zero is not stable. That is the reason why one can see on Figure 3-17 that the area around $p = 0$ is not stable: moving the ailerons deflection about zero causes the airplane to jump to a stable positive or negative value of the roll-rate, whose absolute value is approximatly 3 rad/s in any case. In the region around $p = 0$, one can also notice that there is a range of the ailerons deflection in which two stable roll-rates are present. Thus, for a positive ailerons deflection, the airplane can jump to a negative or to a positive roll-rate. Any control system should thus take care of this phenomenon and avoid this range of the elevator deflection where a given deflection can cause two opposite results.

The kind of peculiar saddle-node bifurcation that was described in the previous paragraph are still present at both ends of the range of the elevator deflection. The presence of the two subcritical Hopf bifurcations gives raise to a dangerous stable branch of equilibria, which must also be avoided in a control system.

Equilibrium diagrams for δe = 0.30 rad

In this set of equilibrium diagrams, presented on Figure 3-22, one can notice first that the area around $p = 0$ is also unstable. Nevertheless, in this case, there are values of the ailerons deflection for which no equilibrium state exists on any branch.

Furthermore, for high values of the rudder deflection, beginning at δr = -0.2 rad, two Hopf bifurcations appear on the same branch. This fact is illustrated on Figure 3-28, where the two Hopf bifurcations are labeled H1 and H2. The unstable branch between H1 and H2 is associated with stable limit cycles, as shown by simulations presented on Figure 3-29, which were made, as usual, on both systems 3.15 and 3.23. A bifurcation diagram showing the possible equilibrium states when one moves on the H1-H2 branch is presented on Figure 3-30: before H1 and after H2, there is a stable attractive sink and between H1 and H2, there is a stable limit cycle associated with an unstable repelling sink. The eigenvalues pattern is presented on Figure 3-31, where one can see that the imaginary axis is crossed twice by pairs of complex eigenvalues.

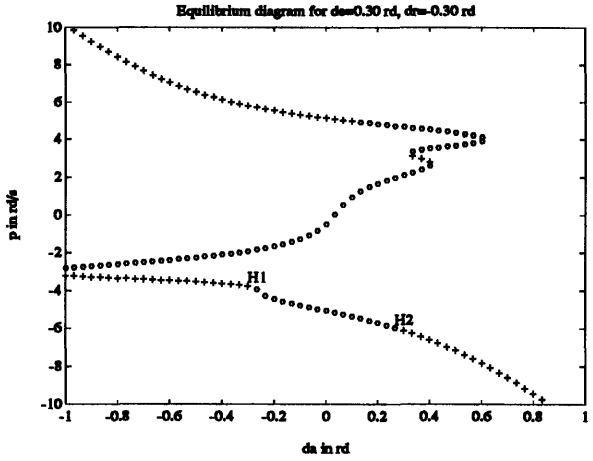

Figure 3-28: Equilibrium diagram for δe = 0.30 rad and δr = -0.30 rad

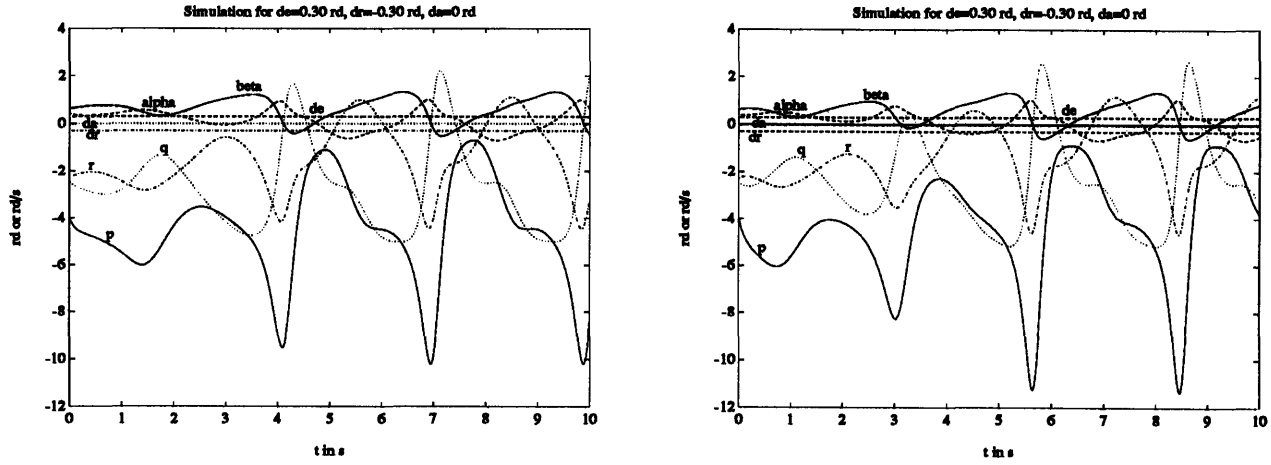

Figure 3-29: Simulation of a limit cycles for δe = 0.30 rad and δr = -0.3 rad. Simulation on the simplified system is on the left.

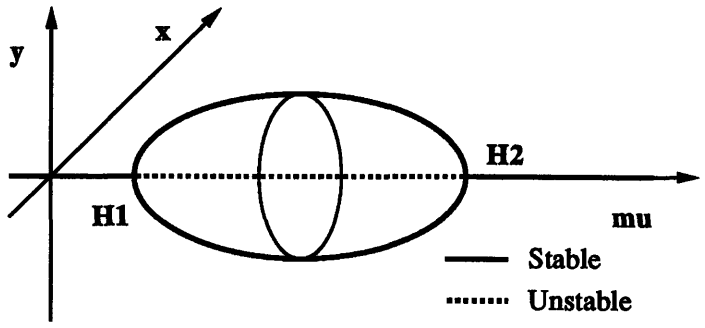

Figure 3-30: Bifurcation diagram for two successive Hopf bifurcations

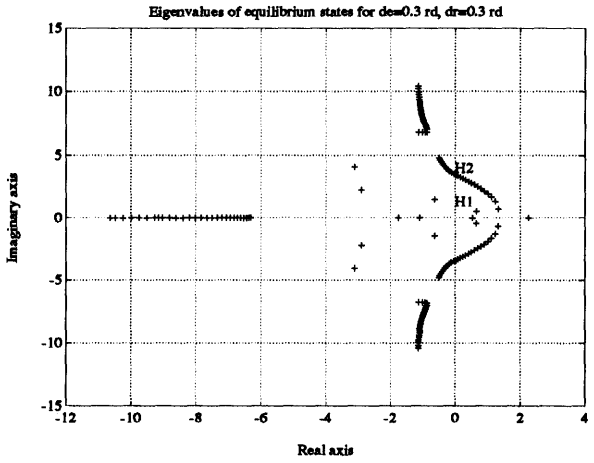

Figure 3-31: Eigenvalues diagram for δe = 0.30 rad and δr = -0.30 rad

Chapter 4

Control strategies

4.1 Introduction

This chapter is intended to provide some control strategies to deal with the nonlinear phenomena due to flight at high angle of attack. Longitudinal and lateral control have been treated separatly. The purpose of the longitudinal control system is to prevent departures into high amplitude limit cycles or jumps to stable high values of the state vector when the elevator deflection reaches extreme values. This is basically done by maintaining a zero roll-rate, using a simple feedback system using p and the aileron deflection.

Similarly, the purpose of the lateral control system is to avoid jumps and limit cycles. However, this goal is attained by sophisticated means since it involves bifurcation theory and more specifically, bifurcation surfaces. The idea of such a control system is to couple the rudder and the aileron deflection so as to avoid values of control deflections (δe, δr, δa) at which more than one stable equilibrium state exists.

Finally, the concept of bifurcation surfaces is applied to the design of a classical control system, namely a yaw damper. It is seen that the use of bifurcation surfaces can provide the control engineer with an additional criterion in chosing the correct value of a control gain.

4.2 Longitudinal control

4.2.1 Control system design

In the longitudinal case, the stability is compromised at both ends of the elevator deflection range: for highly negative δe (δe < -0.33 rad), the airplane is prone to jump phenomena, for highly positive δe (δe > 0.22 rad), the airplane is prone to departure into stable limit cycles.

Nevertheless, these instabilities can be considered as slow: the divergence from the equilibrium case occurs with a relatively long time constant. Thus a simple feedback system can easily take care of these divergences and constrain the airplane to remain on the unstable solution $p = 0$, acting in much the same way than a clown trying to keep a stick on his finger tip.

The feedback control system just measures the roll-rate p and sends a command to the ailerons actuators proportional to the measured p. The primary effect of a positive aileron deflection is to produce a negative roll-rate (coefficient $l_{\delta a}$ is negative); thus an adequate feedback response to a positive perturbation of p is a positive aileron deflection. A big gain is not even needed and the following examples feature a control system with

$$\delta a = 0.2p. \tag{4.1}$$

4.2.2 Examples

Two examples are given, one at each extremity of the range of possible aileron deflection. For large negative δe, Figure 4-1 (left) shows the time history obtained when a step change on δe (δe jumps from 0 to -0.40 rad at t = 5 s) followed by a perturbation on p (p jumps from 0 to 0.05 rad/s at t = 10 s) is introduced on an initial equilibrium state in which δe and all the other control and state variables are zero. When the step on δe is effected, the state vector takes on new equilibrium values. Yet, these new equilibrium values are unstable: the small perturbation applied at t = 10 s causes a divergence of the state variables. Figure 4-1 (right) features exactly the

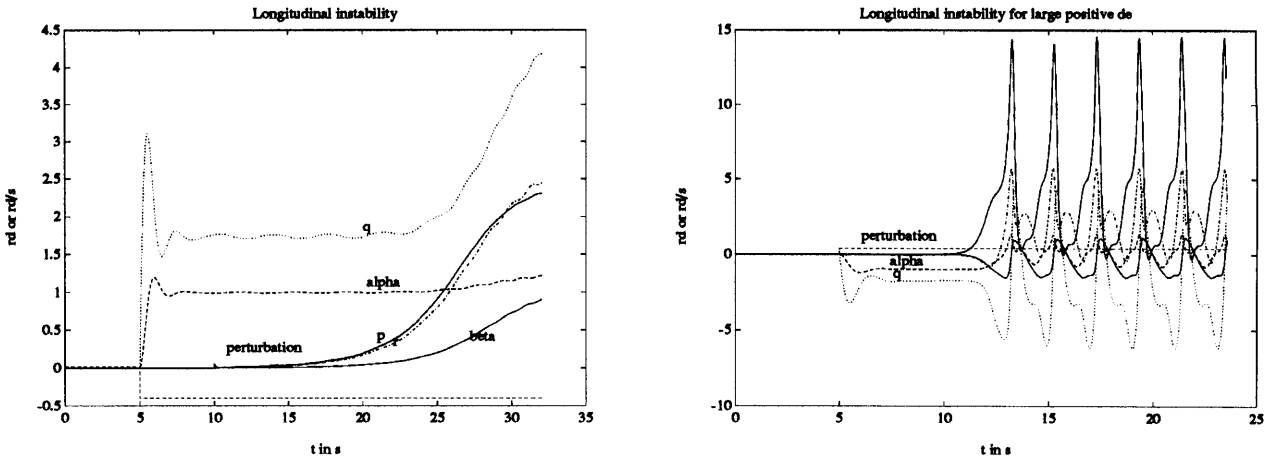

Figure 4-1: Time histories showing the instability of the airplane when either a large positive (right) or negative (left) elevator deflection step is applied

same experiment, except that, in this case, δe jumps from 0 to 0.40 rad. The result of a perturbation is then to initiate a very high amplitude limit cycle.

Figure 4-2 shows how the simple linear feedback system described above is successful in stabilizing the airplane: even after the perturbation is applied, the airplane literally sticks to the assigned solution $p = 0$.

Then, Figure 4-3 displays time histories of the aileron deflection in both cases. The purpose of these figures is essentially to show how fast must be the actuators to respond to such perturbations. The order of magnitude of the angular speed of the ailerons, measured during the initial peak, is 0.15 rad/s, which is a mechanically realizable value.

4.3 Lateral control

Through bifurcation theory and steady state analysis, it was possible to predict the behavior of the fighter aircraft when various combinations of controls were applied. This analysis also showed the necessity for a control system acting on the lateral dynamics of the airplane to avoid jump phenomena, departures into limit cycles and other hazardous "maneuvers". Following ideas provided in [15], a lateral control system can be built based on bifurcation surfaces.

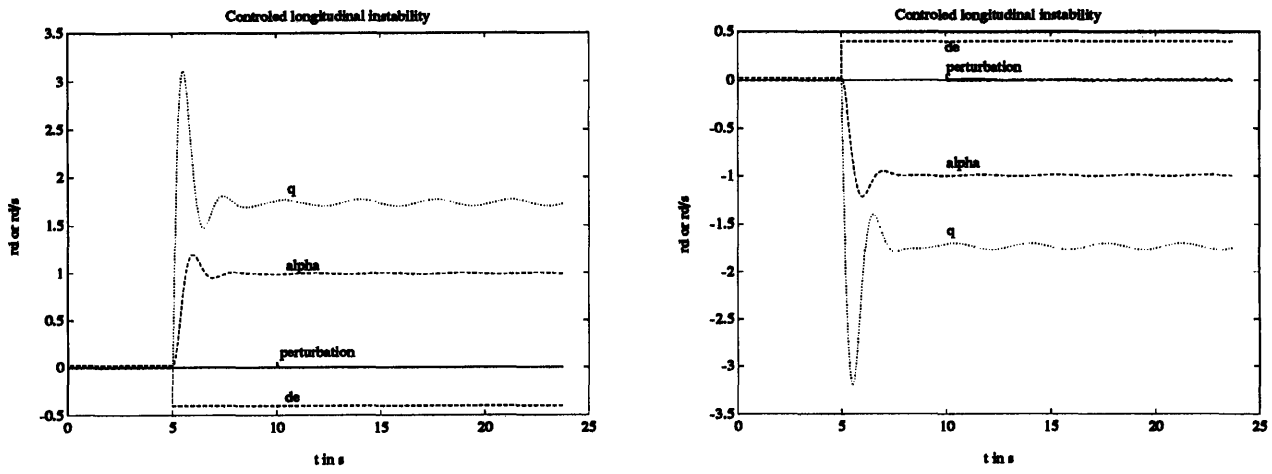

Figure 4-2: Time histories when a control system stabilizes the airplane after a perturbation. Cases of a large negative (left) and positive (right) elevator deflection step.

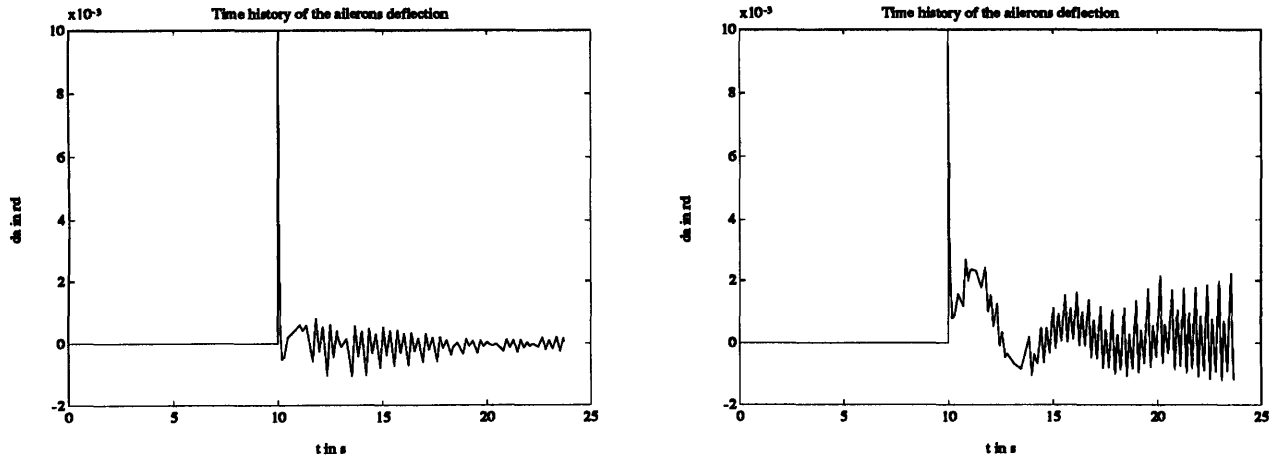

Figure 4-3: Time histories of the aileron deflection when a control system stabilizes the airplane after a perturbation. Cases of a large negative (left) and positive (right) elevator deflection step.

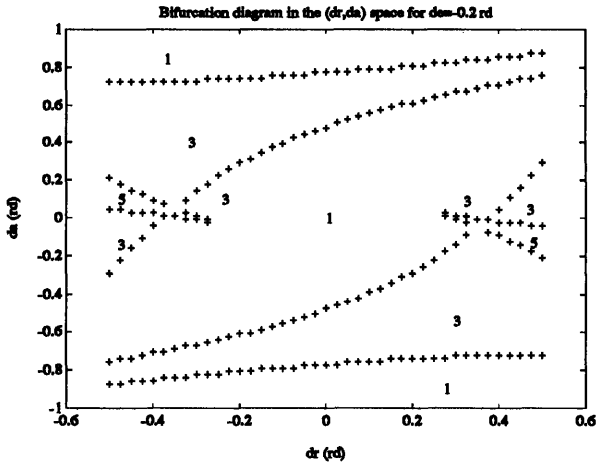

Figure 4-4: Bifurcation surface in the control space (δr, δa), for δe = -0.20 rad. The figures inside the diagram indicate the number of equilibrium states in each area

4.3.1 Bifurcation surfaces

An interesting way of summarizing all the information contained in the equilibrium diagrams for each value of the elevator deflection is to plot the number of equilibrium points in the control space (δr, δa). This yields bifurcation surfaces. A number of these bifurcation surfaces have been plotted on Figures B-1 to B-14, in the Appendix B. A particular example is plotted in this chapter, on Figure 4-4. In these diagrams, crossing a line implies a change in the number of equilibrium solutions. The number of solutions in each area is indicated. Lines corresponding to Hopf bifurcations are not plotted since Hopf bifurcations do not induce a change in the number of equilibrium states. These diagrams will be helpful to design control systems such as an ailerons-rudder coupling because they indicate which relationship should be created between δa and δr to avoid jumps and limit cycles.

4.3.2 Use of bifurcation surfaces to design the lateral control system

An example for δe=-0.20 rad

Figure 4-5 displays the equilibrium surface for δe = -0.20 rad and δr = 0 rad. Since there is no rudder deflection, the equilibrium surface is symmetrical. On the other hand, this equilibrium surface features two jump phenomena, for $\delta a \simeq \pm$ 0.8 rad.

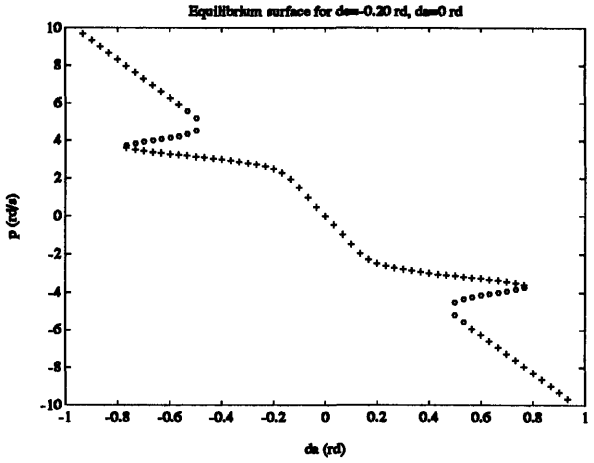

Figure 4-5: Equilibrium surface for δe = -0.20 rad, δr = 0 rad

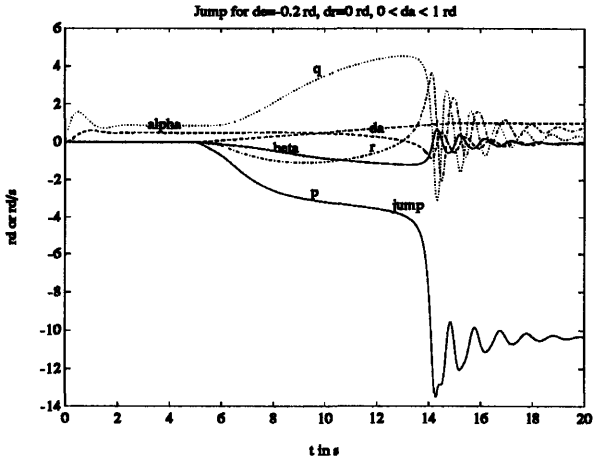

Figure 4-6: Simulation of a jump for δe = -0.20 rad and δr = 0 rad, when δa varies linearly from 0 to 1 rad

This prediction is confirmed by simulations, as shown on Figure 4-6. The principle of this simulation is to keep the rudder and the elevator deflection constant while slowly and linearly moving the ailerons, beginning at t = 5 s, at a rate of 0.1 rad/s. During the first seconds of this maneuver, the airplane reacts "linearly", that is to say in the way "normally" expected by the pilot. Then, a sudden jump on all the variables occurs around t = 13 s.

This jump can happen because there are certain intervals of the aileron deflection where two or more stable equilibrium states coexist. The idea used here to avoid these jump phenomena consists in coupling the ailerons and the rudder so that, for any aileron deflection, there is only one possible equilibrium state. In other words, this coupling consists just in defining the rudder deflection as a function of the aileron

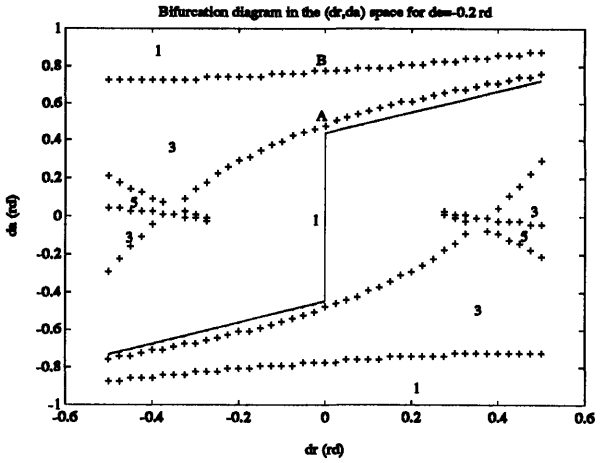

Figure 4-7: Bifurcation surface and definition of the ailerons-rudder coupling in the control space (δr, δa), for δe = -0.20 rad. The figures inside the diagram indicate the number of equilibrium states in each area

deflection so as to remain in the portion of the bifurcation surface in which there is only one possible equilibrium state. This concept is illustrated on Figure 4-7, where a possible relationship between the rudder and the ailerons is superimposed to the bifurcation surface corresponding to δe = -0.20 rad.

On this Figure, the coupling has been chosen so as to minimize the amount of rudder deflection. It is believed that there is no special danger in setting the coupling function to be close from the border between the areas of one and three equilibrium states, since one can observe on the equilibrium surface of Figure 4-5 that crossing this border (for example, at the point labeled A on Figure 4-7) does not imply an immediate jump: the jump would rather happen when crossing the next border, namely that between three and one possible equilibrium state, at a point such as B on Figure 4-7.

The efficiency of such a coupling is demonstrated on the simulation presented on Figure 4-8. In this simulation, a ramp similar to that applied in the previous simulation (cf Figure 4-6) is applied on the ailerons. The elevator deflection remains fixed but the rudder is moved through the previously defined coupling. As a result, one can see that the jump is totally avoided. Figure 4-9 shows how the equilibrium surface is modified by the presence of the coupling.

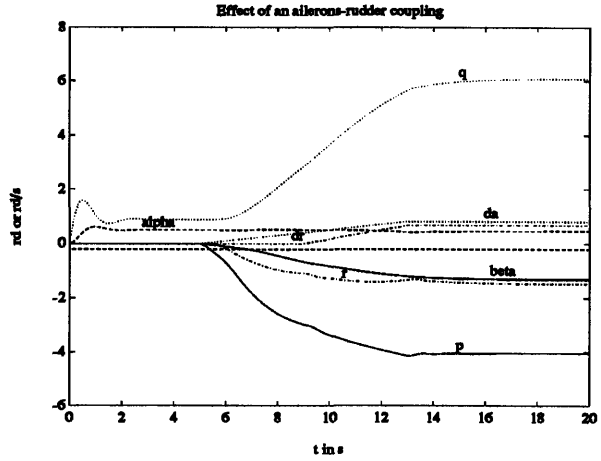

Figure 4-8: Time history for δe = -0.20 rad when δa varies linearly from 0 to 1 rad and δr is coupled to δa

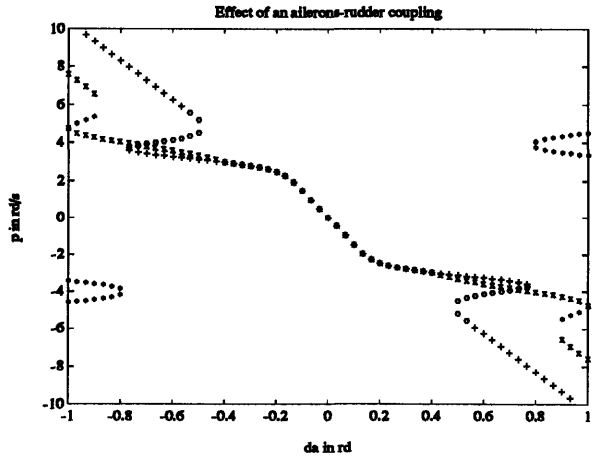

Figure 4-9: Equilibrium surface for δe = -0.20 rad and δr coupled to δa. '+' and '×' are for stable points, 'o' and '*' are for unstable points.

Full design of the lateral control system

In the previous paragraphs, the usefulness of bifurcation surfaces in control design has been demonstrated. However, in this previous example, the control system was designed for only one value of the elevator deflection, namely δe = -0.20 rad. The object of this last section is to show a possible design for the overall lateral control system, based on the same principles. The design presented below covers values of the elevator deflection ranging from -0.30 rad to 0.2 rad.

First of all, making use of Figures B-3 to B-10 in the Appendix B, one can notice that, for δe ranging from -0.30 rad to 0.10 rad and for $\delta r = 0$, there is always a range of aileron deflections that includes 0 and where there is only one possible stable equilibrium state. Thus, in this range of elevator deflection (-0.30 rad $\leq \delta e \leq$ 0.1 rad) and for a sufficiently small aileron deflection, no rudder deflection is needed. Then, for higher aileron deflections, a coupling becomes necessary. The slope of the linear relationship between the ailerons and the rudder deflections and the aileron deflection at which the coupling must be initiated (this aileron deflection can be called δa_0) are both dependent on the elevator deflection. These concepts can be better explicited by the mean of the diagrams presented on Figures 4-10 through 4-12.

On Figure 4-10, one can see that, for -0.30 rad $\leq \delta e <$ -0.15 rad, δa_0 varies continuously with the elevator deflection, ranging between 0.35 rad for δe = -0.30 and 0.52 rad for δe = -0.15 rad. A plot of δa_0 versus the elevator deflection would show that a linear relationship between these two quantities is quite satisfactory. The slope of the linear part of the coupling is such that the line joins ($\delta a = \delta a_0$, $\delta r = 0$) and (δa = 0.72 rad, δr = 0.5 rad).

For -0.15 rad $\leq \delta e <$ -0.05 rad (Figure 4-11), one can see that δa_0, and subsequently, the slope of the linear part of the coupling, remains constant. For -0.05 rad $\leq \delta e <$ +0.10 rad, no coupling is necessary.

One can also try to design a control system in the range +0.10 rad $< \delta e <$ +0.20 rad. On the bifurcation surfaces presented on Figures B-11 and B-12, one can see that, even for δr = 0 rad, there are multiple equilibrium states for small aileron deflections. However, for higher values of the aileron deflection, there is only one, non-ambiguous,

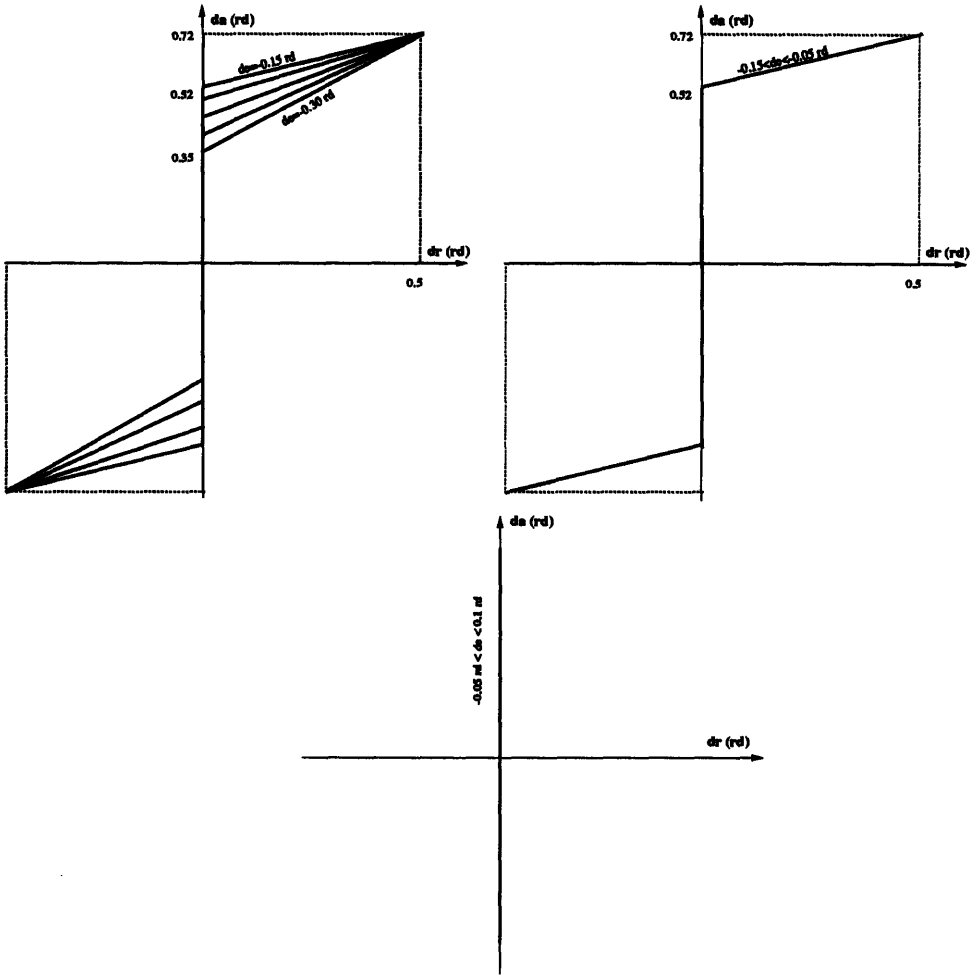

Figure 4-10: Upper left: Ailerons-rudder coupling for -0.30 rad $\leq \delta e <$ -0.15 rad

Figure 4-11: Upper right: Ailerons-rudder coupling for -0.15 rad $\leq \delta e <$ -0.05 rad

Figure 4-12: Down: Ailerons-rudder coupling for -0.05 rad $\leq \delta e \leq +0.10$ rad

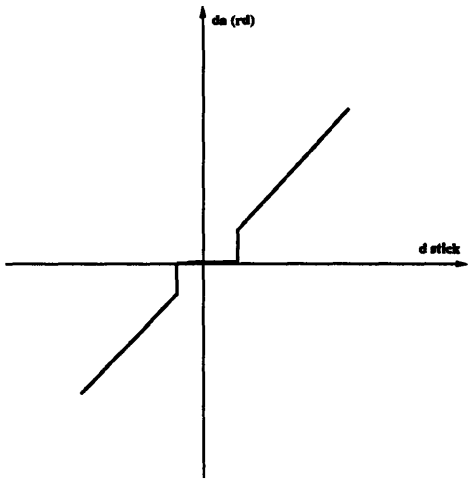

Figure 4-13: Control system valid for 0.10 rad $< \delta e <$ +0.20 rad

stable equilibrium state. One can take advantage of this fact to design a control system which would avoid this area of ambiguous, small aileron deflections: as long as the position of the stick remains in a certain interval centered on zero, there is no aileron deflection and the stability of the airplane is taken care of by the longitudinal stability system designed previously. When the stick moves a greater deal, the aileron deflection jumps to a value at which only one equilibrium state exists. This concept is illustrated on Figure 4-13. The main drawback of this system is that it provides very sudden changes of the roll rate p.

4.4 Another application of bifurcation surfaces

In this final section, the bifurcation surface concept is applied to the design of a yaw damper. This yaw damper is very simply realized: the rudder deflection is driven by the yaw rate with a feedback gain k_r in such a way that

$$\delta_r = k_r r. \tag{4.2}$$

Since classical linear methods of gain selection are not valid in the case of this non-linear system, a simulation has been made to evaluate the effect of increasing gain. In this simulation, presented on Figure 4-14, the initial conditions are the trim con-

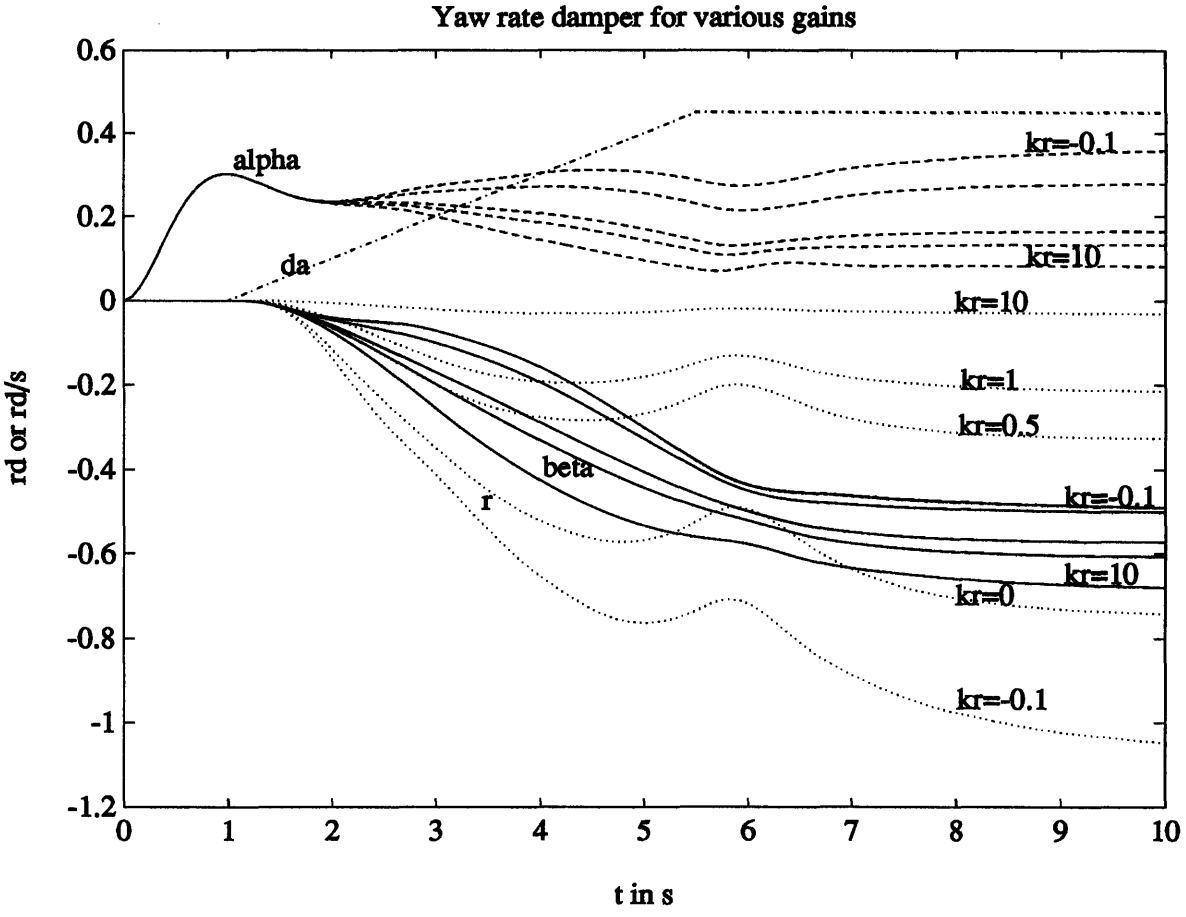

Figure 4-14: Effect of increased gain on a yaw damper

ditions for $\delta_e = 0$. Then a step is applied on the elevator: δ_e jumps from 0 to -0.10 rad. Finally a slow ramp is applied on the ailerons, beginning at t=1 s and lasting 4.5 s at a rate of 0.1 rad/s. Figure 4-14 clearly shows an increased efficiency of the yaw damper for higher positive gains: the yaw rate is close to zero for k_r=10. Thus, one might be tempted to select a high value for k_r.

However, higher gain means higher rudder deflection and higher risk to venture in regions were more than one stable equilibrium state exists. The maneuver described on Figure 4-14 is slow. Thus, the airplane can approximately be considered to be in equilibrium at every instant of the maneuver and the rudder deflection versus the aileron deflection can be plotted in the (δ_r, δ_a) space and superimposed on the bifurcation diagram for δ_e=-0.10 rad. Figure 4-15 shows that the (δ_r, δ_a) profile associated to the maneuver probably goes too deeply into the region where three

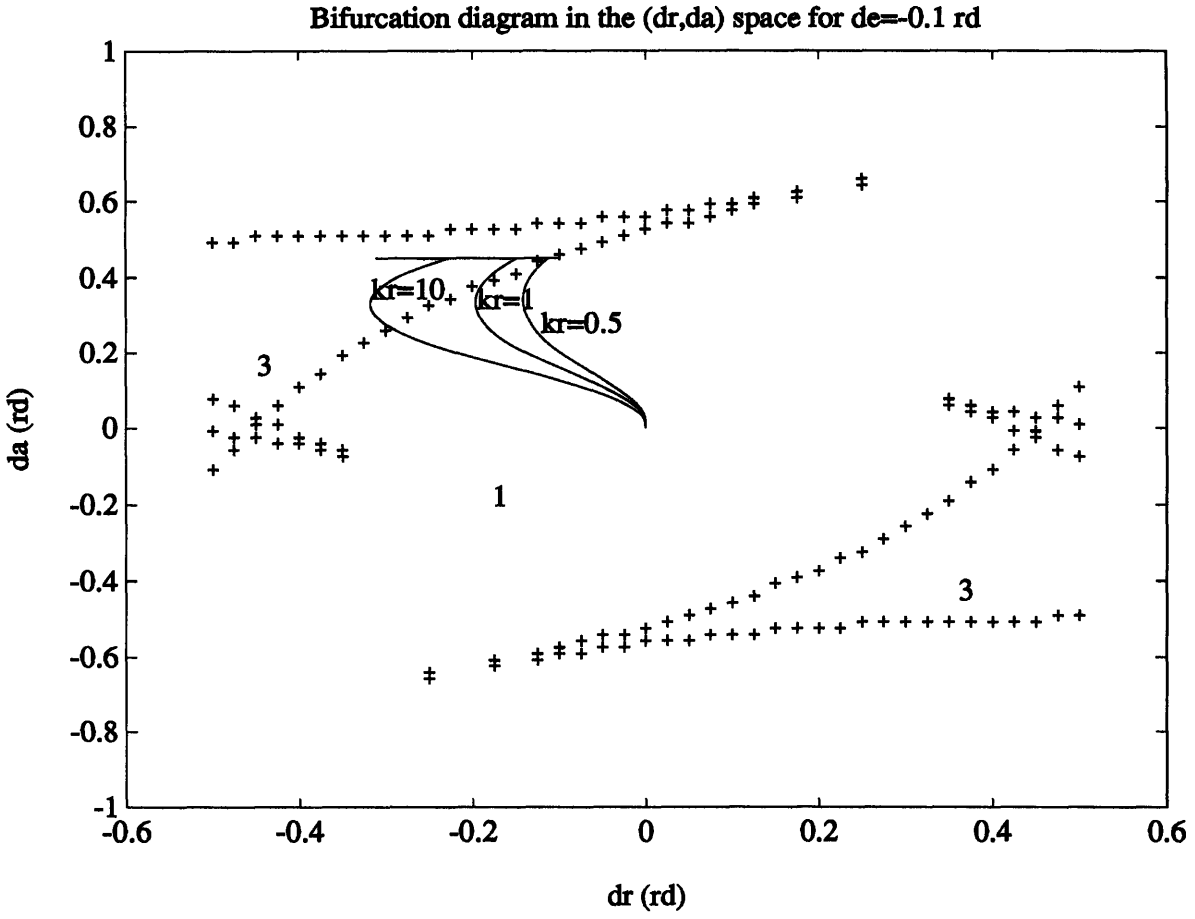

Figure 4-15: (δ_r, δ_a) profile superimposed to the bifurcation diagram for δ_e=-0.10 rad

equilibrium solutions (two of which are stable) exist as soon as the gain k_r is greater or equal to 1. This kind of criterion should probably be incorporated in the studies of control system operating on nonlinear systems.

Chapter 5

Summary and conclusions

5.1 Introduction

One of the most crucial requirements for future combat aircraft is an increase of maneuverabilty[1]. The ultimate goal is to make fighter aircraft able to maneuver at post-stall angles of attack, namely at angles sometimes greater than 50 degrees, and to give them the capability to point their fuselage independently of their flight path [10].

It is quite obvious that classical aerodynamic and dynamic linear models, whose accuracy is strictly confined to small angles of attack and sideslip, are no longer valid. First of all, the mathematical model of the equations of motion of any rigid body is already nonlinear through coupling terms such as pq^2 or nonlinear terms such as $\sin\phi$[3]. The aerodynamic model is also highly nonlinear: ultimately, aerodynamic forces and moments cannot be represented by analytical functions with constant coefficients but need to be represented as tabular data and incorporated in the equations of motion in terms of spline functions. Some of the aerodynamic peculiarities [11, 12] of the flight at high angle of attack are: the dependence of the aerodynamic forces and moments on the past history of the flow, the presence of side forces at zero angle of sideslip,

[1] Well, this has always been the case for any new generation of combat aircraft, but nowdays a change in nature rather than in degree is to be made.

[2] p and q are two angular velocities with respect to the body axis.

[3] ϕ is traditionally the bank angle

the presence of hysteresis, limit cycles and auto-rotationnal rolling.

Bifurcation theory, which is a mathematical tool invented by Poincaré to analyze nonlinear systems, recently showed itself to be very useful in the analysis of nonlinear problems of modern flight dynamics. This theory was first applied to the cross-coupling problem[4] [15, 18] and then extended to the fully nonlinear problem of flight at high alpha [15, 17, 16, 20, 21, 22, 23].

This thesis is basically the application of the bifurcation theory to the particular example of a fighter aircraft whose aerodynamic model includes nonlinear effects in the form of second order polynomials with constant coefficients. The lateral and longitudinal dynamics of this fighter aircraft are studied and used as a preliminary step for the design of a control system aimed at avoiding jumps and limit cycles.

5.2 The bifurcation theory

A necessary introduction for this study is a basic exposition of the principles of the bifurcation theory. This theory arises as an answer to the problem of the stability[5] of a nonlinear systems depending on one parameter, such as

$$\dot{x} = f_\mu(x). \tag{5.1}$$

As a matter of fact, the stability of any nonlinear system is usually given by the stability of the associated linearized system: this is the great result of Poincaré-Liapunov's theory. Nevertheless, in the neighborhood of some equilibrium points, namely the points where the Jacobian matrix[6] of the nonlinear system has zero or imaginary eigenvalues, the stability theory of the linearized system does not give the

[4]Some of the manifestations of cross-coupling phenomena are the instability of the short period lateral and longitudinal oscillations when performing quick rolls and the jumps to high roll-rates with zero input on the ailerons.

[5]By stability, it is meant here local stability. Given an equilibrium point $x = x_0, \dot{x}(x_0) = 0$, this point is said to be locally stable if any trajectory in a neighborhood of x_0 at $t = t_1$ remains in this neighborhood at $t > t_1$. The equilibrium point x_0 is asynptotically stable if, furthermore, $x(t)$ goes to x_0 when t goes to infinity.

[6]The jacobian matrix is defined by $(Df(x))_{i,j} = \frac{\partial f_i}{\partial x_j} for 1 \leq i, j \leq n.$

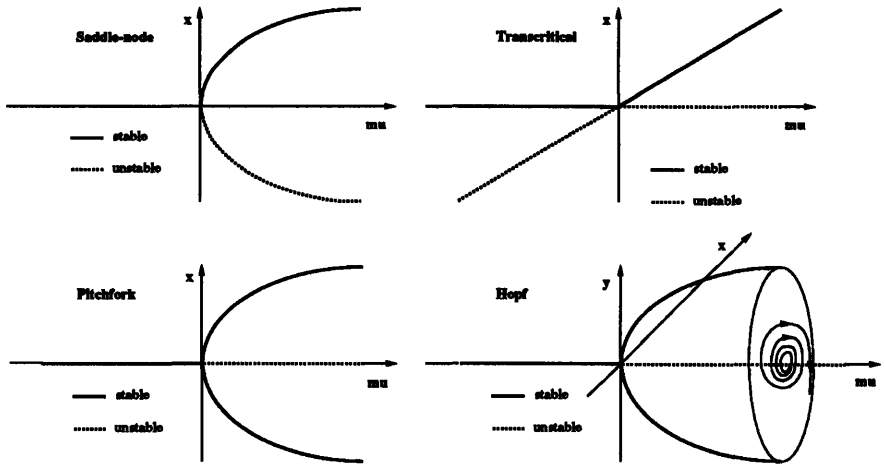

Figure 5-1: Bifurcation diagrams of the four basic types of bifurcation

correct answer. When an eigenvalue or its real part goes through zero, a change in the number and nature of the equilibrium points occurs, which is called a *bifurcation.*

Bifurcations of equilibria depending on one parameter are classified into four types and can be represented on bifurcation diagrams, that is plots of the various equilibrium points versus the value of the parameter μ (cf Figure 5-1). The saddle-node bifurcation is the simplest case. A model for this bifurcation is $\dot{x} = \mu - x^2$: for $x \geq 0$, there are two equilibrium points, of which one is stable and one unstable. The transcritical bifurcation, or exchange of stability, whose model is $\dot{x} = \mu x - x^2$, has not been encountered in this study. In this bifurcation, zero is always present as a solution but exchanges its stability with a non-zero solution. The pitchfork bifurcation, whose model is $\dot{x} = \mu x - x^3$, occurs in situations where 0 is constrained to be an equilibrium solution for any value of the parameter μ and where symmetry with respect to μ is present. Last, the Hopf bifurcation is of special interest because, through it, a stable solution loses its stability and the new attractive stable solution becomes a limit cycle, that is a closed periodic trajectory. The model for this bifurcation is that of a pitchfork in which the coordinate x is replaced by the radius r: $\dot{r} = \mu r - r^3$, $\dot{\theta} = 0$. The models for these bifurcations are one or two dimensional but the point is that multidimensional systems depending on one parameter have also the same type of bifurcations.

5.3 Bifurcation analysis of the longitudinal and lateral dynamics of a fighter aircraft

The bifurcation theory is now to be applied to the equations of motion of a high-performance airplane. For the sake of computationnal simplicity, some approximations have been made: the aerodynamic model is given in the classical form of constant coefficients but includes second order terms, the airspeed is constant and the effects of gravity are neglected. This last approximation is actually a minor one and time histories have been made which either take into account or neglect gravity effects and which show very similar results in both cases. Practically, the system in use for bifurcation analysis is

$$\begin{aligned}
\dot{\beta} &= y_\beta \beta + p\alpha - r, \\
\dot{\alpha} &= z_\alpha \alpha - p\beta + q, \\
\dot{q} &= i_2 rp + \bar{m}_\alpha \alpha + \bar{m}_q q - m_{\dot{\alpha}} p\beta + m_{\delta_e} \delta_e, \\
\dot{r} &= -i_3 pq + n_\beta \beta + n_r r + n_{\delta a} \delta a + n_{\delta r} \delta r, \\
\dot{p} &= l_\beta \beta + l_p p + l_r r + l_{r\alpha} r\alpha + l_{\delta a} \delta a + {}_{\delta r}\, \delta r.
\end{aligned} \tag{5.2}$$

5.3.1 Longitudinal dynamics

In the study of longitudinal dynamics the lateral control deflections in system 5.2 are set to be zero. Then, setting all the time derivatives in 5.2 to be also zero, one can find the equilibrium states in terms of the value of the elevator deflection δe, which is the bifurcation parameter: α_0, β_0, q_0, r_0[7] can be expressed as functions of the equilibrium roll-rate p_0, which, in turn, is the solution of a ninth order polynomial whose coefficients depend on δe,

$$\sum_{i=1}^{9} a_i(\delta e) p^i = 0. \tag{5.3}$$

[7]The subscript 0 means the equilibrium value of the state vector. It has been often omitted when the context was clear enough.

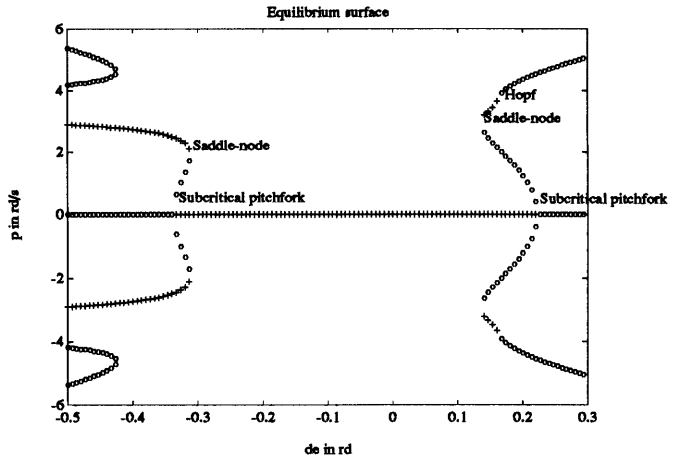

Figure 5-2: Equilibrium diagram in the longitudinal case. Equilibria marked with 'o' are unstable.

There is no constant term in this polynomial since the zero roll-rate is always a solution in the longitudinal case (no input on the ailerons). Retaining only the real solutions of this ninth order polynomial equation, one can draw equilibrium diagrams such as that of Figure 5-2. On this diagram, each equilibrium solution is plotted versus δe and its stability, computed through the Jacobian matrix of 5.2, is indicated. Three of the four basic types of bifurcations are present on this bifurcation diagram. Specifically, this diagram shows that the trivial solution $p = 0$ is unique and stable for moderate elevator deflections. Then, when the absolute value of δe grows, $p = 0$ becomes unstable through two subcritical pitchfork bifurcations[8]. Hopf bifurcations, which affect so much the dynamics of the airplane, and saddle-node bifurcations are also present. Limit cycles, due to Hopf bifurcation were simulated (cf Figure 5-3).

5.3.2 Lateral dynamics

The same type of analysis is applied to the lateral dynamics. However, a much greater number of equilibrium diagrams is needed to fully account for the lateral dynamics since the three control deflections can now be varied. Due to the great number of possible combinations of δe, δa and δr, many different phenomena are present and each one cannot be accounted for in this summary. Nevertheless, the most recurrent

[8]A pitchfork bifurcation is said to be *subcritical* when, unlike in the regular case mentionned above, there is one unstable solutions that bifurcate into one stable solution and two unstable.

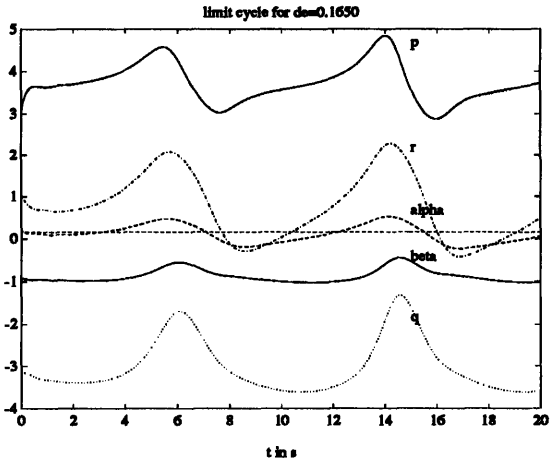

Figure 5-3: Simulation just beyond the Hopf bifurcation on simplified system 3.16

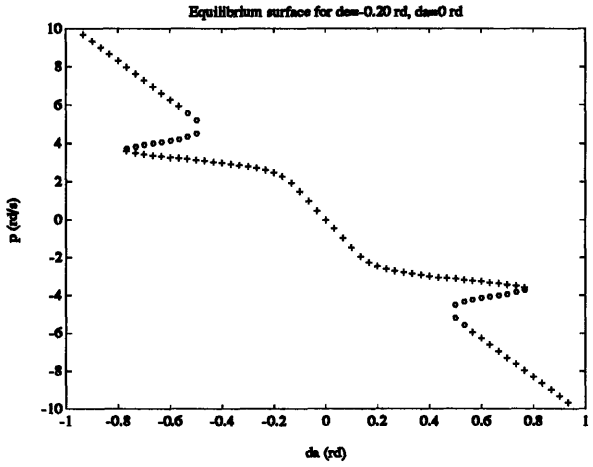

Figure 5-4: Equilibrium surface for δe = -0.20 rad, δr = 0 rad

of these nonlinear phenomena is the jump phenomenon. An example of jump is given on Figure 5-4 and 5-5: at δe = 0.20 rad and δr = 0 rad fixed, a ramp is applied to the ailerons. The airplane first reacts linearly and then, for $\delta a \simeq 0.8$ rad, undergoes a sudden jump on all the state variables. This jump can be predicted on the basis of the equilibrium diagram of Figure 5-4, where the basic stable solution stops existing at $\delta a \simeq 0.8$ rad: moving the ailerons further causes the airplane to be attracted towards an other stable solution of much greater amplitude. The time history presented on Figure 5-5 confirms this prediction.

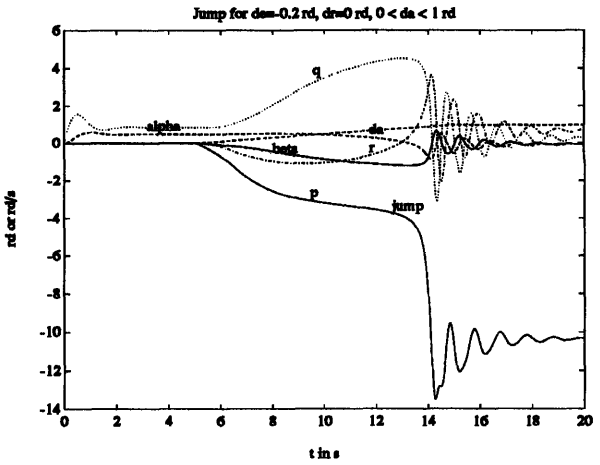

Figure 5-5: Simulation of a jump for δe = -0.20 rad and δr = 0 rad, when δa varies linearly from 0 to 1 rad

5.4 Control strategies

The goal assigned to the control system designed in this thesis is to avoid this kind of jumps and limit cycles. In longitudinal dynamics this purpose can be easily met through a classical linear feedback between the roll-rate p and the ailerons delection δe: when the aircraft departs into an unwanted roll, the ailerons react with an appropriate deflection.

The lateral control system was designed using concepts from the bifurcation theory: for a given elevator deflection, a so-called *bifurcation surface* is plotted, which indicates what is the number of equilibrium solutions for a given (δa, δr) couple (cf Figure 5-6). Area of different number of equilibrium solutions are separated by continuous lines. The principle of the lateral control system is to constrain the airplane to remain in the area where a unique equilibrium solution exists, by coupling the ailerons and the rudder. The diagram of such a coupling is superimposed on the bifurcation surface on Figure 5-6. Using this coupling, a simulation was done where the same ramp on the ailerons was applied on the airplane (cf Figure 5-7): the jump disappeared. This type of lateral control system was then extended to elevator deflections ranging from -0.30 rad up to +0.10 rad.

Eventually, the bifurcation surface concept was applied to the design of a classical control system, namely a yaw damper and seemed to give useful information for gain

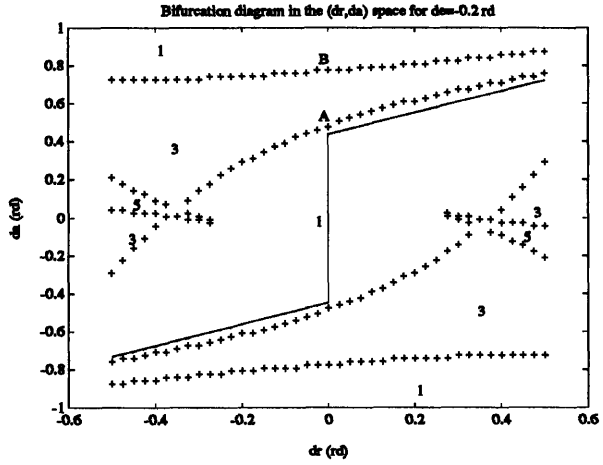

Figure 5-6: Bifurcation surface and definition of the ailerons-rudder coupling in the control space (δr, δa), for δe = -0.20 rad. The figures inside the diagram indicate the number of equilibrium states in each area

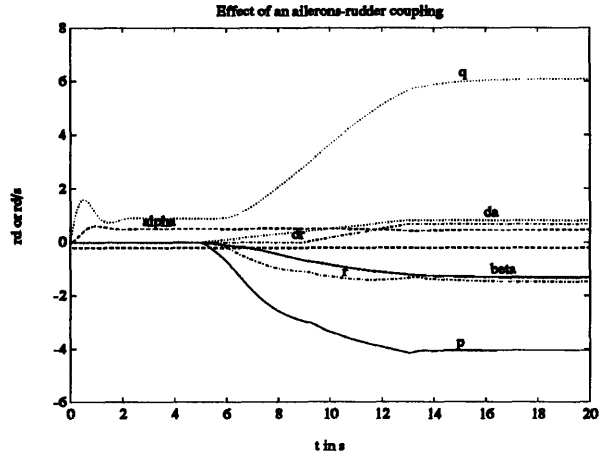

Figure 5-7: Time history for δe = -0.20 rad when δa varies linearly from 0 to 1 rad and δr is coupled to δa

selection.

5.5 Conclusions and recommendations for further work

5.5.1 Conclusions

The usefulness of the bifurcation theory was demonstrated through this relatively simple example since it was the basis for both the lateral and longitudinal dynamics analysis and for the control system design. Even more than useful, bifurcation analysis is totally necessary when facing nonlinear systems whose Jacobian matrix has zero eigenvalues. From a more remote standpoint, this shows once more the enormous deal of information that pure mathematics can bring to all the fields of applied sciences ...

However, the realism of the analysis done in this thesis is somewhat limited by the many approximations made on the aerodynamic model of the airplane: concepts must be taken into account rather than quantitative results.

5.5.2 Recommendations for further work

There are three areas in which further work can be done regarding the applications of bifurcation theory to flight dynamics: numerical simulations, experimental verifications and theoretical investigations.

Numerical simulations

The model used in this thesis was very simple though it featured all the aspects of a complex, coupled, nonlinear system. To fully represent a fighter at high angle of attack, a good model should include fully nonlinear equations of motions (no linearization in α and β), fully nonlinear aerodynamic model and must take into account the influence of modern control surfaces such as flaperons, canards and thrust vectoring.

Experimental verifications

If a such good model is developed, it might be worthwhile correlating the numerical results with experiments in a wind tunnel, though these experiments would require a heavily instrumented model with moving and controlable control surfaces.

Theoretical investigations

However, the most exciting work to be done is in the theoretical field. One of the major shortcomings of the numerical method used in this thesis is that it does not give any evaluation of the amplitude of the limit cycles. Numerical methods have been developped recently [22] to compute the amplitude of the limit cycles but it seems that even more information could be obtained through the application of the multiple scales method , as developed by R.V. Ramnath (cf [27] for basic concepts about multiple scaling and [28, 29] for a complete presentation). As a matter of fact, not only numerical results but approximative analytical representations of the limit cycles in the neighborhood of a Hopf bifurcation could be obtained through multiple scaling. Thus, one would probably get great insight into mechanisms of departures into limit cycles and would know which parameter have the greatest influence on limit cycles amplitude and onset.

Appendix A

Matlab routine used to compute the value and the stability of the equilibrium states of the system 2.16

```
yb=-0.28;
za=-1.746;
mapt=-0.251;
mab=-10.2618;
mqb=-1.419;
i2=0.949;
i3=0.7160;
mde=-31.64;
nb=8.88;
nr=-0.377;                                                    10
lb=-20.91;
lr=0.221;
lp=-5.786;
lra=13.16;
lda=-60.27;
ldr=-10.05;
nda=-1.282;
ndr=-8.30;
demin=-0.50;
demax=0.30;                                                   20
da=0;
dr=0;
% These instructions compute the nineth order polynomial.
```

```
a1=[i2 0 mab-mqb*za];
a2=[0 i3*za+nr 0];
b1=[0 i2*yb+mqb-mapt 0];
b2=[-i3 0 nb+nr*yb];
c2=[0 0 -nda*da-ndr*dr];
for i=1:61
        de=demin+(i-1)*(demax-demin)/60;                                    30
        c1=[0 0 -mde*de];
        Na=conv(c1,b2)-conv(b1,c2);
        Nb=conv(a1,c2)-conv(a2,c1);
        D=conv(a1,b2)-conv(a2,b1);
        pooly=conv(D,conv([0 lb+lr*yb],Nb)+conv([lr 0],Na))+conv(conv(D,D),
[lp lda*da+ldr*dr])+conv([lra 0],conv(Na,Na))+conv([0 lra*yb],conv(Na,Nb));
% This instruction computes the roots of the nineth order polynomial.
        cc31(:,i)=roots(pooly);
% These instructions select the real roots.
        for j=1:9                                                           40
                if imag(cc31(j,i)) ~=0
                        cc31(j,i)=0;
                end
        end
end
cc32=sort(sort(cc31));
for i=1:61
        de=demin+(i-1)*(demax-demin)/60;
        c1=[0 0 -mde*de];
        Na=conv(c1,b2)-conv(b1,c2);                                         50
        Nb=conv(a1,c2)-conv(a2,c1);
        D=conv(a1,b2)-conv(a2,b1);
        for j=1:9
                p=cc32(j,i);
% These instructions compute the state vector for each equilibrium p
and for each de.
                a=polyval(Na,p)/polyval(D,p);
                b=polyval(Nb,p)/polyval(D,p);
                q=p*b-za*a;
                r=p*a+yb*b;                                                 60
                vecta(j,i)=a;
                vectb(j,i)=b;
                vectq(j,i)=q;
                vectr(j,i)=r;
% These instructions compute the stability matrix and its eigenvalues.
                M=[yb p 0 -1 a;-p za 1 0 -b;-mapt*p mab mqb i2*p
i2*r-mapt*b;nb 0 -i3*p nr -i3*q;
                lb lra*r 0 lra*a+lr lp];
                vp=eig(M);
                compt=0;                                                    70
                for k=1:5
                        if real(vp(k)) > 0
                        compt=compt+1;
                        end
                end
                if compt > 0
                        plot(de,p,'o')
```

```
                else
                        plot(de,p,'+')
                end                                                    80
                        if j == 1
                                cc42(:,i)=vp;
                        end
                        if j == 2
                                cc52(:,i)=vp;
                        end
                        if j == 3
                                cc62(:,i)=vp;
                        end
                        if j == 4                                      90
                                cc72(:,i)=vp;
                        end
                        if j == 5
                                cc82(:,i)=vp;
                        end
                if j == 6
                                cc92(:,i)=vp;
                        end
                        if j == 7
                                cc102(:,i)=vp;                         100
                        end
                        if j == 8
                                cc112(:,i)=vp;
                        end
                        if j == 9
                                cc122(:,i)=vp;
                        end
        end
end
                                                                       110
```

Appendix B

Bifurcation surfaces

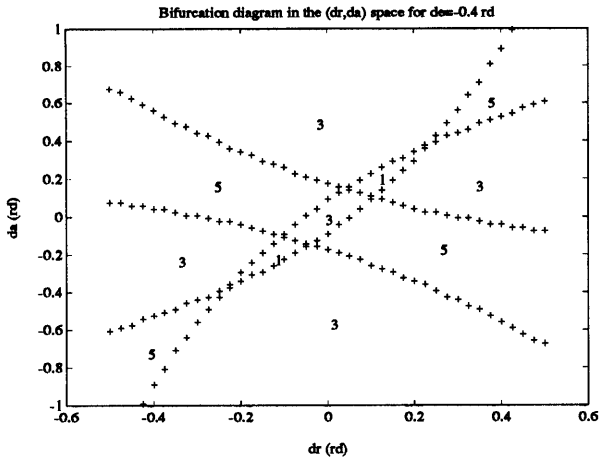

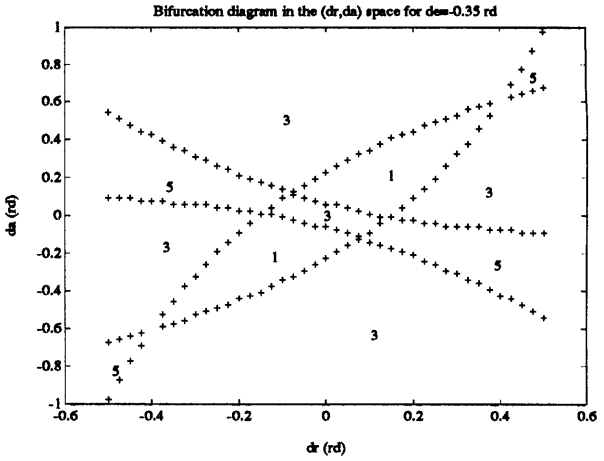

Figure B-1: Left: bifurcation surface in the (δr, δa) space for δe = -0.40 rd. The figures inside the diagram indicate the number of equilibrium states in each area

Figure B-2: Right: bifurcation surface in the (δr, δa) space for δe = -0.35 rd. The figures inside the diagram indicate the number of equilibrium states in each area

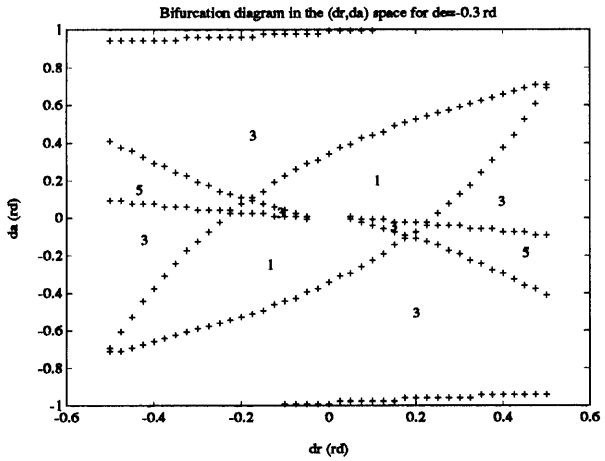

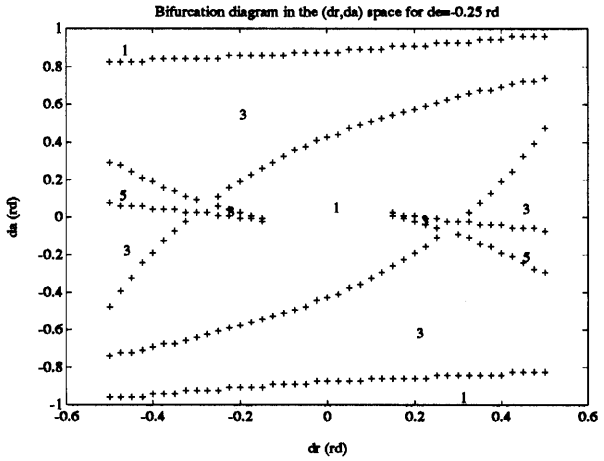

Figure B-3: Left: bifurcation surface in the (δr, δa) space for δe = -0.30 rd. The figures inside the diagram indicate the number of equilibrium states in each area

Figure B-4: Right: bifurcation surface in the (δr, δa) space for δe = -0.25 rd. The figures inside the diagram indicate the number of equilibrium states in each area

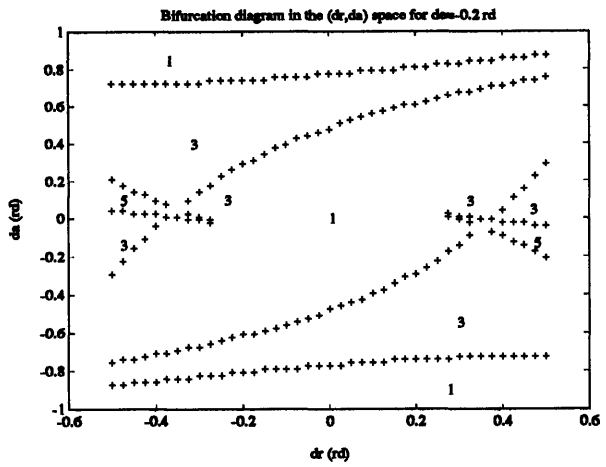

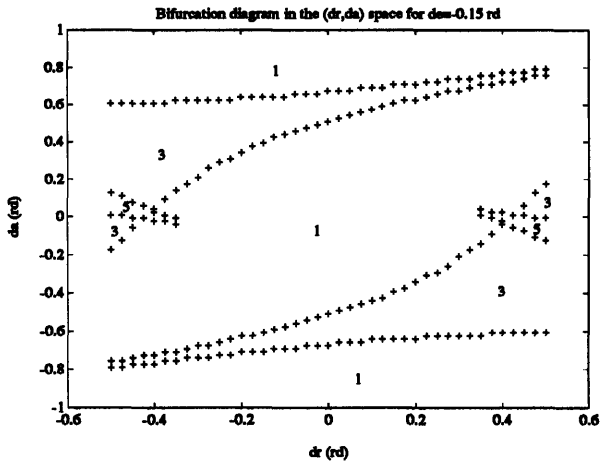

Figure B-5: Left: bifurcation surface in the (δr, δa) space for δe = -0.20 rd. The figures inside the diagram indicate the number of equilibrium states in each area

Figure B-6: Right: bifurcation surface in the (δr, δa) space for δe = -0.15 rd. The figures inside the diagram indicate the number of equilibrium states in each area

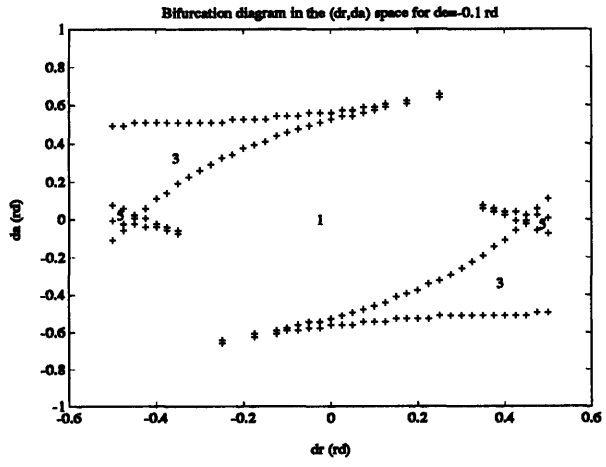

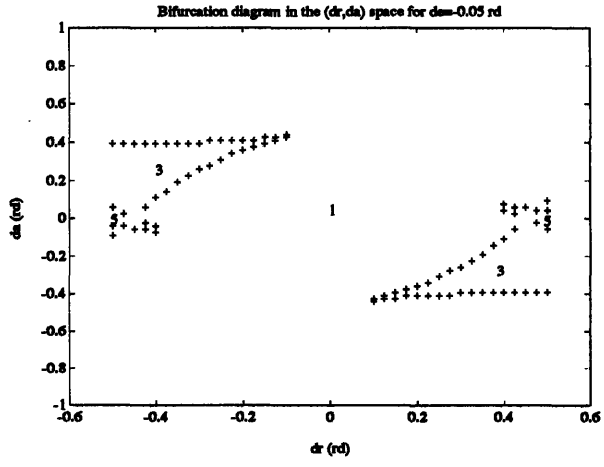

Figure B-7: Left: bifurcation surface in the (δr, δa) space for δe = -0.10 rd. The figures inside the diagram indicate the number of equilibrium states in each area

Figure B-8: Right: bifurcation surface in the (δr, δa) space for δe = -0.05 rd. The figures inside the diagram indicate the number of equilibrium states in each area

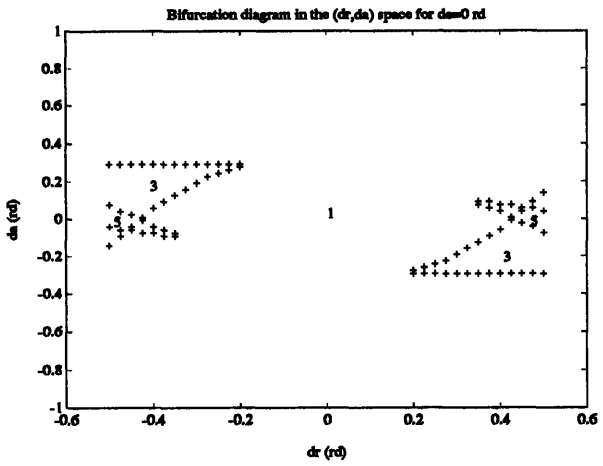

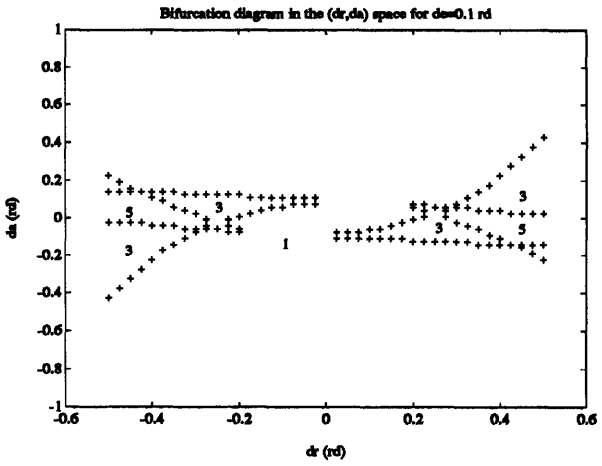

Figure B-9: Left: bifurcation surface in the (δr, δa) space for $\delta e = 0$ rd. The figures inside the diagram indicate the number of equilibrium states in each area

Figure B-10: Right: bifurcation surface in the (δr, δa) space for $\delta e = 0.10$ rd. The figures inside the diagram indicate the number of equilibrium states in each area

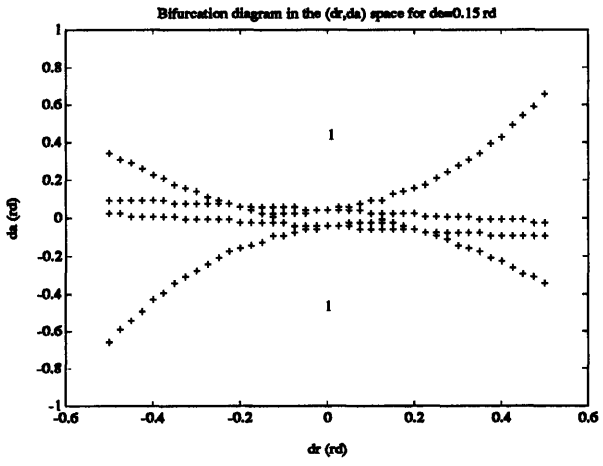

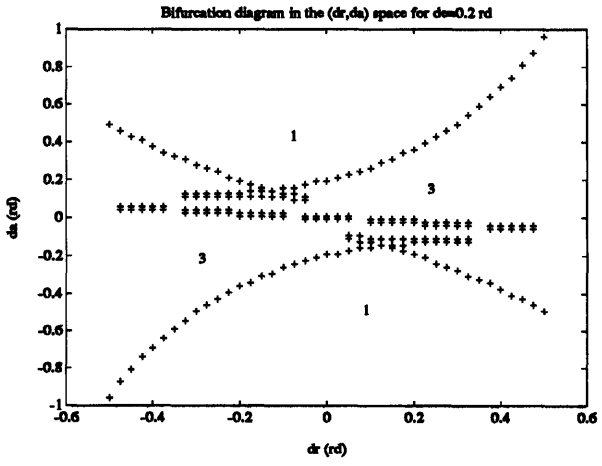

Figure B-11: Left: bifurcation surface in the (δr, δa) space for $\delta e = 0.15$ rd. The figures inside the diagram indicate the number of equilibrium states in each area

Figure B-12: Right: bifurcation surface in the (δr, δa) space for $\delta e = 0.20$ rd. The figures inside the diagram indicate the number of equilibrium states in each area

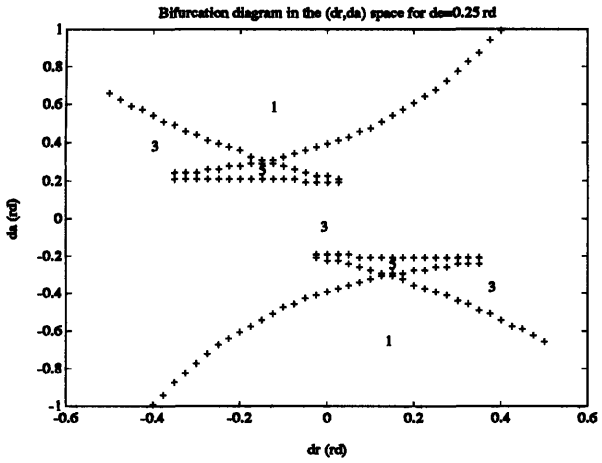

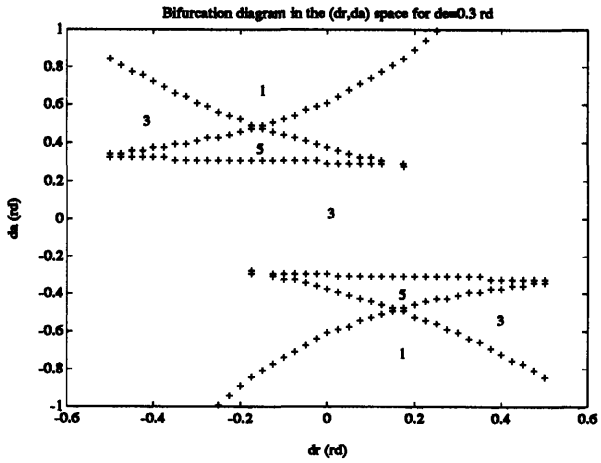

Figure B-13: Left: bifurcation surface in the (δr, δa) space for $\delta e = 0.25$ rd. The figures inside the diagram indicate the number of equilibrium states in each area

Figure B-14: Right: bifurcation surface in the (δr, δa) space for $\delta e = 0.30$ rd. The figures inside the diagram indicate the number of equilibrium states in each area

Bibliography

[1] B. Etkin. *Dynamics of Flight. Stability and Control.* Wiley and Sons, NY, 1982.

[2] D. Mc Lean. *Automatic Flight Control Systems.* Prentice Hall, Englewood (NJ), 1990.

[3] W. H. Phillips. Effect of steady rolling on longitudinal and directional stability. Technical Note 1627, NACA, 1948.

[4] I. Czinczenheim. Le couplage par inertie et ses répercussions sur les qualités des avions. *La Documentation Aéronautique*, 1958.

[5] M. Bismut. Régime de tonneaux non controlés. *La Recherche Aéronautique*, 58, 1958.

[6] D. W. Rhoads and J. M. Schuler. A theoretical and experimental study of airplane dynamics, in large-disturbance manoeuvres. *Journal of Aeronautical Sciences*, 7, 1957.

[7] J. D. Welch and R. E. Wilson. Cross-coupling dynamics and the problem of automatic control in rapid rolls. *Journal of Aeronautical Sciences*, 10, 1957.

[8] L. Sternfield. A simplified method for approximating the transient motion in angle of attack and sideslip during a constant rolling manoeuvre. Report 1344, NACA, 1958.

[9] F. Clifton Berry. High alpha. *Air Force Magazine*, October 1990.

[10] W.B. Herbst. Future fighter technologies. *Journal of Aircraft*, 7, August 1980.

[11] K.J. Orlik Ruckmann. Aerodynamic aspects of aircraft dynamics at high angles of attack. *Journal of Aircraft*, 20(9), 1983.

[12] Ames Research Center, Dryden Flight Research Facility. *High Alpha Technology Program Workshop*, November 1989.

[13] J. Rom. *High angle of attack aerodynamics.* Springer-Verlag, NY, 1992.

[14] R. Thom. *Stabilité structurelle et morphogénèse.* Ediscience, Paris, 1972.

[15] P. Guicheteau. Bifurcation theory applied to the study of control losses on combat aircraft. *La Recherche Aérospatiale*, (2), 1982.

[16] J. V. Carroll and R. K. Mehra. Bifurcation analysis of nonlinear aircraft dynamics. *Journal of Guidance and Control*, 5(5), 1982.

[17] R. K. Mehra and J. V. Caroll. Global stability and control analysis of aircraft at high-angles of attack. Annual Technical Report CR215-248-2, Office of Naval Research, 1978.

[18] A. A. Schy and M. E. Hannah. Prediction of jump phenomena in roll coupled maneuvers of airplanes. *Journal of Aircraft*, 14, 1977.

[19] A. A. Schy, J. W. Young, and K. G. Johnson. Prediction of jump phenomena in aircraft maneuvers, including nonlinear aerodynamic effects. *Journal of Guidance and Control*, 1(1), 1978.

[20] A. A. Schy, J. W. Young, and K. G. Johnson. Pseudosteady state analysis of nonlinear aircraft maneuvers. *AIAA paper*, (80-1600), 1980.

[21] J.B. Planeaux and T.J. Barth. High-angle-of-attack dynamic behavior of a model high-performance fighter aircraft. *AIAA paper*, (4368), 1988.

[22] J.B. Planeaux and J.A. Beck. Bifurcation analysis of a model fighter aircraft with control augmentation. *AIAA paper*, (2836), 1990.

[23] B. Wigdorowitz. Application of linearization analysis to aircraft dynamics. *Journal of Guidance, Control and Dynamics*, 15(3), May-June 1992.

[24] D. A. Sánchez. *Ordinary Differential Equations and Stability Theory: an Introduction.* Dover, New-York, 1979.

[25] J. Guckenheimer and P. Holmes. *Nonlinear Oscillations, dynamical systems and bifurcations of Vectors Fields.* Springer-Verlag, New-York, 1986.

[26] T. Hacker and C. Oprişiu. A discussion of the roll-coupling problem. *Progress in Aerospace Sciences*, 15, 1974.

[27] R.V. Ramnath. Class notes, M.I.T. course 16.17, 1992.

[28] R.V. Ramnath, J.K. Hedrick, and H.M. Paynter, editors. *Nonlinear system analysis and synthesis*, volume 2. The American Society of Mechanical Engineers, NY, 1980.

[29] R.V. Ramnath and G. Sandri. A generalized multiple scales approach to a class of linear differential equations. *J.M.A.A.*, 28(2), 1969.